

Alma Mater Studiorum - Università di Bologna

**DOTTORATO DI RICERCA IN
BIOLOGIA CELLULARE E MOLECOLARE**

Ciclo XXIX

Settore Concorsuale di afferenza: 05/E1

Settore Scientifico disciplinare: BIO/10

**BIOCHEMICAL AND STRUCTURAL CHARACTERIZATION
OF THE CHLOROPLASTIC ENZYME TRANSKETOLASE
FROM THE GREEN MICROALGA**

Chlamydomonas reinhardtii

Presentata da: Miriam Pasquini

Coordinatore Dottorato:

Relatore:

Prof. Giovanni Capranico

Prof. Francesco Francia

Correlatore:

Dr. Mirko Zaffagnini

Esame Finale Anno 2017

***“It is through science that we prove,
but through intuition that we discover.”***

Henri Poincare (1854-1912)

Index	1
Introduction	5
Chapter 1: Chlamydomonas reinhardtii	6
1. Chlamydomonas reinhardtii: an interesting alga.....	6
1.1 Chlamydomonas as a model organism.....	6
1.2 Chlamydomonas as source of energy: hydrogen and fuels' production.....	7
2. The chloroplast in Chlamydomonas reinhardtii.....	7
2.1 C. reinhardtii chloroplast as a protein production factory.....	8
Chapter 2: The Calvin cycle	9
1. Steps of the cycle.....	9
2. The regulation of the Calvin cycle.....	10
Chapter 3: The non-redox regulation of the Calvin cycle: influence of magnesium and pH	12
1. The crosstalk between magnesium and pH regulatory activity.....	12
1.1 Physiological significance of the fluctuations of Mg ²⁺ and pH in the stroma and the lumen	12
Chapter 4: The redox regulation of the Calvin Cycle: Cysteine residues, disulfide bonds and other redox post-translational modifications (PTMs)	14
1. Cysteines and disulfide bonds.....	14
2. The role of the thioredoxins (TRXs).....	16
3. Other Redox Post-translational modifications (PTMs).....	18
3.1 H ₂ O ₂ -mediated modifications of protein thiols.....	18
3.2 •NO-mediated modifications of protein thiols.....	19
3.3 H ₂ S-mediated modification of protein thiols.....	20
3.4 S-Glutathionylation.....	20
4. Proteomic identifications of disulfide bonds and other redox PTMs.....	21
4.1 Bioinformatic tools for studying disulfide bonds: Molecular Dynamics (MD) simulation.....	23
Chapter 5: The transketolase	25
1. General features.....	25
2. Enzymatic structure.....	28
2.1 Cofactor-induced optical properties of transketolase.....	31
3. Kinetic mechanism.....	33
3.1 Double-substrate and single-substrate reactions.....	35
4. Industrial applications for the transketolase.....	37
Chapter 6: THI and TPP as gene expression regulators	38
1. Biosynthesis pathway of THI/TPP.....	38

2. TPP riboswitches.....	39
3. Cellular effects of THI and TPP.....	40
Materials and Methods.....	43
1. Aim of the study.....	44
Chapter 1.....	45
1. Plasmid Construction for Expression of CrTK and EcE4PDH in <i>E. coli</i>	45
2. Preparation of competent BL21 <i>Escherichia coli</i> cells.....	46
3. Transformation of BL21 <i>Escherichia coli</i> cells.....	47
4. Extraction of Plasmidic DNA.....	47
5. <i>E. coli</i> cultures and protein expression induction with IPTG.....	48
6. Protein purification and quantification.....	49
7. SDS-PAGE (Sodium Dodecil Sulphate-Protein Acrylamide Gel Electrophoresis).....	50
8. CrTK Molecular Mass Determination through Gel Filtration.....	52
9. CrTK analysis through Dynamic Light Scattering (DLS).....	52
10. Absorption and CD spectroscopy.....	52
10.1 Binding studies with thiamine pyrophosphate (TPP).....	52
10.2 Secondary structure estimation for CrTK in its reduced form.....	53
11. Mass Spectrometry.....	53
12. Crystallization and Data Collection.....	54
12.1 Structure Solution and Refinement.....	54
12.2 Accession number.....	55
13. Choice of the CrTK-EcE4PDH activity assay and assay description.....	55
14. Activity Measurement for EcE4PDH.....	56
15. Reconstitution of the CrTK.....	56
16. Treatment with NEM (Alkylation) of CrTK _{TPP}	57
17. Treatment with DTNB of CrTK _{TPP}	57
18. Treatment with CuCl ₂ and Activity Recovery of CrTK _{TPP}	57
19. Treatment with oxidized DTT and Activity Recovery of CrTK _{TPP}	57
20. BIO-GSSG Western Blot on CrTK _{TPP}	58
21. Treatment with H ₂ O ₂ of CrTK _{TPP}	58
22. Assays for determining temperature and pH optimum.....	58
23. Determination of Kinetic Parameters.....	58

Chapter 2	59
1. Strain, medium and treatments of <i>Chlamydomonas</i> cultures.....	59
2. RNA Extraction from <i>Chlamydomonas reinhardtii</i> , using the RNAeasy Mini Kit (QIAGEN).....	60
3. DNase treatment of RNA samples, using TURBO DNA-free kit (Ambion).....	60
4. cDNA synthesis, using SuperScript III First-Strand Synthesis System for RT-PCR (Invitrogen).....	61
5. Gene sequences and primer design.....	61
6. Polymerase Chain Reaction - PCR, using BioTaq (Bioline).....	62
7. Agarose gel electrophoresis.....	62
8. Real Time PCR - or quantitative PCR (qPCR), using the SYBR Green JumpStart Taq Ready Mix (Sigma).....	62
Results	63
Chapter 1	64
1. Quaternary structure of apo- and holo-forms of CrTK.....	64
2. Crystal structure of CrTK _{apo} and CrTK _{TPP/Mg}	65
3. CrTK in comparison with other TK structures.....	68
4. CrTK _{TPP/Mg} structure reveals a number of interactions between TPP, Mg ²⁺ and active site residues.....	68
5. Comparison between CrTK _{apo} and CrTK _{TPP/Mg} structures.....	71
6. pH optimum.....	74
6.1 Determination of the pH optimum for the EcE4PDH.....	74
6.2 Comparison between CrTK and EcE4PDH pH dependence.....	75
7. Magnesium and TPP role in the reconstitution of the fully active CrTK.....	76
8. Mg ²⁺ is required for the formation of a TPP-induced absorption band.....	79
9. CD spectra of the CrTK _{TPP} and CrTK _{TPP/Mg}	83
10. Effect of DTT on the CrTK activity.....	83
11. Effects of oxidation with CuCl ₂ on the CrTK _{TPP} activity.....	85
12. Induced Circular Dichroism (ICD) spectra of CrTK _{TPP/Mg}	86
13. CD study of the TPP binding in the reduced and oxidized CrTK _{TPP} forms.....	87
14. Affinity constant (K _m) for the F6P in the reduced and oxidized CrTK _{TPP}	89
15. Effect of NEM-induced irreversible alkylation on the CrTK _{TPP}	90
16. Glutathionylation of the CrTK _{TPP} by BIO-GSSG.....	91
17. Effect of DTNB -induced reversible alkylation on the CrTK _{TPP}	91
18. Titration of CrTK _{TPP} free thiols with DTNB.....	92
19. Mass spectrometry on CrTK _{TPP}	93

19.1 LC-ESI-MS-MS analysis on reduced CrTK _{TPP}	94
19.2 LC-ESI-MSMS analysis on oxidized CrTK _{TPP}	96
Chapter 2	98
1. Influence of intermediates of the TPP biosynthetic pathway on the TRK1 gene expression levels.....	98
2. Influence of stress agents on TRK1 gene expression.....	100
Discussion	102
Chapter 1	103
1. Comparison between the structure of the CrTK and the CrTK _{TPP/Mg}	103
2. ICD signal analysis on the reduced and oxidized CrTK _{TPP/Mg}	103
3. The importance of Mg ²⁺ for the CrTK activity.....	104
4. The role of the Mg ²⁺ in the TPP-induced absorption band.....	104
5. The redox sensitivity of the CrTK and the role of the Mg ²⁺	105
6. Effects of NEM and DTNB treatments on the CrTK _{TPP} activity.....	106
7. Gluthathionylation in the CrTK.....	107
8. Titration of the free thiol residues and mass spectrometry analysis: identification of the Cys470-Cys484 disulfide bond.....	108
Chapter 2	110
1. Influence of intermediates of the TPP biosynthetic pathway on the TRK1 gene expression levels.....	110
2. Influence of stress agents on TRK1 gene expression.....	111
Conclusions	113
References	115
Acknowledgements	133

Introduction

Chapter 1: *Chlamydomonas reinhardtii*

1. *Chlamydomonas reinhardtii*: an interesting alga

Chlamydomonas reinhardtii is a eukaryotic photosynthetic unicellular green microalga, belonging to the order of *Volvocales*, family *Chlamydomonadaceae* (Pröschold et al., 2001) that is distributed worldwide in soil and freshwater. Systematic investigations on aquatic microalgae belonging to the genus *Chlamydomonas* began in the early 19th century. The first wild type strain, called c137 (mt+), was collected in 1945 in Massachusetts, USA, for scientific purposes by Gilbert M. Smith (Smith, 1946) - for this reason, this alga is also called *Chlamydomonas smithii*.

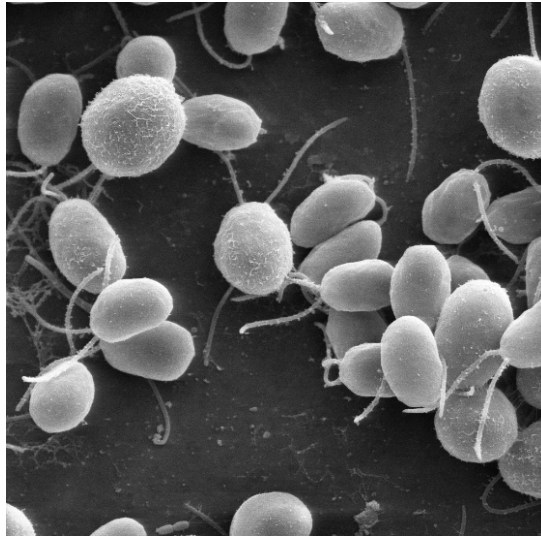


Figure 1. Scanning electron microscope image, showing green algae *Chlamydomonas reinhardtii* (from Wikipedia).

As shown in Figure 1, *Chlamydomonas* cells are oval shaped. They are approximately 10 μm in length and 3 μm in width and present a cell wall made of hydroxyproline-rich glycoproteins, a big cup-shaped chloroplast (occupying 40% of the cell volume), several mitochondria, a large pyrenoid and an "eyespot" that senses light (Lacoste-Royal and Gibbs, 1987). *Chlamydomonas* can swim thanks to two apically localized flagella (anchored in basal bodies), maintained at an equal and appropriate length through a fine mechanism of regulation of flagellar length (Wilson et al., 2008). Flagella are important not only to optimize the exposure to light and nutrients (Rochaix, 1995; Govorunova, 2005), but even for the sexual mode of reproduction (Harris, 2001; Pan et al., 2003) since they mediate the recognition and fusion processes that take place between cells of two opposite mating types, called *plus* (+) and *minus* (-).

1.1 *Chlamydomonas* as a model organism

C. reinhardtii is the best investigated microalgal species today, partly due to its ease of culturing and manipulating its genetics, and, as pointed out in (Merchant et al., 2007), represents a common ancestor of animals and plants. The mitochondrial, chloroplast and nuclear genomes have been fully sequenced and can be accessed via public databases (Blaby et al., 2014). Cultivation in the laboratory can be carried out from photo-litho-autotrophic (light and CO_2 as inorganic compound) to chemo-organo-heterotrophic (dark and acetate as the organic carbon source) conditions. Fast vegetative growth rates with generation times of less than seven hours are common (Sager and

Granick, 1953), allowing fast creation of biomass. Because of these reasons, a continuously growing number of researchers have joined the “*Chlamy* community” to study such diverse research topics as photosynthesis and light acclimation (Allahverdiyeva et al. 2015; Heinnickel and Grossman, 2013; Minagawa, 2011; Rochaix et al., 2012); respiration (Salinas et al., 2014); flagella and basal bodies organization and function (Dutcher, 2014); life cycle and mating (Umen, 2011); carbon metabolism (Johnson and Alric, 2013); nutrient membrane transport (Blaby-Haas and Merchant, 2012; Grossman, 2000); circadian clock (Matsuo and Ishiura, 2011); photoreceptors (Kianianmomeni and Hallmann, 2014); photosynthetic hydrogen production (Grossman et al., 2011; Philipps et al., 2011; Melis et al., 2007) and high-value compounds’ production (Merchant et al., 2012; Rasala and Mayfield, 2015; Rosales-Mendoza et al., 2012; Skjanes et al., 2013).

1.2 Chlamydomonas as source of energy: hydrogen and fuels’ production

More recently, as greater focus has been placed on the development of renewable fuel sources, *C. reinhardtii* and other algal species have also been used to study the production of renewable biofuels in the form of hydrogen gas or oils (Grossman et al., 2011; Merchant et al., 2012). Photosynthetic microbes, such as algae and cyanobacteria, are promising renewable energy production vehicles for such compounds because they can utilize atmospheric CO₂ as their carbon source, grow in sea water or waste water, propagate quickly on otherwise non-arable land and use sunlight as an energy source (Merchant et al., 2012).

2. The chloroplast

The chloroplast is a specific organelle surrounded by two membranes (the outer and the inner ones) and it is present in the cytoplasm of eukaryotic photosynthetic cells that carry out the photosynthetic process (Kirk, 1971; Bishop, 1974). The inner membrane delimits the chloroplast stroma. The stroma contains a complex membrane network called thylakoids (Figure 2). They represent a highly dynamic collection of membranous interconnected sacks where photosynthetic pigments, chlorophylls and carotenoids, are found and catch the light to drive photosynthesis. In many vascular plants, thylakoids are arranged in lamellae and grana (Mustardy et al., 2008), while in some C₄ plant and algal chloroplasts, they are organized in free-floating appressed and non-appressed lamellae in the stroma (Pribil et al., 2014).

A part of the chloroplast is taken up by the pyrenoid, containing its own set of enzymes, among which the ribulose-bisphosphate carboxylase (Rubisco) - in both atmospheric and CO₂-limiting conditions (Borkhsenius et al., 1998). To improve its carbon dioxide organization pathway, *Chlamydomonas* has evolved a number of transporters and other proteins able to “pump” CO₂/bicarbonate in the pyrenoid, making it more easily available in the action site of the Rubisco (Brueggeman et al., 2012; Fang et al., 2012). This mechanism permits an efficient photosynthesis even in water, where carbon dioxide availability is much restricted than in soil environments (Wang et al., 2011). The creation of different mutants showing impairments in the Carbon Concentrating Metabolism (CCM) has contributed to the characterization of this complex pathway (Wang et al., 2011) and could be important in the future to enhance the photosynthetic rate of important land plants.

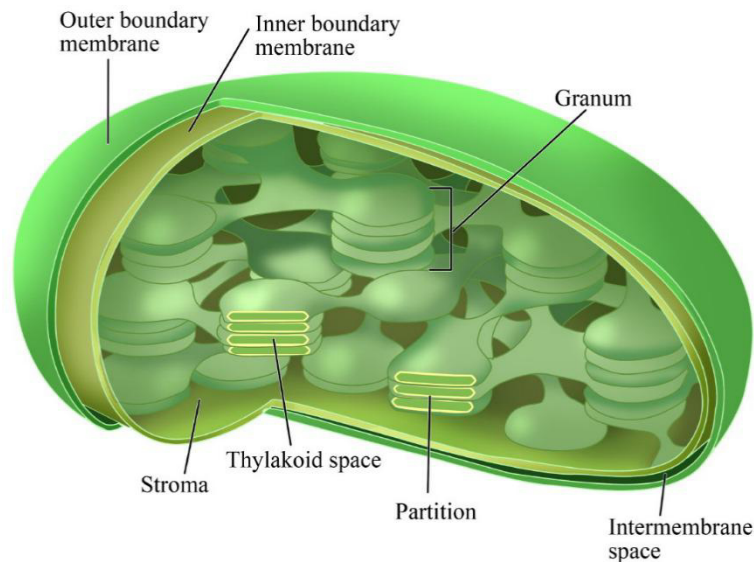


Figure 2. Chloroplast organization.

2.1 *C. reinhardtii* chloroplast as a protein production factory

The *C. reinhardtii* chloroplast genome consists of approximately 80 redundant copies of an approximately 200 kb circular plasmid (Rosales-Mendoza et al., 2012). Stable transformation of all 80 copies with a transgene is achieved by prolonged selection at high antibiotic concentrations, which allows the creation of a number of transgene copies whose expression level is high. In addition, the transcriptional stability of transgenes incorporated into the chloroplast genome is high because silencing is not a concern (Leon-Banares et al., 2004). Consequently, expression of valuable proteins from the *C. reinhardtii* chloroplast commonly results in nearly 1%, and in rare cases up to 20%, of total cellular protein consisting of the transgenic product (Leon-Banares et al., 2004). To date, a copious number of reports has been published describing the expression of high value proteins with therapeutic or other biotechnological purposes from the *C. reinhardtii* chloroplast (Mayfield et al., 2007; Rosales-Mendoza et al., 2012; Rosales-Mendoza, 2013).

Chapter 2: The Calvin Cycle

1. Steps of the cycle

In the stroma of chloroplasts in photosynthetic organisms (plants, algae and cyanobacteria), long-term energy storage in the form of sugars is produced by a subsequent sequence of biochemical reactions called Calvin cycle. This cycle was discovered by Melvin Calvin, James Bassham and Andrew Benson at the University of California, Berkeley (Bassham et al., 1950), who found that the inorganic carbon (*i.e.* CO₂) is converted into organic compounds that can be exploited by the organism (and by animals that feed on it). For this reason, this process is also defined as “organication” or “fixation” of the carbon. The most outdated name is “dark reactions”, which can be misleading because it implies incorrectly that the reactions only occur in the night or are independent of light, which is why most scientists no longer use it: in fact, the Calvin cycle is not independent from light since it relies on ATP and NADH molecules, which are products of the light-dependent reactions of the photosynthesis.

There are three phases identified in the Calvin cycle: (1) the carbon fixation, (2) the reduction reactions and (3) the ribulose 1,5-bisphosphate (RuBP) regeneration, as shown in the Figure 3. In the first stage, the enzyme Rubisco incorporates carbon dioxide into an organic molecule, the 3-phosphoglyceric acid (3-PGA). In the second stage, this molecule is reduced using electrons supplied by NADPH. In the stage 3, the ribulose bisphosphate (RuBP), the molecule at the beginning of the cycle, is regenerated in order to restart the cycle itself. Only one carbon dioxide molecule per cycle is incorporated, so the cycle must be completed three times to produce a single three-carbon molecule, the glyceraldehyde 3-phosphate (GA3P), and six times to produce a six-carbon glucose molecule (Bassham et al., 1950).

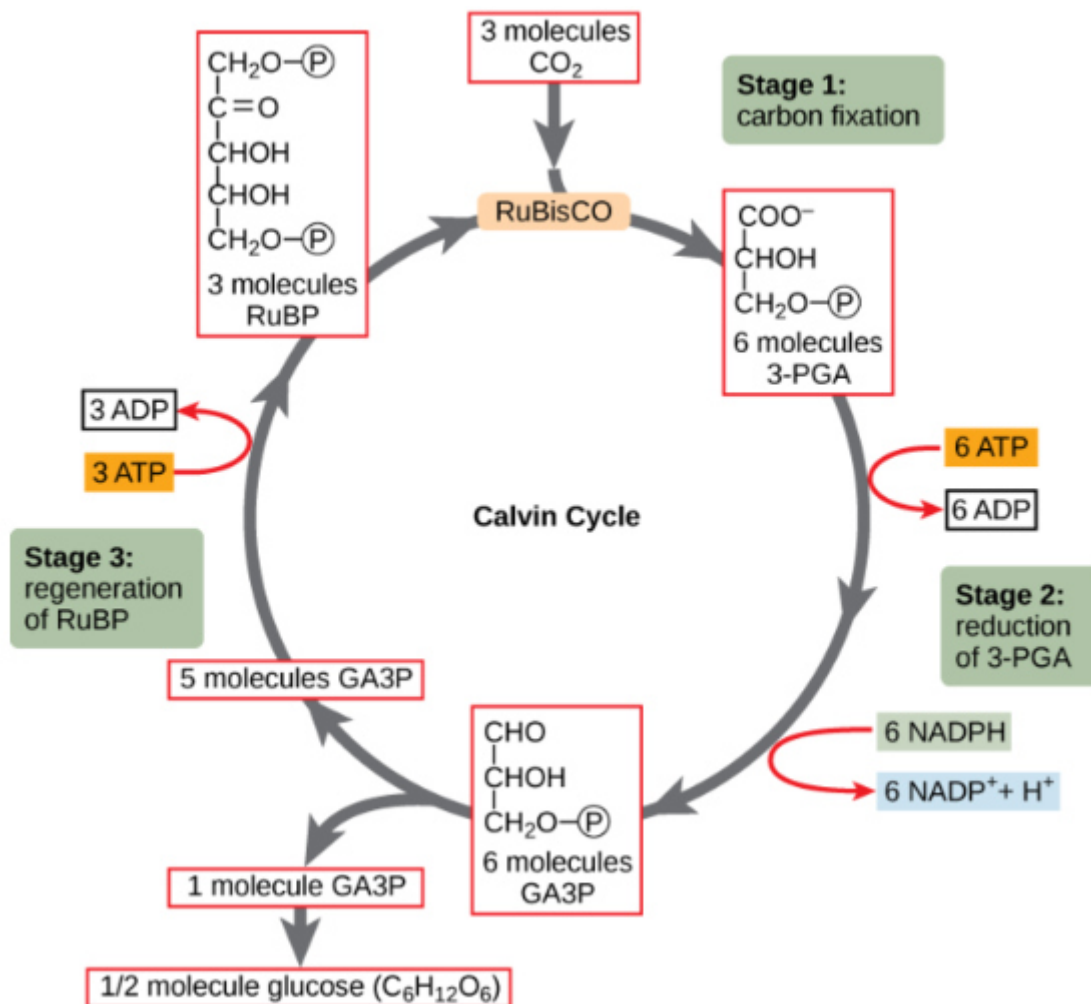


Figure 3. Steps of the Calvin cycle: (1) the carbon fixation, (2) the reduction reactions and (3) the ribulose 1,5-bisphosphate (RuBP) regeneration.

2. The regulation of the Calvin cycle

Carbon dioxide assimilation through Calvin cycle has to be promptly down-regulated as some steps would be wasteful if allowed to occur in the dark, counteracting the reactions of glycolysis and using up all available ATP and NAD(P)H required for other metabolic processes. The modulation of the Calvin cycle is very complex and includes changes, from dark-to-light conditions, that can be categorized in (1) “non redox” and (2) “redox” regulatory events:

1) The “non redox” events include a regulatory action linked to the increase of the Mg²⁺ content in the chloroplasts’ stroma upon illumination, with a simultaneous increase of the pH level at the same site (Barber et al., 1974; Portis and Heldt, 1976);

2) The “redox” mechanisms are indeed connected to the ferredoxin/thioredoxin activation system: when light is available, the reduced/activated ferredoxin (Fd_{red}) reduces and therefore activates the thioredoxin (TRX) proteins, through the ferredoxin-thioredoxin reductase (Figure 4). The reduced TRX can now disrupt disulfide bond(s) found in the photoactivable target enzymes of the Calvin cycle. This last will be “switched off” in the dark, when the formation of disulfide bonds will occur with the consequent inactivation of its enzymes (Wolosiuk et al., 1993; Schürmann and Buchanan, 2008).

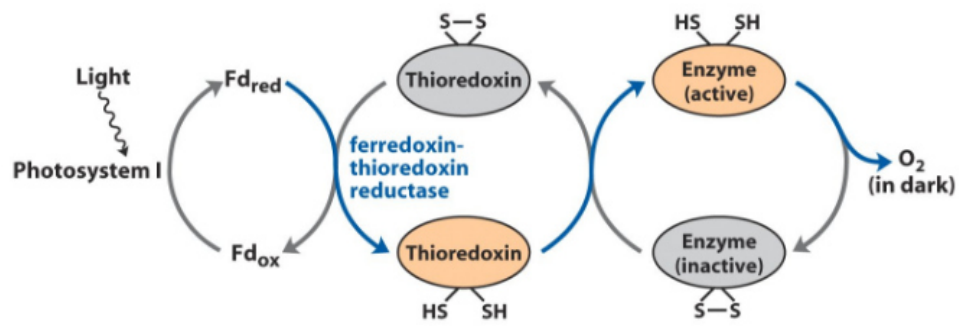


Figure 4. Scheme of the ferredoxin-thioredoxin system.

Chapter 3: The non redox regulation of the Calvin cycle: influence of magnesium and pH

1. The crosstalk between magnesium and pH regulatory activity

Magnesium (Mg^{2+}) is one of the most important cations in plant systems, being involved in the photophosphorylation, in the formation of both the chlorophylls (*a* and *b*) and the catalytically active form of many respiratory enzymes, in the protein synthesis, in the RNA generation and in the formation of functional cell membranes. In a plant cell, the total Mg^{2+} concentration is reported to be in the millimolar range, distributed among the cytosol, the chloroplast and the mitochondria, while most metabolically inactive Mg^{2+} is located in the vacuole (Kobayashi et al., 2015).

The light-induced increase in the Mg^{2+} concentration of the stroma was found to be between 1-5 mM, depending on the assay conditions, particularly the pH (Portis and Heldt, 1976). However, these values may greatly vary according to plant species, cell type or nutritional and light conditions (Shaul et al., 2002).

Proton pumping from the stroma into thylakoids in the light results in acidification of the thylakoid lumen. The accompanied electrical gradient across the thylakoid membrane is compensated by concomitant fluxes of Cl^- , K^+ and Mg^{2+} ions (Dilley and Vernon, 1965; Hind et al., 1974). This compensation allows the prolongation of H^+ transport into the thylakoids and the generation of ΔpH of 2–3 pH unit between the lumen and the stroma – in the light, the pH of the stroma is about 8 and that of the thylakoid lumen is less than 6 (Höhner et al., 2016). In general, the concentrations in the stroma are on the order of 150 mM for K^+ (Demmig and Gimmler, 1983), 50 mM for Cl^- (Demmig and Gimmler, 1983), and 5 mM for Mg^{2+} (Portis and Heldt, 1976). Anions seem to compensate only about half of the H^+ taken into thylakoids after illumination (Thaler et al., 1992), and thus the remaining part of charge balance has to be mediated by efflux of cations from the lumen to the stroma. Cation channels across the thylakoid membrane were mainly investigated in spinach (Tester and Blatt, 1989; Fang and Berkowitz, 1995; Pottosin and Schönknecht, 1996). Pottosin & Schönknecht (1996) have demonstrated that the dominant cation channel in spinach thylakoid membrane is almost equally permeable to K^+ , Ca^{2+} , and Mg^{2+} ion. These authors have calculated that, considering the relative volume of the stroma and the lumen, Mg^{2+} concentration in the lumen of spinach thylakoids should be in the range of 30–50 mM to account for the observed 2 mM increase in stromal Mg^{2+} levels during illumination. They have even calculated that, considering the abundance and the conductance of the spinach thylakoid cation channel, Mg^{2+} efflux from the lumen through this channel can be itself responsible for the observed increase of about 2 mM in the Mg^{2+} concentration of the stroma.

1.1 Physiological significance of the fluctuations of Mg^{2+} and pH in the stroma and the lumen

A speculation by (Barber, 1976) affirms that the change of stromal Mg^{2+} concentration affects thylakoid stacking and hence the efficiency of energy transfer between photosystems I and II. Mg^{2+} and pH levels were shown to affect also the activity of the thylakoid ATPase complex.

The fluctuations in Mg^{2+} and pH levels also have an important regulatory role on key stromal enzymes. Illuminated chloroplasts accumulate fixed CO_2 in form of starch, which is broken down in the dark to supply the energy needs of the cell. Some of the intermediates of starch synthesis and breakdown are identical. Thus it is essential to ensure that the photosynthetic enzymes of CO_2

reduction would be active only after illumination, to avoid redirection of starch breakdown products into starch synthesis (Berkowitz and Wu, 1993). This is accomplished by the tight regulation of key stromal CO₂ reduction enzymes by pH and Mg²⁺ levels in this compartment. Increased Mg²⁺ levels in the light activate the enzymes fructose 1,6-bisphosphatase (FBPase) and sedoheptulose 1,7-bisphosphatase (SBPase), which contribute to the creation of the CO₂ acceptor Ru5P (Purczeld et al., 1978; Gardemann et al., 1986). This regulation was also found to act in concert with TRX-dependent modulation of FBPase redox state, indicating that both factors are undoubtedly important to control the activity of this enzyme (Gutle et al., 2016). Mg²⁺ also activates the enzyme Rubisco driving the carboxylation of Ru5P resulting in CO₂ fixation (Wang and Portis, 1992). Activation of the enzymes FBPase and Rubisco also requires a high stromal pH of about 8 (Gardemann et al., 1986; Wang and Portis, 1992). As a result of H⁺ sequestration to the lumen in the light, the pH of the stroma reaches a level of about 8, while that of the cytosol remains about 7. Artificial lowering of the stromal pH of illuminated chloroplast eliminates photosynthesis, even when the ΔpH between the stroma and thylakoid is maintained (Enser and Heber, 1980; Werdan et al., 1975). Thus, this high stromal pH is essential for the activity of CO₂ assimilating enzymes.

Chapter 4: The redox regulation of the Calvin Cycle: Cysteine residues, disulfide bonds and other redox post-translational modifications (PTMs)

1. Cysteines and disulfide bonds

Cysteine residues in proteins can be categorized based on a variety of parameters. These parameters include (1) the redox state of the sulfur atom, (2) the molecular geometry of the cysteinyl residue with its bond lengths and angles, (3) the accessibility and environment of the residue within a protein, and (4) the properties as an acid/base or as a nucleophile/electrophile. All these parameters determine the reactivity and therefore affect whether a cysteine has (I) a structural role, (II) acts as a catalyst or (III) as a redox switch.

1. The versatile redox states of the sulfur atom in cysteinyl residues comprise thiyl radicals, thiols, disulfides and sulfenic, sulfinic and sulfonic acids (Figure 5). Thiols and thiyl radicals can be essential for enzyme catalysis, for example, to generate deoxyribonucleotides with the help of ribonucleotide reductases (Jordan and Reichard, 1998; Nordlund and Reichard, 2006). Protein thiols also form intra- or intermolecular disulfide bonds. These can be classified as catalytic or structural disulfides based on their half-life. Short-lived disulfides are usually involved in catalytic redox cycles and are therefore formed *and* broken within milliseconds or seconds. Such catalytic cysteines are, *e.g.*, found in many proteins of the TRX superfamily (Deponate, 2013). In contrast, structural disulfides are formed under partially oxidizing conditions and usually stabilize a protein in a defined tertiary or quaternary structure until the protein is degraded. However, selected structurally relevant disulfide bonds of secreted proteins were shown to be susceptible to reduction, which can result in altered protein conformations and functions (Hogg, 2003; Butera et al., 2014). Philip Hogg therefore introduced the term ‘allosteric disulfides’ to discriminate these bonds from classical structural and catalytic disulfides (Schmidt et al., 2006; Butera et al., 2014). Other non-catalytic and non-structural disulfides with intermediate half-lives and regulatory functions are the redox switches, that include intramolecular disulfide bonds as well as intermolecular disulfide bonds between proteins or between a protein and a low molecular weight compound such as glutathione (Mieyal et al., 2008; Brigelius-Flohé and Flohé, 2011; Deponate, 2013).

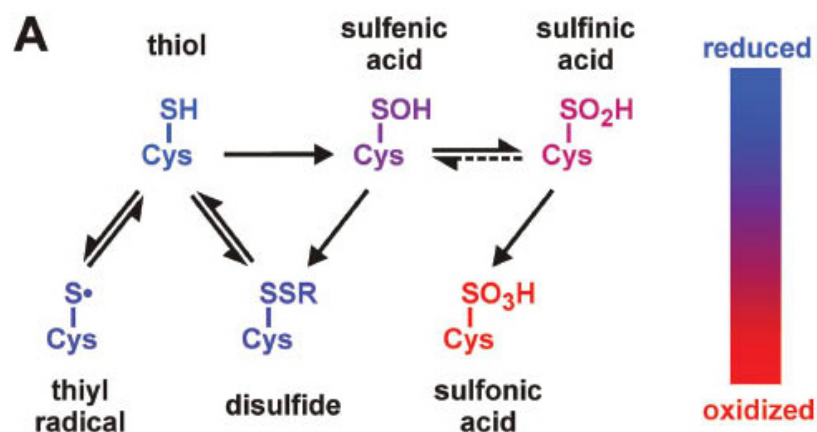


Figure 5. Common cysteinyl redox states in proteins and their reversible or irreversible interconversion.

2. The molecular geometry of cysteinyl residues and disulfide bonds includes three classical structural parameters: bond lengths, bond angles between three atoms and dihedral angles between three bonds. The geometry directly affects the reactivity as demonstrated for the TRX-catalyzed

reduction of disulfides (Wiita et al., 2007). A systematic classification of the five dihedral angles between the $C\alpha$ atoms of disulfide-bonded cysteines in annotated protein structures yielded 20 distinct disulfide configurations (Schmidt et al., 2006). Among these configurations, allosteric disulfides were predominantly found to have a minus right-handed staple bond (-RHStaple) (Schmidt et al., 2006). A minus left-handed spiral configuration (LHSpiral) was found for many structural disulfide bonds, and catalytic disulfides in oxidoreductases often have a plus/minus right-handed hook configuration (+/-RHHook), as shown in Figure 6 (Schmidt et al., 2006).

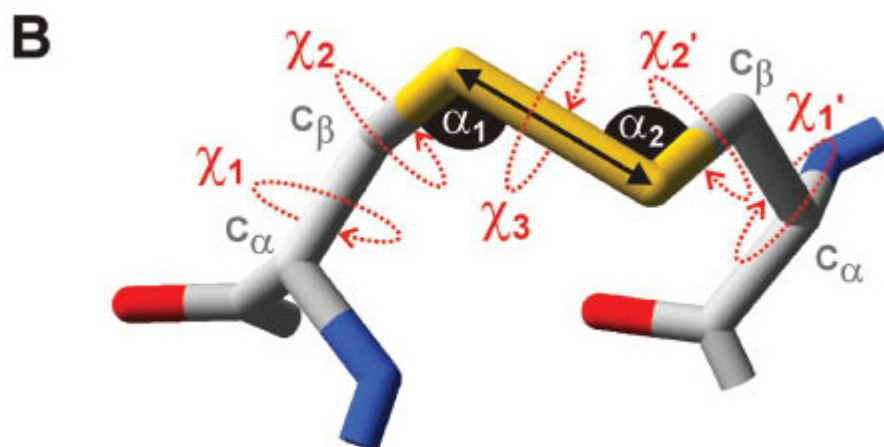


Figure 6. Molecular geometry of a disulfide bond. The shown glutaredoxin disulfide bond adopts a +/-RHHook configuration.

3. and 4. The reactivity and properties of a cysteinyl residue are determined by the accessibility, the position and the environment of the residue within a protein. For example, the -RHStaple bond of allosteric disulfides is often found as a crosslink between antiparallel β -strands (Schmidt et al., 2006). This secondary structure presumably contributes to an activation of the disulfide bond (Zhou et al., 2014) based on a correlation between a stressed molecule geometry and an increase of the redox potential (Baldus and Gräter, 2012). The reactivity of catalytic cysteines, e.g., in enzymes of the TRX superfamily, is analogously influenced by the microenvironment that is generated by neighboring residues (Roos et al., 2009; Hall et al., 2011; Deponte, 2013; Lillig and Berndt, 2013; Van Laer et al., 2014). For example, lowering the pK_a of the thiol group with the help of proton acceptors or via ionic interactions with positively charged residues will not only affect the nucleophilicity of the cysteine but also make it a much better leaving group (Figure 7) (Deponte, 2013; Nagy, 2013). Hence, the formation and the half-life of disulfides can be influenced by the pK_a value and the stability of the corresponding cysteine thiolates. Nevertheless, pK_a values and redox potentials are irrelevant for redox switches as long as the cysteinyl side chain is inaccessible for an interacting redox agent. But even accessibility is not enough, because the kinetics of a productive interaction with a redox agent depends on a correct reaction geometry, in particular with regard to the transition state (Figure 7; Deponte, 2013; Nagy, 2013). Correct reaction geometries, together with complementary surfaces for signal molecules and interacting partners, are therefore crucial parameters for the specificity of thiol switches.

Taken together, redox switches should be accessible, have intermediate half-lives and sufficient reactivity. These parameters as well as the specificity of thiol switches are determined by the protein environment, resulting in activated molecular geometries as well as appropriate redox potentials, pK_a values and complementary surfaces.

There are two major dilemmas for the prediction of redox switches. First, redox switching is often coupled to significant conformational changes (Choi et al., 2001; Wood et al., 2004; Hall et al.,

2011; Nishii et al., 2015) and it is therefore difficult to predict the properties of a specific residue in the absence of structures that reflect the whole reaction pathway. Second, even for proteins that are structurally and functionally well-characterized, we often do not really understand the complex cysteine interactions at an atomistic level. Future studies will not only have to employ a quantum mechanical approach to precisely characterize the reactivity of the sulfur atoms, but will also have to take into account the protein environment and its alteration during signal sensing and transduction.

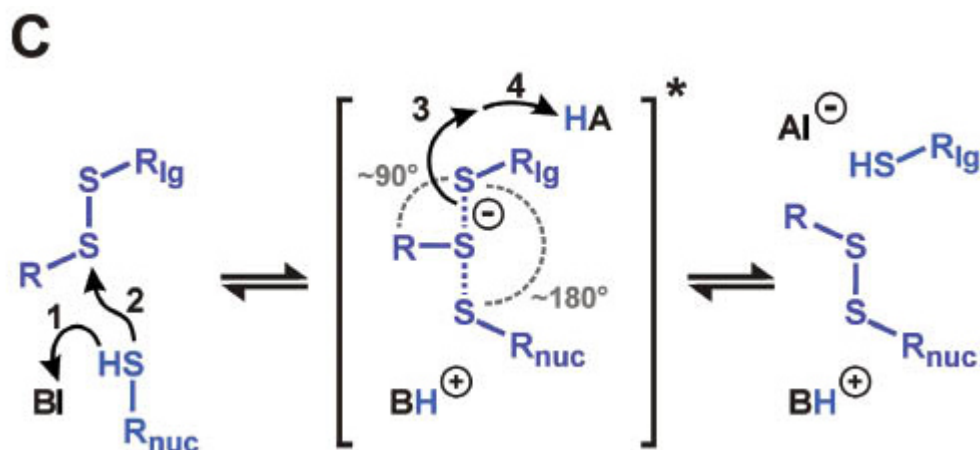


Figure 7. General mechanism of a thiol-disulfide exchange reaction with a trigonal bipyramidal transition state. Whether the nucleophile $R_{nuc}\text{-S}^-$ is deprotonated (step 1) before or during the nucleophilic attack (step 2) depends on the thiol pK_a and the environment of the reaction partners. Analogously, the liberation of the leaving group $R_{lg}\text{-S}^-$ (step 3) might be independent or coupled to a protonation (step 4).

2. The role of the thioredoxins

The majority of enzymes catalyzing thiol-disulfide exchange reactions belongs to the TRX superfamily. TRXs can both form and disrupt disulfide bridges. All the redoxins (RX) rely on cysteinyl residues in a Cys-X-X-Cys/Ser active site motif. TRXs and most of the glutaredoxins (GRXs) that contain in both active site cysteinyl residues reduce protein disulfides using a so-called dithiol mechanism (Hashemi et al., 2007; Deponate, 2013; Scütte et al., 2013). The first step is a nucleophilic attack of the N-terminal cysteinyl residue of the redoxin in its deprotonated thiolate form on the target disulfide, resulting in an intermolecular disulfide between the N-terminal cysteinyl residue and the attacked target cysteinyl side chain in RX. This intermediate disulfide is immediately attacked by the C-terminal thiol(ate) of the redoxin active site, releasing the reduced target dithiol and leaving a disulfide at the active site of the redoxin (Figure 8).

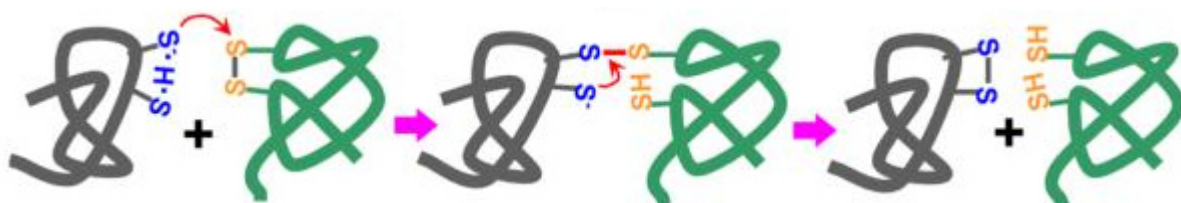


Figure 8. Catalytic mechanism of a standard thioredoxin (in grey). The attacking Cys is shown as thiolate (S^- , in blue), stabilized by hydrogen bond with the second Cys. A transient intermolecular disulfide bond (in red) is formed with a cysteine (in yellow) of the target protein (in green) during the reaction. The second Cys in the thiol oxidoreductase attacks this intermolecular disulfide forming a disulfide with the catalytic Cys, releasing the reduced substrate (figure from Fomenko et al., 2008).

The TRX disulfide is subsequently reduced in a very similar thiol-disulfide exchange reaction by thioredoxin reductase (TRX-R), whereas the GRX disulfide is reduced in two steps by reduced glutathione (GSH). In the first step a mixed disulfide between GSH and the N-terminal active site cysteinyl residue of GRX is formed. In the second step the glutathionylated GRX is reduced by a second molecule of GSH, yielding reduced GRX and oxidized glutathione (GSSG).

The classification of the TRXs, based on their cellular localization and sequence omology, has identified 15 subgroups (Meyer et al., 2012). In the chloroplasts, five types of TRXs are present (*f*, *m*, *x*, *y* and *z*), whereas in the cytosol and in the mitochondria, there are two different TRXs - named TRX-*h* (heteroplasmic) and TRX-*o* (*organellar*), respectively. Phylogenetic analysis on plastidial TRXs have shown that while TRX *m*, *x*, *y* and *z* are of prokaryotic origin (Sahrawy et al., 1996; Arsova et al., 2010), TRX-*f* is closely related to eukaryotic TRXs (Sahrawy et al., 1996; Issakidis-Bourguet et al., 2001). The diversification of the plastidial TRXs seems to reflect the complexity of the chloroplastic redox network: in *Chlamydomonas*, recent proteomic studies identified two *f*, one *m*, *x*, *y* and *z* (Michelet et al., 2013).

According to the present literature, three TRXs functional categories can be inferred (Figure 9). The first subset, related to photosynthesis and carbon metabolism, would be composed of the TRXs *f* and *m* isoforms, coupling light and redox-signaling pathways (Michelet et al., 2013).

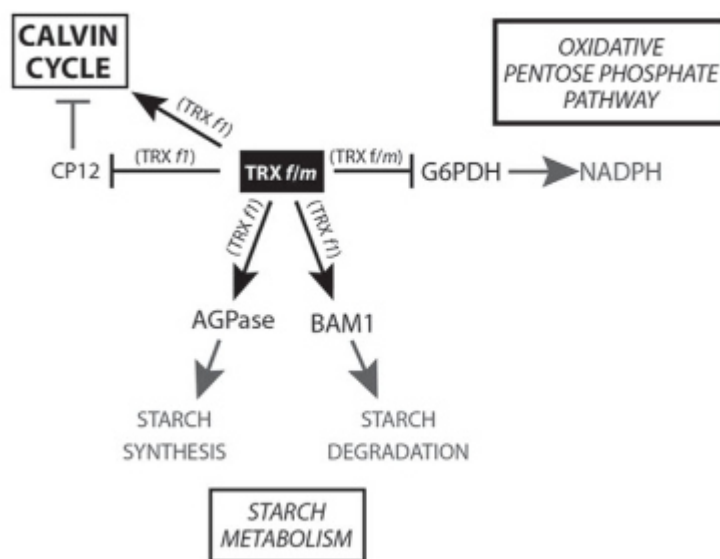


Figure 9. Interactions of the TRXs *f*- and *m*-type with other proteins and pathways.

In the second subgroup, we could find the *x*- and *y*-type TRXs (Figure 10), basically involved in ROS detoxification and taking part of the complex redox-signaling network regulating plant development. The last subcategory, connected to the regulation of photosynthesis-related transcription in chloroplasts, would be composed of only the TRX-*z*. Intriguingly, TRXs *f* and *m* can efficiently reduce the TRX-*z*: for this reason, we can affirm that *f*- and *m*-type isoforms, in addition to regulate the photosynthesis-linked processes, could also act as indirect regulators of the plastidial transcription (Michelet et al., 2013).

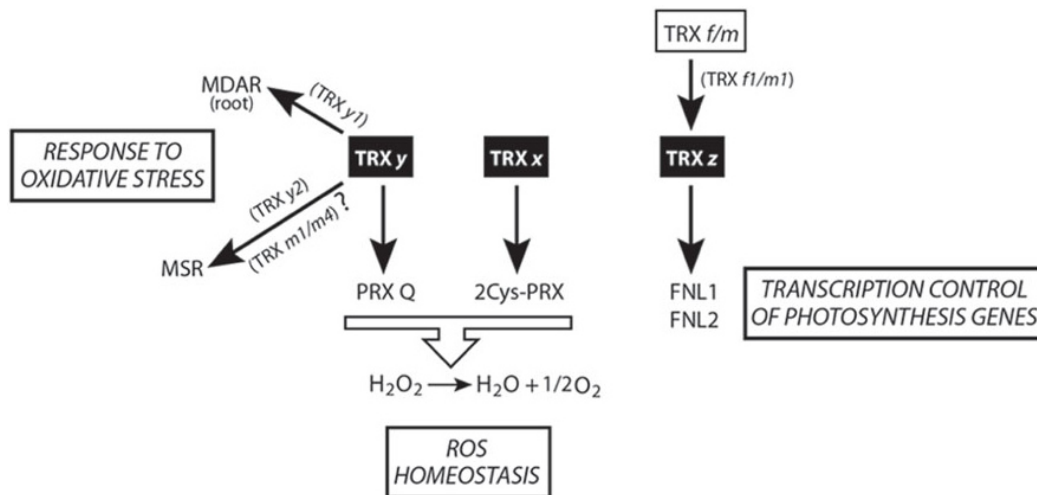


Figure 10. Interactions of the TRXs x-, y- and z-type with other proteins and pathways.

3. Other Redox Post-translational modifications (PTMs)

Due to their unique physico-chemical properties, cysteinyl residues participate in catalytic reactions, serve as metal ligands and are also susceptible to various PTMs. Whereas free cysteines have an ionization constant (pKa) of about 8.3, in proteins, some cysteines defined as reactive cysteines, possess lower pKa, ranging from 3 to 7 (Couturier et al., 2013). In TRXs and GRXs, the lowering of the pKa results, as already mentioned above, from the protein microenvironment as these thiolates are stabilized by proximal positively charged amino acids, by specific hydrogen bonding and/or by a dipole effect induced at the N-terminus of an α -helix. This implies that, at physiological pH, these residues will be predominantly found as thiolates, which are much stronger nucleophiles than thiol groups. Consequently, proteins containing these reactive cysteines can undergo many different oxidation states in response to different redox signals (Couturier et al., 2013). It is for instance not yet clear which protein properties favor one modification respect to another, but the local protein environment and the proximity to the oxidant source may be important. In these last years, a special importance was conceded to protein thiol groups modified via H₂O₂, •NO, and H₂S: the main reason lies in the fact that these three molecules, which were initially thought to be exclusively toxic, may in fact represent key regulators for various biological processes and in particular for signaling purposes, considering their relative stability, their capacity to diffuse across membranes (•NO and H₂S are gases and the uncharged H₂O₂ is channeled via aquaporins) and their propensity to react with thiolates (Bienert et al., 2007).

3.1 H₂O₂-mediated modifications of protein thiols

Together with methionines, cysteines are the most H₂O₂-sensitive residues. The two-electron oxidation of a cysteine thiolate (-S⁻) by H₂O₂ forms a sulfenic acid (-SOH; Figure 11 and 5). Due to its unstable and highly reactive nature, the sulfenic acid will be further modified (Reddie and Carroll, 2008). In the absence of other proximal thiolates, sulfenic acid can further react with one or two additional peroxides, forming sulfinic (-SO₂H) and sulfonic (-SO₃H) acids (Figure 11). These two modifications are usually considered as irreversible reactions, except for the SO₂H in the specific case of the peroxiredoxin (PRX) catalytic cycle. Alternatively, sulfenic acids can react with the main chain nitrogen of a neighboring residue to form a sulfenyl-amide or condensate with another sulfenic acid leading to thiosulfinate, but the physiological relevance of these

possibility would be the transfer of haem-bound NO to a free thiol group. Once formed *de novo*, another physiologically relevant mechanism for S-nitrosothiol formation is trans-nitrosylation, *i.e.*, the transfer of an NO moiety from a S-nitrosylated protein to another (Kovacs and Lindermayr, 2013). Incidentally, the NO moiety can also be transferred to glutathione forming nitrosogluthione, a possible transport and/or reservoir form (Lee et al., 2008). In support of an important role of nitrosogluthione in plants, mutants for the nitrosogluthione reductase gene exhibit important growth defects and modified responses to abiotic and biotic constraints (Feechan et al., 2005; Lee et al., 2008; Lee et al., 2012).

3.3 H₂S-mediated modification of protein thiols

The involvement of H₂S as a signaling molecule is emerging both in plants and animals. Like •NO, H₂S can play regulatory roles and modulates protein activity by binding to some protein haems. Besides, H₂S can promote the formation of persulfide groups, a process known as S-sulfhydration, through several potential mechanisms. H₂S could perform a nucleophilic attack on oxidized protein cysteine residues either as sulfenic acid, disulfide bond or glutathione adducts (Finkel, 2002). Another possibility is that the sulfenyl-amide intermediate, as shown for human protein tyrosine phosphatase 1B (PTP1B), can also react with H₂S, the resulting persulfide being reduced by TRX (Salmeen et al., 2003). These reaction mechanisms are uncertain considering that H₂S is a poor reductant compared to glutathione and that it is also less abundant and reactive. Another potential mechanism involves oxidation of H₂S into H₂S₂ by reaction with ROS and subsequent nucleophilic attack by a protein thiolate. Similarly to trans-nitrosylation, S-sulfhydryls could eventually react with another thiol, forming either a disulfide or more likely transferring its sulfur to an acceptor protein in a trans-sulfhydration reaction (Papenbrock et al., 2011).

3.4 S-Glutathionylation

Glutathione is the major low molecular weight antioxidant in most cells and exists in the reduced (GSH) and oxidized (GSSG) forms. GSH is the major form due to constant reduction of GSSG to GSH by glutathione reductase (GR) using NADPH. In plants, glutathione is considered as a major cellular antioxidant and redox buffer but also plays an important role in a myriad of cellular and physiological functions including detoxification of heavy metals and xenobiotics, root growth or pathogen responses (Noctor et al., 2012). Glutathionylation is a post-translational modification triggered by oxidative stress conditions and consisting of the formation of a mixed-disulfide between a protein free thiol and the thiol of a molecule of glutathione. Although the precise mechanism leading to glutathionylation is still unclear *in vivo*, it is considered to occur mainly either through reactive oxygen species (ROS)-dependent sulfenic acid formation followed by reaction with reduced glutathione (GSH) or by thiol/disulfide exchange with oxidized glutathione (GSSG). The reverse reaction, named deglutathionylation, is mainly catalyzed by GRXs (Couto et al., 2016).

4. Proteomic identifications of disulfide bonds and other redox PTMs

While the identification of reactive cysteines is crucial for understanding protein function and regulation, there is no universal signature allowing their recognition. Analyses based on the strict conservation of cysteines between homologous proteins (in particular in CxxC/S motifs), or their replacement by seleno-cysteines in orthologs found in some organisms, often proved to be valuable. However, it neither provides an exhaustive list of proteins containing these reactive cysteines nor indicates which redox PTMs exist in a cellular context and how large proportion of a reactive cysteine is modified.

Thus, besides computational and biochemical approaches using purified recombinant proteins, many gel-based or gel-free wide-scale proteomic approaches have been designed to identify reactive cysteines and associated redox PTMs from complex protein extracts. A direct proteomic method to detect proteins with disulfide bonds and called Redox 2D-PAGE or diagonal SDS-PAGE is based on the differential migration of proteins containing intra- or intermolecular disulfides under non-reducing (first dimension) and reducing (second dimension) conditions (Cumming, 2008). In this second dimension, proteins without disulfide bonds will lie in a diagonal line on the 2D gel, whereas proteins with inter- or intra-molecular disulfide bonds will migrate below or above this diagonal.

Alternatively, assuming that disulfide bonds are preferentially reduced by TRXs, the identification of TRXs targets was thought to constitute a good representative, although non-exhaustive, list of disulfide bond-containing proteins. Hundreds of putative plant TRXs target proteins (Montrichard et al., 2009) have been isolated using affinity chromatography columns with mutated immobilized TRXs in order to “freeze” a covalent interaction with their targets or using thiol labeling after TRXs reduction (Hisabori et al., 2005). With the observation that some TRXs can reduce sulfenic acids, S-nitrosothiols, glutathionylated and sulfhydrated cysteines and could promote trans-nitrosylation reactions, this approach may have detected most reversible redox PTMs (Mitchell and Marletta, 2005; Benhar et al., 2008).

Most of the current methods designed to detect reactive cysteines and redox PTMs are indirect and are based on the differential alkylation of reduced and oxidized thiols. They require an initial step of thiol alkylation of free unreactive cysteines using generally N-ethylmaleimide (NEM) or iodoacetamide (IAM) for irreversible modifications or MMTS (methyl methanethiosulfonate) for reversible modifications. In a second step, the various types of PTMs are reduced by general tris(2-carboxyethyl)phosphine, dithiothreitol (TCEP, DTT) or specific chemical compounds or enzymes (Leonard and Carroll, 2011). Finally, nascent thiols are labeled by derivation with biotinylated- or fluorescent- forms of these alkylating reagents (Figure 12). The biotinylated proteins are recovered on avidin columns and identified preferentially using a gel-free method by LC-MS-MS. More recently, quantitative thiol trapping techniques (namely OxICAT, isotope-coded affinity tag for the identification of Oxidized cysteines; isoTOP-ABPP, isotopic tandem orthogonal proteolysis–activity-based protein profiling), essentially based on the use of isotopic light ¹²C- and heavy ¹³C-forms of IAM, have been developed to identify the site(s) of modifications and assess the degree of modification and reactivity (Hagglund et al., 2008; Leichert et al., 2008; Weerapana et al., 2010). For sulfenic acids, reduction was initially achieved through arsenite, but other probes derived from dimedone, namely DAz-2 and DYn-2, have recently been engineered (Roos and Messens, 2011). For S-glutathionylated and S-nitrosylated proteins, reduction is usually performed using GRXs and ascorbate, respectively. The latter strategy was called biotin switch method (Jaffrey and Snyder, 2001).

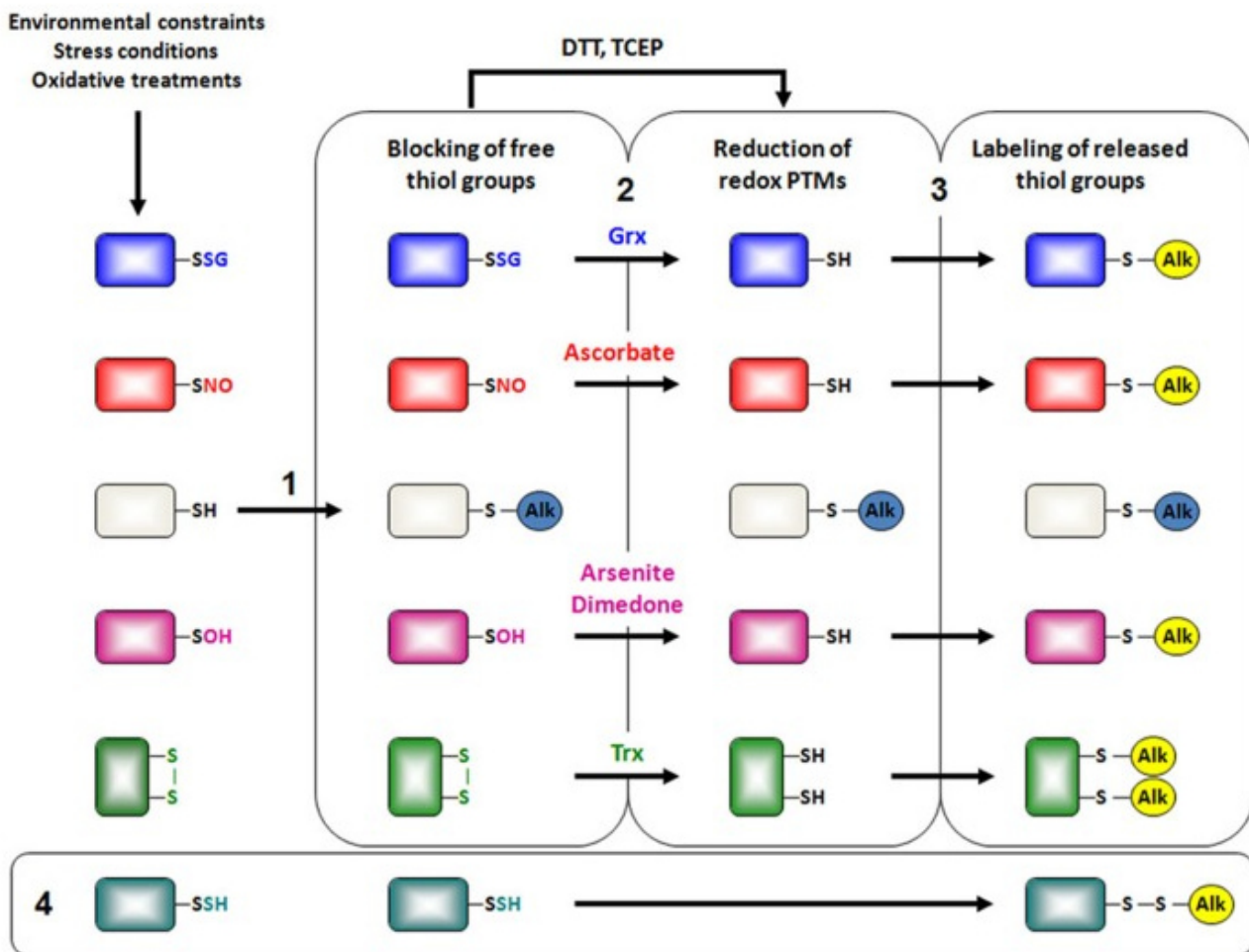


Figure 12. Indirect chemical detection of redox PTMs by proteomics. Besides the wish for detecting basal redox PTMs, experiments are usually designed to assess *in vivo* redox changes after applying an oxidative stress treatment. Most current approaches to detect redox PTMs rely on the same three-step strategy. The first step consists of blocking free thiol groups with alkylating agents such as *N*-ethylmaleimide (NEM), iodoacetamide (IAM) and its isotopically light ^{12}C - derivative or methyl methanethiosulfonate (MMTS) (1). The second step consists of the reduction of reversibly oxidized cysteine residues (2). General reductants as dithiothreitol (DTT) or Tris(2-carboxyethyl)phosphine hydrochloride (TCEP) are used to identify all types of oxidized cysteines. In contrast, selective chemical agents (ascorbate, arsenite, dimedone) or enzymes (glutaredoxins, thioredoxins) are used for the reduction of specific redox PTMs. Finally, the third step corresponds to the labeling of liberated thiol groups by reaction with biotinylated-, fluorescent- or isotopically heavy ^{13}C -derivatives of alkylating reagents mentioned previously, keeping in mind that fluorescent reagents are rather devoted to the detection of modified proteins, whereas biotinylated reagents are devoted to protein enrichment for subsequent mass spectrometry analyses (3). Persulfide groups could be detected without the reduction step if MMTS is used for the first alkylation step (4).

The proteins identified through these different methods show only partial overlap, indicating that a significant portion of modifications is specific, being dependent on the protein local environment and/or on the applied oxidizing conditions. Long lists of plant proteins undergoing various redox PTMs, especially glutathionylation and nitrosylation, and involved in other cellular processes were published a few years ago (Astier et al., 2012; Zaffagnini et al., 2012a and b).

All these methods are usually subject to the same limitations. Alkylation, reduction and labeling are usually performed on cell lysates and though protein extraction is performed using acidic or sometimes anaerobic conditions, it does not entirely preclude that modifications of the cysteine redox state occur during the procedure or that the modifications are insufficiently trapped. To circumvent this problem, cell permeable probes were developed, in particular for sulfenic acids

(Leonard and Carroll, 2011). An other major drawback of such studies concerns the specificity of a given reductant for a given PTM (Wang and Xian, 2011). This will clearly need to be addressed in the future. Moreover, protein abundance is often a limiting factor, mostly for gel-based methods. Possibilities to solve this problem are to perform pre-fractionation or to use biotin affinity for avidin in order to increase the amount of modified proteins and decrease complexity of the sample. Another very important question that often remains unanswered is to determine the site of modification and to what extent a given cysteine is modified. Answering this question requires ICAT-derived gel-free strategies that were used only in rare cases (Hagglund et al., 2008; Leichert et al., 2008).

4.1 Bioinformatic tools for studying disulfide bonds: Molecular Dynamics (MD) simulation

Some early computational studies on disulfide bond properties have been limited to small systems with often only tens to hundreds of atoms, where Density Functional Theory (DFT) or Car–Parrinello Molecular Dynamics (CPMD) and QM/MM methods have been employed to investigate potential reaction pathways (Fernandes and Ramos, 2004; Hofbauer and Frank, 2010). Studying disulfide bond dynamics beyond the single molecule level remains a computational challenge, due to the prohibitive cost of quantum calculations. As a result, efficient interatomic MD force fields are in demand to extend the length and time-scale of simulations involving chemical reactions. Scientists have recently reported progress in addressing this challenge for proteins using molecular dynamics simulations with the ReaxFF reactive force field (Keten et al., 2012). ReaxFF is derived from first-principles calculations and is capable of modelling chemical reactions (including transition states during reactions, changes in bond order, charge equilibration) while retaining computational efficiency, which has been previously demonstrated for a variety of reactive systems including oxidation of hydrocarbons, silicon fracture and catalysis of carbon nanotube formation (Nielson et al., 2005). Keten et al. (2012) considered a simple model system consisting of two cysteine amino acids covalently linked by a single disulfide bond to gain a fundamental insight into the nanomechanics of disulfide bonds in proteins under varied chemical and physical conditions. In the Figure 13, (A) and (B) show the general molecular setup and simulation protocol. As depicted in (C), reactions are explored by using a variable biasing potential that tethers the hydrogen atoms to the sulfur atoms to enhance the sampling of reactions (Bonomi and Parrinello, 2010). All simulations are carried out in a periodic box of water with explicit solvent, as shown in (D) in a system containing about 1000 fully reactive protein and water solvent atoms, to capture solvent effects (hydrophobicity, viscosity, screening, possible reactions etc.) accurately.

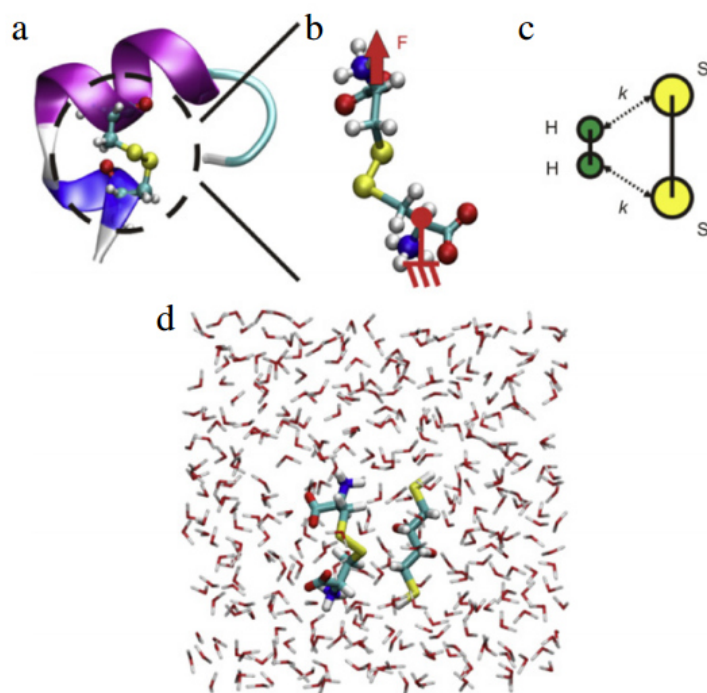


Figure 13. Schematic views illustrating the simulation setup. The disulfide bond model is taken from a small protein (Protein Data Bank identification code 1AKG) shown in panel A. Steered Molecular Dynamics simulations are carried out, where one of the amino acids is fixed and the other is pulled at the alpha-carbon atom as depicted in panel B. Panel C shows the method for inducing reactions. To induce a reducing potential, hydrogen atoms (in the schematic shown as a hydrogen molecule) are tethered towards the S–S bond with a harmonic bias potential, thereby sampling the reaction at a shorter time-scale accessible to Molecular Dynamics. Panel D shows the overall system solvated in an explicit water box (approximately 1000 atoms) with periodic boundary conditions.

Chapter 5: The transketolase

1. General features

Studies of thiamine pyrophosphate (TPP)-dependent enzymes have commenced in 1937, with the isolation of the coenzyme of the yeast pyruvate decarboxylase, which was demonstrated to be a diphosphoric ester of thiamine. For quite a long time, these studies were largely focused on enzymes decarboxylating keto acids, such as pyruvate decarboxylase and pyruvate dehydrogenase complexes. The transketolase, discovered independently by Racker and Horecker in 1953 (and named by Racker) (Horecker et al., 2002), did not receive much attention until 1992, when crystal X-ray structure analysis of the enzyme from *Saccharomyces cerevisiae* was obtained (Lindqvist et al., 1992).

The transketolase (TK or TKT, EC 2.2.1.1.) is an enzyme catalyzing cleavage of ketoses (donor substrates) and subsequent transfer of a two-carbon fragment thus formed (glycolaldehyde residue) onto aldoses (acceptor substrates) (Figure 14).

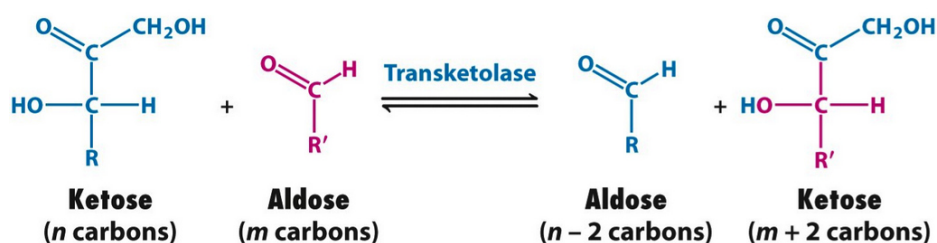


Figure 14. Standard reaction of TK. The double arrow indicates the reversibility of the reaction.

D-xylulose 5-phosphate (X5P), fructose 6-phosphate (F6P), sedoheptulose 7-phosphate (S7P) and L-erythrulose are typical donor substrates of TK (they are ketoses containing hydroxyl groups at C3 and C4 positions in *trans* conformation), while glyceraldehyde 3-phosphate (G3P), D-ribose 5-phosphate (R5P) and D-erythrose 4-phosphate (E4P) are typical acceptor substrates of TK. Reactions are reversible, with the sole exception of cases where hydroxypyruvate (HPA) is used as substrate (Kochetov et al., 1982; Schenk et al., 1998; Horecker et al., 2002). The enzyme exhibits little specificity towards the length of the carbon chain, but the presence of the phosphate group in the substrate molecule significantly increases the affinity of the substrate to the enzyme (Kochetov et al., 1982).

TK is a key enzyme in the non-oxidative branch of the pentose phosphate pathway (PPP) in every organisms and it is involved in the photosynthetic Calvin cycle in plants and autotrophic bacteria. It catalyzes two important reactions, which operate in opposite directions in these two pathways. In the first reaction of PPP, the cofactor TPP accepts a 2-carbon fragment from a 5-carbon ketose (X5P), then transfers this fragment to a 5-carbon aldose (R5P) to form a 7-carbon ketose (S7P). The abstraction of two carbons from X5P yields the 3-carbon aldose G3P. In the Calvin cycle, TK catalyzes the reverse reaction, the conversion of S7P and G3P to pentoses, the aldose R5P and the ketose X5P (Figure 15) (Horecker et al., 2002).

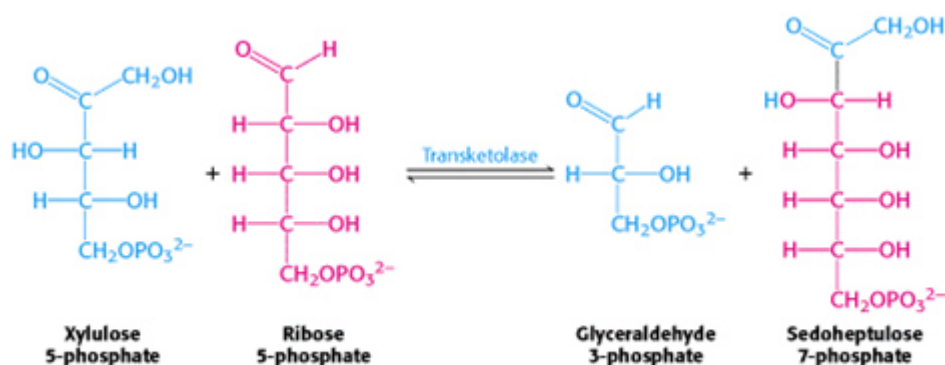


Figure 15. First TK-catalyzed reaction in PPP. The double arrow indicates the reversibility of the reaction.

The second reaction catalyzed by TK in the PPP involves the same TPP-mediated transfer of a 2-carbon fragment from X5P to the aldose E4P, generating F6P and G3P. Again, in the Calvin cycle the same reaction occurs exactly in the opposite direction (Figure 16). Moreover, in the Calvin cycle this is the first reaction catalyzed by transketolase, rather than the second (Horecker et al., 2002).



Figure 16. Second TK-catalyzed reaction in PPP. The double arrow indicates the reversibility of the reaction.

In mammals, TK connects the PPP to the glycolysis, routing excess sugar phosphates into the main carbohydrate catabolic pathway. Its presence is necessary for the production of nicotinamide adenine dinucleotide phosphate (NADPH): it provides hydrogen atoms for chemical reactions that result in the production of coenzymes, steroids, fatty acids, aminoacids, glutathione and neurotransmitters. Reduced TK activity interferes with all these essential biochemical pathways (Martin et al., 2003). Alterations in the activity of human TK have been reported to cause and/or accompany different pathological disorders, including the Wernicke-Korsakoff syndrome, Alzheimer disease or diabetes (Hammes et al., 2003). Furthermore, cumulative evidences support the hypothesis that the majority of nucleic acid ribose in cancer cells is provided by the non-oxidative part of the PPP through altered activity of TK and transaldolase (TA).

TKs from different species show a remarkably high degree of sequence similarity (Figure 17). Whereas the bacterial, yeast and plant enzymes comprise about 45–60% identical amino acids, mammalian TKs share less identity with TKs from other organisms (Schenk et al., 1998).

CrTK $\alpha 1$ $\alpha 2$ $\eta 1$
 40 50 60 70 80 90
 CrTK VAQAAPAAKAAAPSIKRDVLRKCTIAFLAIDAVNKAAGRRGRRFNSDAGYGLWNE
 VcTK LAQAAPATAKVDPAISRDVLRKCTIAFLAIDAVNKAAGRRGRRFNSDAGYGLWNE
 CvTKMAKGEIKDKTALAINAFLAIDGVNKAAGRRGRRFNSDAGYGLWNE
 ZnTKGAVEILQGGKAATGDLLEKSVNTFLAIDAVNKAAGRRGRRFNSDAGYGLWNE
 AtTK RPLVRAAAVETVETTTDSSIVDKSVNSFLAIDAVNKAAGRRGRRFNSDAGYGLWNE
 SyTKMVTATGSLDELAINAFLAVDAIKKAAGRRGRRFNSDAGYGLWNE
 ScTKNAQPSDIDKLAVTIRLLSVDQVKAAGRRGRRFNSDAGYGLWNE
 HsTKMESYHKPDDQRLQALVDTANRILSSIQASAAAGRRRTRCCDAGYGLWNE

CrTK $\beta 1$ $\eta 1$ $\alpha 3$ $\alpha 4$ TT
 100 110 120 130 140 150
 CrTK VMKYNFKNFDFNDRFVLSGHSMTQYAMHLSTGDTDFLDGIKQFQWNGDITGRRP
 VcTK VMKYNFKNFDFNDRFVLSGHSMTQYAMHLSTGDTDFLDGIKQFQWNGDITGRRP
 CvTK FMTVDFKDTKFNDRFVLSGHSMLNYLLHLNGDLSIDDLKQFQWNGDITGRRP
 ZnTK VMKYNFKNFDFNDRFVLSGHSMLQYALLHLAGDYSVKEKDLKQFQWNGDITGRRP
 AtTK VMKYNFKNFDFNDRFVLSGHSMLLYALLHLAGDYSVQEDLQFQWNGDITGRRP
 SyTK VMKYNFKNFDFNDRFVLSGHSMLQYALLYLLGDSVTIEDLQFQWNGDITGRRP
 ScTK LRCHFNFDFNDRFVLSGHSMLLYMLHLGDTYTEDLQFQWNGDITGRRP
 HsTK VMKYNFKNFDFNDRFVLSGHSMLLYMLHLGDTYTEDLQFQWNGDITGRRP

CrTK $\alpha 5$ TT $\beta 2$ $\alpha 6$ TT
 160 170 180 190 200 210
 CrTK HFVITFCVEVITGGLGGCNAVGSNAVAALAAAFNKFQVRFVVDHYTVCILGDCMRRG
 VcTK HFVITFCVEVITGGLGGCNAVGSNAVAALAAAFNKFQVRFVVDHYTVCILGDCMRRG
 CvTK HFVITFCVEVITGGLGGCNAVGSNAVAALAAAFNKFQVRFVVDHYTVCILGDCMRRG
 ZnTK HFVITFCVEVITGGLGGCNAVGSNAVAALAAAFNKFQVRFVVDHYTVCILGDCMRRG
 AtTK HFVITFCVEVITGGLGGCNAVGSNAVAALAAAFNKFQVRFVVDHYTVCILGDCMRRG
 SyTK HFVITFCVEVITGGLGGCNAVGSNAVAALAAAFNKFQVRFVVDHYTVCILGDCMRRG
 ScTK HFVITFCVEVITGGLGGCNAVGSNAVAALAAAFNKFQVRFVVDHYTVCILGDCMRRG
 HsTK FHOAFVTVACGLGGCNAACGAYTGRVFDL.....LASYRVVCLGDCMRRG

CrTK $\alpha 7$ $\beta 3$ $\beta 4$ $\beta 5$ $\eta 2$ $\alpha 8$ $\beta 6$ TTT
 220 230 240 250 260 270
 CrTK IESACISASHWGKELALVDRNRISIDGHTDISFTEDVAKRFRALGWVIVHINGN
 VcTK IESACISASHWGKELALVDRNRISIDGHTDISFTEDVAKRFRALGWVIVHINGN
 CvTK IESACISASHWGKELALVDRNRISIDGHTDISFTEDVAKRFRALGWVIVHINGN
 ZnTK IASACISASHWGKELALVDRNRISIDGHTDISFTEDVAKRFRALGWVIVHINGN
 AtTK IESACISASHWGKELALVDRNRISIDGHTDISFTEDVAKRFRALGWVIVHINGN
 SyTK IESACISASHWGKELALVDRNRISIDGHTDISFTEDVAKRFRALGWVIVHINGN
 ScTK VESACISASHWGKELALVDRNRISIDGHTDISFTEDVAKRFRALGWVIVHINGN
 HsTK SYWCMARASISYEDNRVATGIDRLQSDPAPLHQMDIYCRCAFQWVATVDR...

CrTK $\alpha 9$ $\beta 7$ $\eta 3$ $\alpha 10$
 280 290 300 310 320 330
 CrTK DYGGRRAATAGAAVQKDFIIRVSRLLDQCFNFKADSDHGRAPFPIITAAATKRLN
 VcTK DIDGRRAATAGAAVQKDFIIRVSRLLDQCFNFKADSDHGRAPFPIITAAATKRLN
 CvTK DIDGRRAATAGAAVQKDFIIRVSRLLDQCFNFKADSDHGRAPFPIITAAATKRLN
 ZnTK GYDGRRAATKAAVTDNPTIIVKVTIICGCFNFKANGSYHGAALAEKVEATRNKLN
 AtTK GYDGRRAATKAAVTDNPTIIVKVTIICGCFNFKANGSYHGAALAEKVEATRNKLN
 SyTK DLAAAKAAIKAAVTDNPTIIVKVTIICGCFNFKSOTAGHGAALTDVVAATKRLN
 ScTK DMSGSSALERAKLSDKPTIIVKVTIICGCFNFKSOTAGHGAALTDVVAATKRLN
 HsTK ..HSEELCKAFQKQKQPTIIVKVTIICGCFNFKSOTAGHGAALTDVVAATKRLN

CrTK TT $\alpha 11$ $\alpha 12$ $\alpha 13$
 340 350 360 370 380 390
 CrTK P...GDFEYVFDVYDVRGAIKRAEAEANRHKACAEKAKYFKRMAEFELTSCMLP
 VcTK E...YDFEYVFDVYDVRGAIKRAEAEANRHKACAEKAKYFKRMAEFELTSCMLP
 CvTK P...YDFEYVFDVYDVRGAIKRAEAEANRHKACAEKAKYFKRMAEFELTSCMLP
 ZnTK P...YDFEYVFDVYDVRGAIKRAEAEANRHKACAEKAKYFKRMAEFELTSCMLP
 AtTK P...YDFEYVFDVYDVRGAIKRAEAEANRHKACAEKAKYFKRMAEFELTSCMLP
 SyTK D...YDFEYVFDVYDVRGAIKRAEAEANRHKACAEKAKYFKRMAEFELTSCMLP
 ScTK DPKSDFVYFDVYDVRGAIKRAEAEANRHKACAEKAKYFKRMAEFELTSCMLP
 HsTK ..MAKGIHDFEYVFDVYDVRGAIKRAEAEANRHKACAEKAKYFKRMAEFELTSCMLP

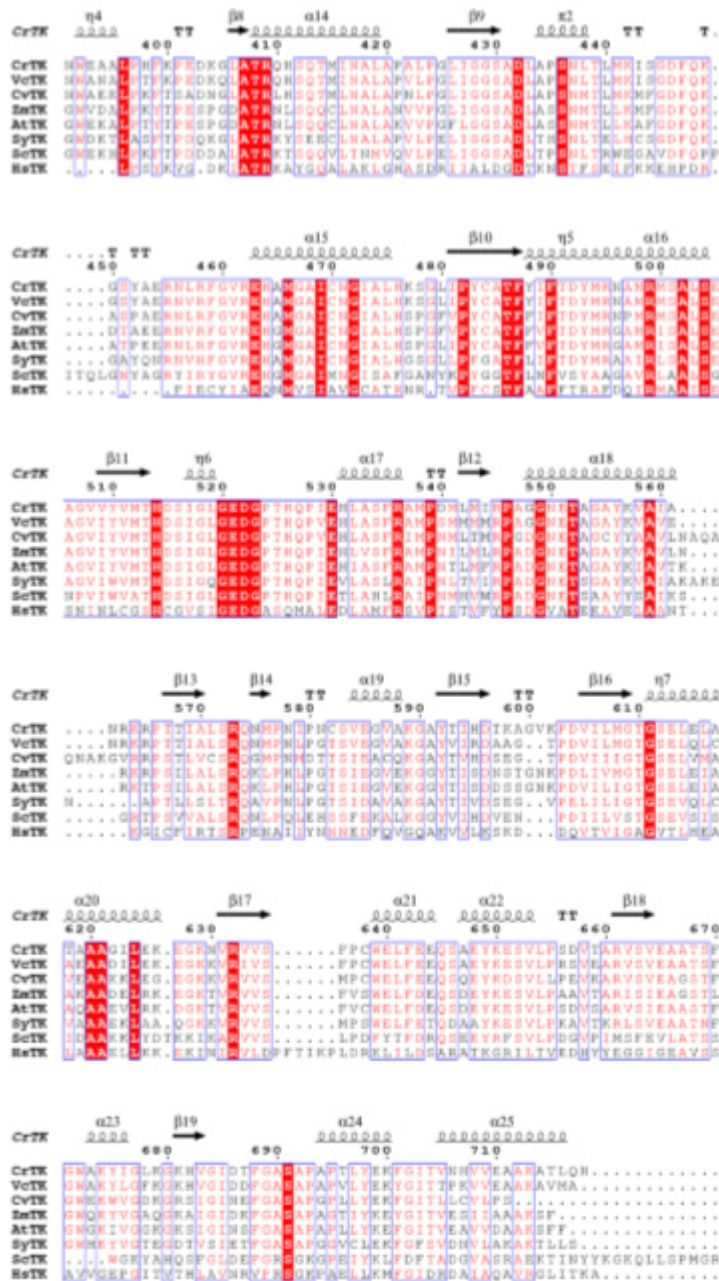


Figure 17. Sequence alignment among *Chlamydomonas reinhardtii* TK (CrTK), *Volvox carteri* TK, *Chlorella variabilis* TK, *Zea Mays* TK, *Arabidopsis thaliana* TK, *Synechocystis sp. (strain PCC 6803)* TK, *Saccharomyces cerevisiae* TK, *Homo Sapiens* TK, using Esprpt 3.0. Numbering corresponds to the mentioned sequences. Identical residues are indicated by a red background, and conserved residues are indicated by red characters. The secondary structure elements of CrTK are shown above the sequences.

2. Enzymatic Structure

TK is a conserved homodimeric protein, and its two active sites are equivalent in terms of their catalytic activities. TPP and bivalent cations, such as Ca^{2+} or Mg^{2+} , function as cofactors (Heinrich et al., 1972). Each subunit, possessing one TPP molecule and one metal ion, comprises three domains: the N-terminal domain (called PP domain since it binds the pyrophosphate moiety of TPP), the middle domain (or Pyr domain since it is bound to the aminopyrimidine ring of TPP), and C-terminal (Figure 18).

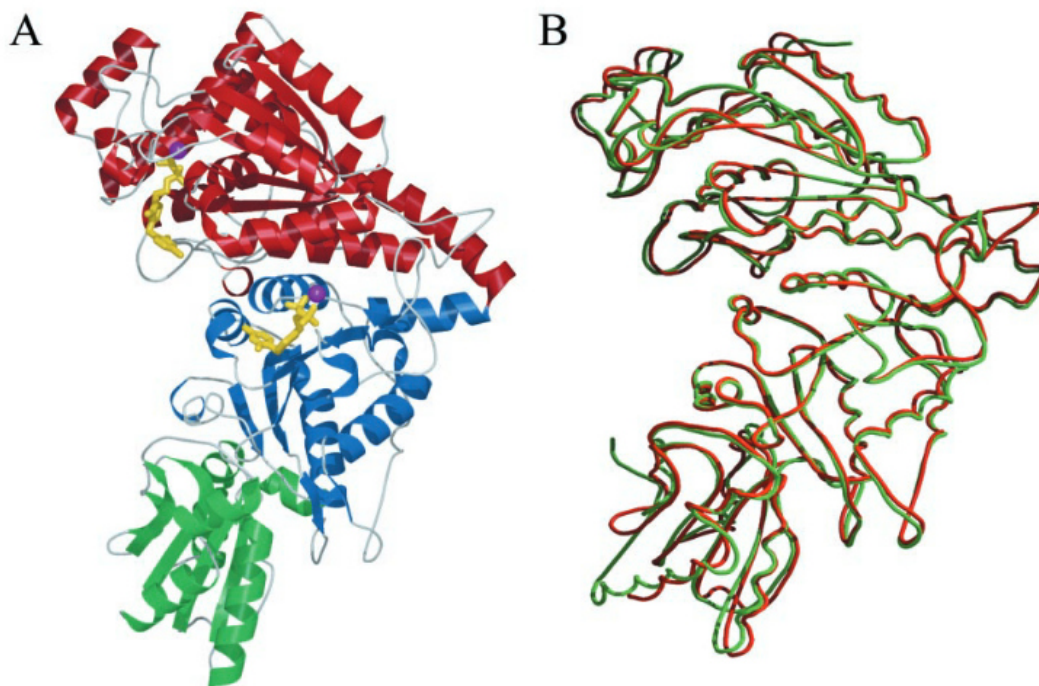


Figure 18. *A) Domain arrangements (red, N-terminal, so-called PP domain; blue, middle domain, therefore called Pyr domain; and green, C-terminal domain) of one maize TK monomer with bound TPP cofactor (yellow) and one Mg^{2+} (purple). B) Superposition of one subunit of TK from maize (red) and yeast (green). Generated by Bobscrip (Esnouf, 1997).*

Binding of TPP involves the PP and Pyr domains of both subunits. In this process, the pyrophosphate moiety of TPP (whose structure is shown in Figure 19) is bound by the PP domain of one subunit, while the aminopyrimidine ring is located in the hydrophobic pocket largely formed by side chains of aromatic aminoacids constituting the Pyr domain of the other subunit (Figure 20). Because the thiazole ring is located in the cleft between PP domains, it interacts with amino acid residues of both subunits (Lindqvist et al., 1992; Nikkola et al., 1994).

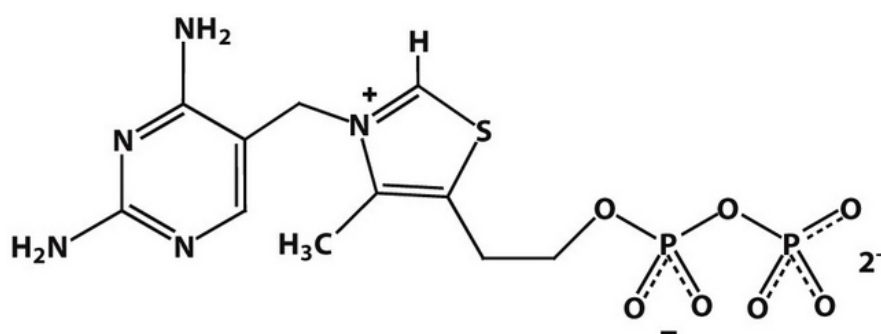


Figure 19. *Molecular structure of TPP: on the left, the amino-pyrimidine ring, in the middle, the thiazole ring and, on the right, the pyrophosphate moiety.*

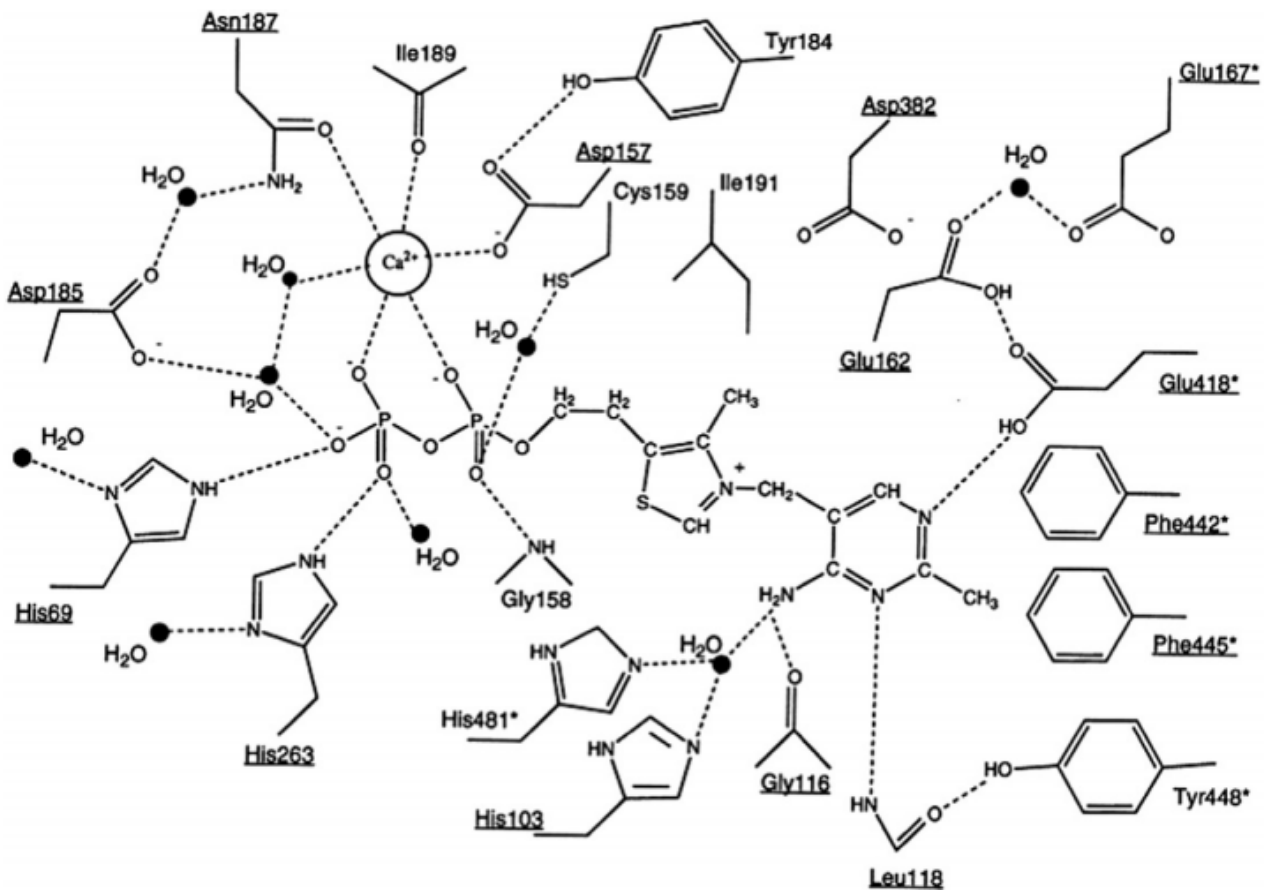


Figure 20. Cofactor–protein interactions in the TPP binding site of yeast transketolase (Schneider et al., 1998) Conserved residues are underlined and residues from the second subunit are marked by *.

Following the interaction with apo-TK, the aminopyrimidine ring of the coenzyme falls into the hydrophobic environment of the active site (Nikkola et al., 1994) and, as a consequence, undergoes conversion from the 4'-aminotautomeric into the N1'H-imminotautomeric form, which is further stabilized via the interaction with Glu-418 (forming a hydrogen bond with the N1'-atom of the aminopyrimidine ring) and Phe-445 residues (Figure 21).

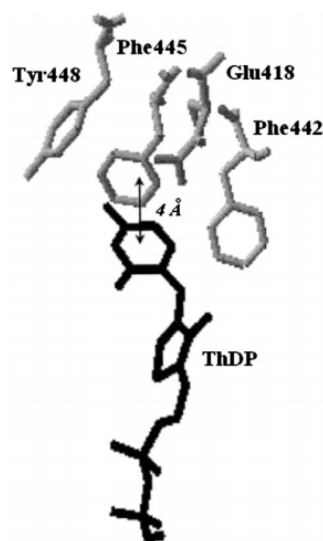


Figure 21. The hydrophobic pocket of the aminopyrimidine ring of ThDP in the yeast holo-TK (Kovina et al., 2002). The double arrow indicates a stacking phenomenon.

These processes account for the appearance of the induced circular dichroism and absorption band (*e.g.*, the optical properties of the coenzyme itself are changed on its embedding into the hydrophobic pocket of the active site) (Kovina et al., 2002). The fast and readily reversible switch between amino and imino tautomeric forms of TPP is critical for the ability of TK to perform its catalytic function (Schellenberger., 1998). The direct involvement of the N1 'H-imino tautomeric form of TPP in the catalytic act is a common feature of all TPP-dependent enzymes, like the pyruvate dehydrogenase (Khailova et al., 1982; Kovina et al., 2004).

2.1 Cofactor-induced optical properties of transketolase

Studying the yeast TK, researchers found that the interaction of TPP with apo-TK is associated with the appearance of a band in its absorption (in the range 285– 370 nm, Figure 22-A) and CD (in the range 300–380 nm; Figure 22-B) spectra. A clear-cut linear relationship between the intensity of this band and the enzymatic activity was observed in addition to apo-TK of different amounts of TPP (Kochetov et al., 1976; Meshalkina et al., 1979). TPP analogs failing to induce such changes in TK spectra were likewise not able to support the catalytic function.

The presence of a donor substrate changes the spectrum of holo-TK in both the region of absorption of the thiazole ring (the amplitude of the peak at 270 nm is decreased) and the longer wavelength end of the spectrum; subsequent addition of an acceptor substrate restores the original appearance of the spectrum (Figure 22-A). Changes in the spectrum (recorded in the presence of the donor substrate) and its restoration (observed on addition of the acceptor substrate) characterize, respectively, the first stage of TK reaction (donor substrate binding and cleavage) and the subsequent transfer of the active glyceraldehyde residue (GA) from DHE-TPP (dihydroxyethyl-TPP) onto the acceptor substrate. The absorption spectrum was also restored in the absence of the acceptor substrate, but the process was considerably slower. In the latter case, the restoration of the spectral properties was created by the cleavage of a GA residue from DHE-TPP and the formation of the holo-enzyme (Kochetov and Izotova, 1973).

Similar phenomena were observed in CD spectra (Figure 22-B). In the presence of a reversibly cleaved substrate (in this case, F6P), the induced absorption band disappeared, whereas, in the presence of an irreversibly cleaved substrate, its inversion was observed. The spectral changes in both cases were created by the formation of DHE-TPP, resulting from donor substrate cleavage. With the irreversibly cleaved substrate, DHE-TPP was formed in both active sites; when the substrate was cleaved reversibly, DHE-TPP formation was restricted to one half of them. Band inversion (characteristic of DHE-TPP formation in both active sites) could also be observed on addition of a reversibly cleaved substrate, if its cleavage is made irreversible (*e.g.*, by removing from the medium the first reaction product) (Solovjeva et al., 2001). The original appearance of the spectrum was restored by the acceptor substrate added subsequently (*e.g.*, after the addition of the donor substrate). GA residue was transferred from DHE-TPP onto the acceptor substrate, restoring the original form of the coenzyme. Addition to holoTK of the acceptor substrate alone caused no spectral changes. The spectral changes described make it possible to study the process of the coenzyme interaction with the apoenzyme and undertake a stepwise exploration of the conversion of the substrates: ketose cleavage with the formation of the intermediate, DHE-TPP (step 1 of TK reaction) and the transfer of the active GA onto the acceptor substrate (step 2 of TK reaction) (Solovjeva et al., 2001).

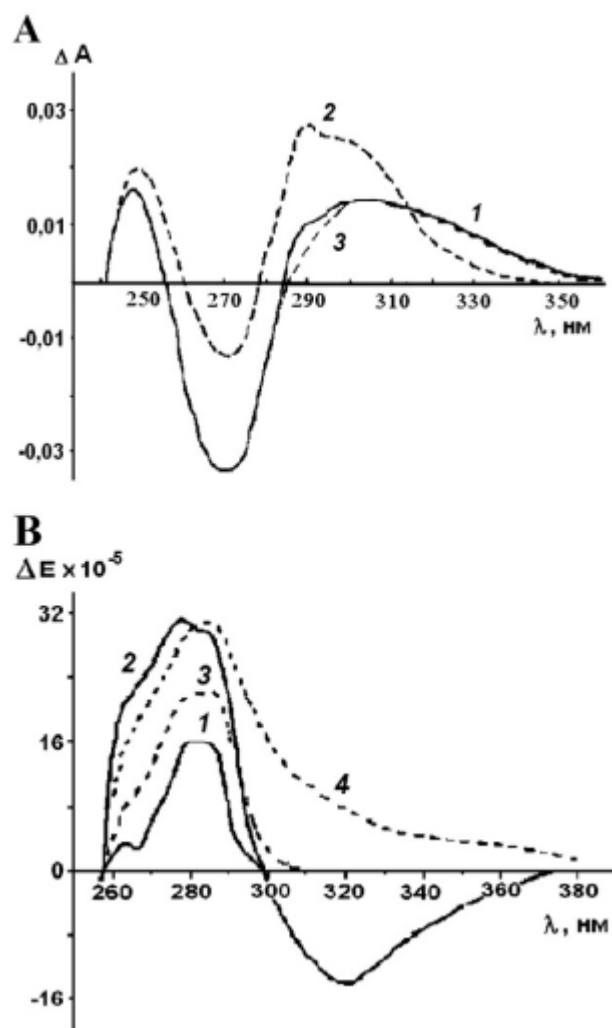


Figure 22. A) Difference absorption spectra of holoTK in the absence (1) and in the presence (2) of the donor substrate, HP; the acceptor substrate, GA is added after the addition of HP (3) (Kochetov et al., 1973). B) CD spectra of TK in the presence of TPP and the substrates: apoTK (1), holoTK (2), holoTK + F6P (3) or HP (4) (Pustynnikov et al., 1986).

Thus, the appearance of an absorption band induced by the coenzyme–apoenzyme binding is indicative of the formation of the active site; changes in its intensity, observed on sequential addition of the donor and acceptor substrates, result from the reaction catalyzed by TK. Changes in the optical activity of holo-TK, associated with substrate binding and cleavage, indicate that the microenvironment of the coenzyme (e.g., mutual orientation of the coenzyme, the substrates, and the functional groups of the apoprotein within the active site) is altered in the course of the catalytic act. In aqueous solutions, TPP is largely present in an amino form (I in Figure 23), which lacks absorption bands in the near-UV range (Kovina et al., 2002).

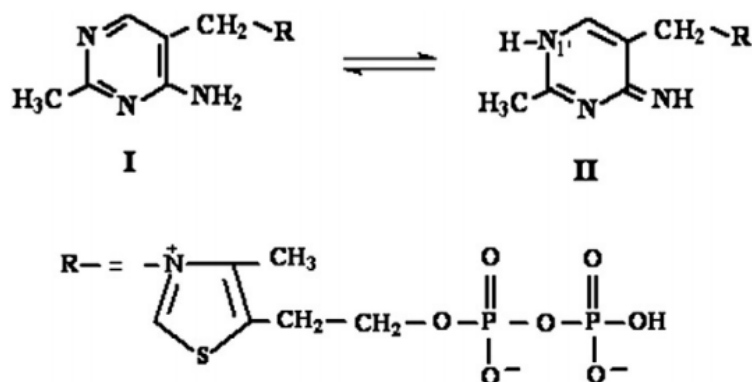
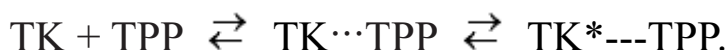


Figure 23. Amino (I) and imino (II) forms of the TPP molecule.

3. Kinetic mechanism

TPP is bound by the apo-form of the TK in at least two stages, as reported in (Kochetov et al., 1973). The first stage, which is fast and readily reversible, results in the formation of a catalytically inactive intermediate, the coenzyme-protein complex $\text{TK}\cdots\text{TPP}$. The catalytically active holoenzyme $\text{TK}^*\text{---TPP}$ is formed at the second stage (slower than the first one), associated with changes in the protein conformation:



The structures of the apo- and holo-TK differ in the position of two loops: in apoTK, loops are unordered and characterized by high mobility; in holoTK, they are ordered and directly contact the TPP (Sundstrom et al., 1992; Nikkola et al., 1994). It is possible that the interdependent antiphase motion of these loops determines the interchangeable destabilization of the secondary complexes ($\text{TK}^*\text{---TPP}$) between the active centers of TK and the coenzyme (Kovina and Kochetov, 1998).

According to X-ray data, the original structures of both TK active centers are equivalent (Lindqvist et al., 1992; Nikkola et al., 1994). Scatchard and Hill plots of TPP binding curves show negative cooperativity of the active centers in TPP binding in yeast TK (at least in the presence of Ca^{2+}) (Egan and Sable, 1981; Kochetov et al., 1975). Thus, the initially identical TK active centers become non-equivalent in the course of TPP binding. In yeast TK, the affinity of both TK active centers towards TPP is higher in the presence of Ca^{2+} than in the presence of Mg^{2+} ; however, with either cation TPP binding exhibits the negative cooperativity, albeit with Mg^{2+} it is less pronounced (Selivanov et al., 2003) and is distinctly revealed only in the presence of donor substrate (Esakova et al., 2004).

In Figure 24, it is considered the cooperative interaction of two originally identical active centers of apo-TK in the two-step mechanism of TPP binding (Kovina et al., 1997). The non-equivalence of the active centers towards coenzyme binding was due to an increase of the reverse conformational transition rate constants for the second active center (k_{-3}) compared to that of the first one (k_{-1}). Thus non-equivalence of the active centers within the holo-dimer results from conformational instability of one of them. In other words, there is no cooperative interaction between the active centers until the TPP binding is completed in both of them. After that, a destabilization of the secondary complex occurs in one of the centers. The destabilization is reversible and can take place in either of the two active centers with equal probability (Kovina et al., 1997).

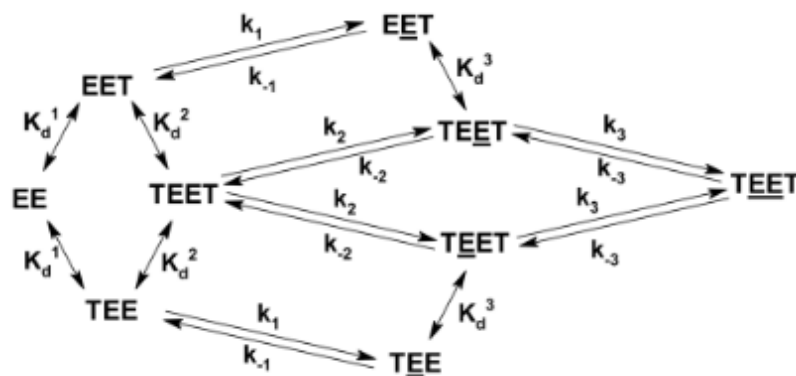


Figure 24. TPP interaction with apoTK. E is the apoenzyme's active center; T is the TPP; ET is the primary, readily dissociating, catalytically inactive complex of apoTK with TPP; ET and TEET are the holoenzymes, catalytically active at one and both active centers, respectively; K_d^1 , K_d^2 and K_d^3 are the dissociation constants for the primary apoTK complexes with ThDP; k_i and k_{-i} ($i=1,2,3$) are the rate constants of the forward and reverse conformational transition reactions for the different enzyme species (from Kochetov and Solovjeva, 2014).

TK substrates are embedded into a deep, narrow channel, spanning the molecule from the surface of the apoprotein to the second carbon atom of the thiazole ring of the coenzyme (Nilsson et al., 1997). The channel is so tight that it cannot accommodate the donor substrate and the acceptor substrate at the same time. They approach the active site alternately, in accordance with the kinetic ping-pong mechanism. Figure 25 shows the model of the interaction of a donor substrate (in this case, X5P) with the active site of yeast TK, based on mutagenesis data and results of crystal structure analysis. The conserved amino acid residues His-69 and His-103 form hydrogen bonds with the C1-OH functionality of the donor substrate and stabilize the DHE-TPP, the major intermediate of TK reaction), determining its orientation in the active site in an optimal manner for the catalytic process. In addition, these residues account for the substrate specificity of TK - phosphorylated substrates have higher affinity to this enzyme (Usmanov and Kochetov, 1982).

For the tight binding of and the high affinity for phosphorylated substrates (exceeding that observed with their nonphosphorylated counterparts) highly conserved residues of the yeast TK Arg-528, Arg-359, and His-469 are required (Nilsson et al., 1997). The residue Asp-477 interacts with the hydroxyl at C4 of X5P, whereas His-263 and His-30 interact with the hydroxyl group at C3 of the same substrate. Moreover, one of the known requirements to be met by a donor substrate is the trans-configuration of its hydroxyl groups at C3 and C4. Crystal structure of the complex E4P-TK demonstrated that Asp-477 forms a hydrogen bond with the hydroxyl at C2 of the acceptor substrate. Taken together, all the observations and also the data obtained with Asp477 mutants (Nilsson et al., 1998) provide evidence that the conserved residues of the substrate-harboring channel likely determine the stereospecificity of TK.

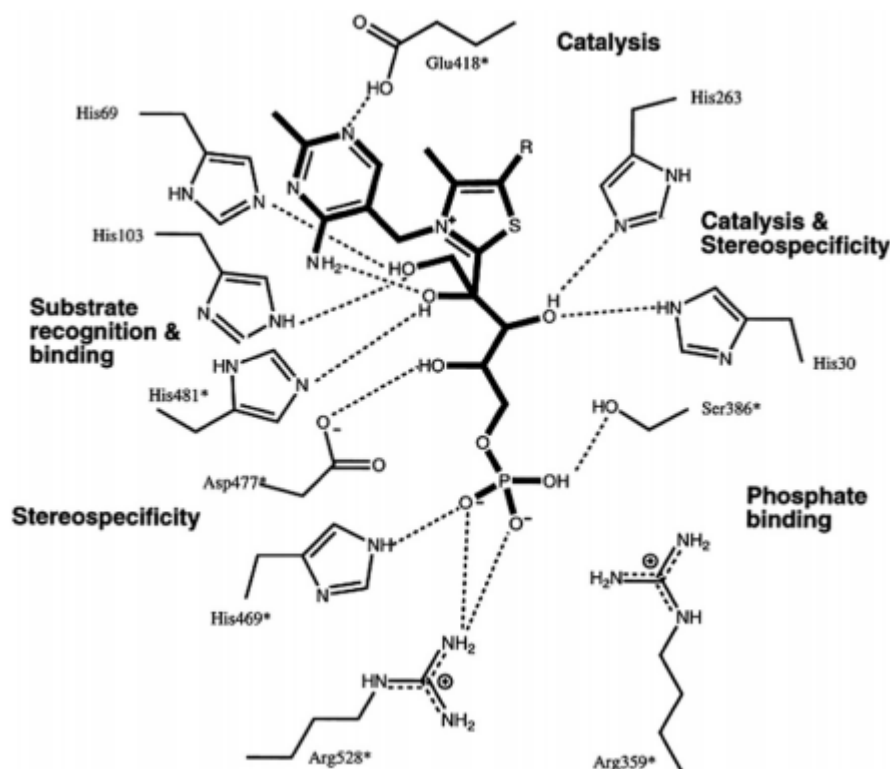


Figure 25. Model of the covalent donor substrate-TPP adduct in the active site of the *Saccharomyces cerevisiae* transketolase (Kochetov and Solovjeva, 2014).

3.1 Double-substrate and single substrate reactions

A simplified reaction scheme for the TK-catalyzed conversion of substrates X5P and R5P into products S7P and G3P is shown in Figure 26.

The reaction cycle can be subdivided into a donor half-reaction (donor ligation and cleavage) and an acceptor half-reaction (acceptor ligation and product liberation) (Mitschke et al., 2010). After formation of the reactive ylide form of TPP, the C2 carbanion of TPP attacks the carbonyl of donor X5P in a nucleophilic manner to yield the covalent donor-TPP adduct X5P-TPP (step 1). Ionization of C3-OH and cleavage of the C2–C3 bond of X5P-TPP (or Michaelis complex) results in the formation of the product G3P and of the DHE-TPP carbanion/enamine intermediate (step 2). This intermediate may then react with either G3P (reverse reaction of step 2) or R5P, in competing equilibria. In the latter case, C2 of DHE-TPP ligates to C1 of R5P (in the acyclic form), yielding the covalent S7P-TPP adduct (step 3). Eventual liberation of product S7P completes the reaction cycle (step 4).

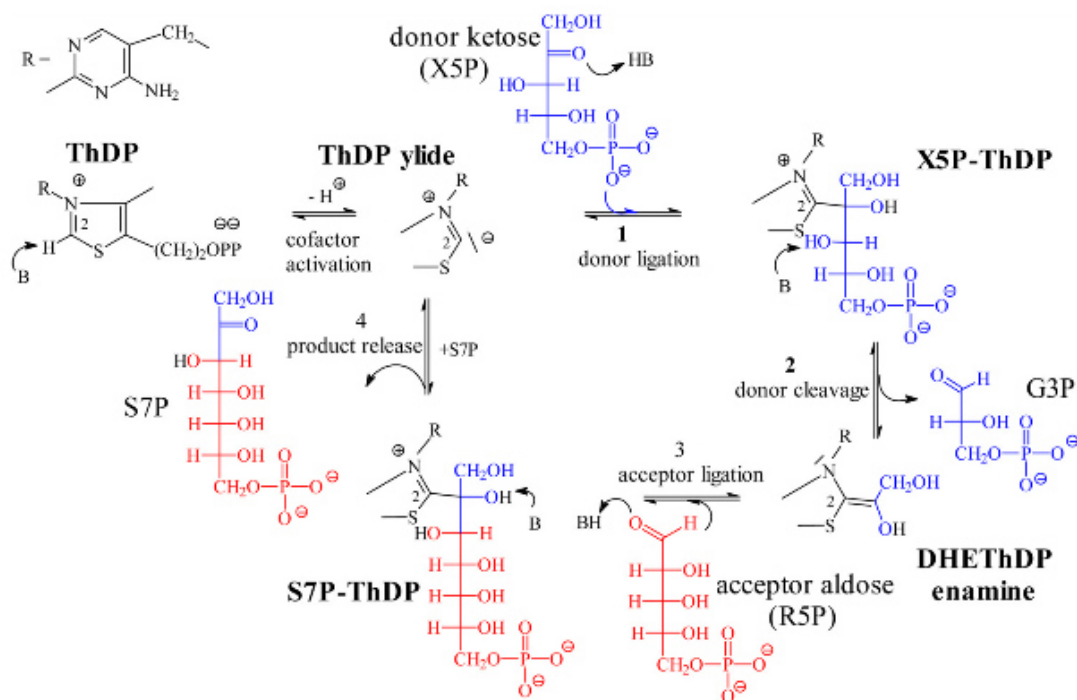


Figure 26. Minimal reaction mechanism of TK for the conversion of donor ketose X5P (in blue) and acceptor aldose R5P (in red) into S7P and G3P with intermediates and elementary steps of catalysis (Mitschke et al., 2010).

It is noteworthy that TK is also capable of catalyzing single substrate reactions (Figure 27), such as ketose transformation in the absence of aldose (Solovjeva et al., 2001; Bykova et al., 2001). In the schematic depiction of a TK catalyzed single substrate reaction, glycolaldehyde formed as result of donor substrate cleavage is further used by TK as an acceptor substrate for another glycolaldehyde residue, which results in the formation of erythrulose. When X5P serves as the sole substrate, the reaction products are represented by G3P and erythrulose (Solovjeva et al., 2001). The rate of the single substrate reaction is relatively low, accounting for about 2% of that of its double substrate counterpart (Solovjeva et al., 2001).

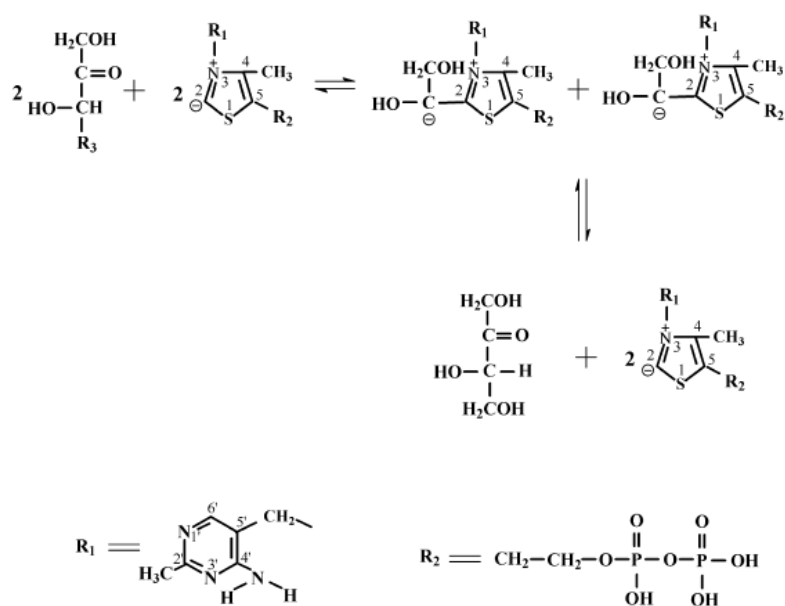


Figure 27. Schematic representation of single substrate transketolase reaction.

4. Industrial applications for the transketolase

TK finds an increasing number of applications for industrial purposes, in particular in the synthesis of chemicals. One example is the biosynthesis of the aromatic amino acids L-phenylalanine, L-tryptophan and L-tyrosine from D-glucose (Ganem et al., 1978). These amino acids are used as precursors for the organic synthesis of various products; e.g. L-phenylalanine can be transformed into the artificial sweetener aspartame (Vinick et al., 1982), L-tryptophan into the dye indigo (Ensley et al., 1983) and L-tyrosine into eumelanin, a UV-absorbing substance (Della Cioppa et al., 1990).

TK is also an important biocatalyst in stereospecific carbon-carbon bond synthesis. TK accepts a large number of aldehydes as substrates (Humphrey et al., 1995; Morris, 1996), in particular those containing an α -hydroxy group in 2R configuration; the products are ketoses with a 3 S,4R configuration (threo-configuration) (Effenberger et al., 1992). For instance, TK from spinach can catalyze a reaction between 2,3-dihydroxybutyraldehyde and hydroxypyruvate, yielding a mixture of 6-deoxy-D-fructose and 6-deoxy-L-sorbose, which can serve as precursors of 2,5-dimethyl-4-hydroxy-3(2H)-furanone (furanol), an important industrial aromatic product with caramel-like flavour used in the food industry (Hecquet et al., 1996). One of the major problems for the large scale industrial use of TK-catalysed biotransformations is that high concentrations of substrate strongly decrease its turnover number (Bongs et al., 1997; Mitra et al., 1998).

Chapter 6: THI and TPP as gene expression regulators

1. Biosynthesis pathway of THI/TPP

Thiamin (THI, vitamin B1) plays a vital role in all organisms as a cofactor for enzymes of the glycolysis, the Krebs cycle, the PPP and also the Calvin cycle in photosynthetic organisms. Animals are dependent on a source of THI in their diet, whereas microorganisms and plants can perform biosynthesis *de novo*. The THI biosynthesis is composed by two branches that culminate in the production of heterocyclic moieties, hydroxyethylthiazole phosphate (HET-P) and hydroxymethylpyrimidine pyrophosphate (HMP-PP) (Figure 28, representing the pathway in *Chlamydomonas*). These moieties are condensed to form thiamin monophosphate (TMP), which in eukaryotes is dephosphorylated by a phosphatase to form THI and is subsequently pyrophosphorylated by a pyrophosphokinase to the active cofactor thiamin pyrophosphate (TPP) (Moulin et al., 2013). Despite the importance of THI, regulation of its metabolism is only beginning to be unraveled in eukaryotes.

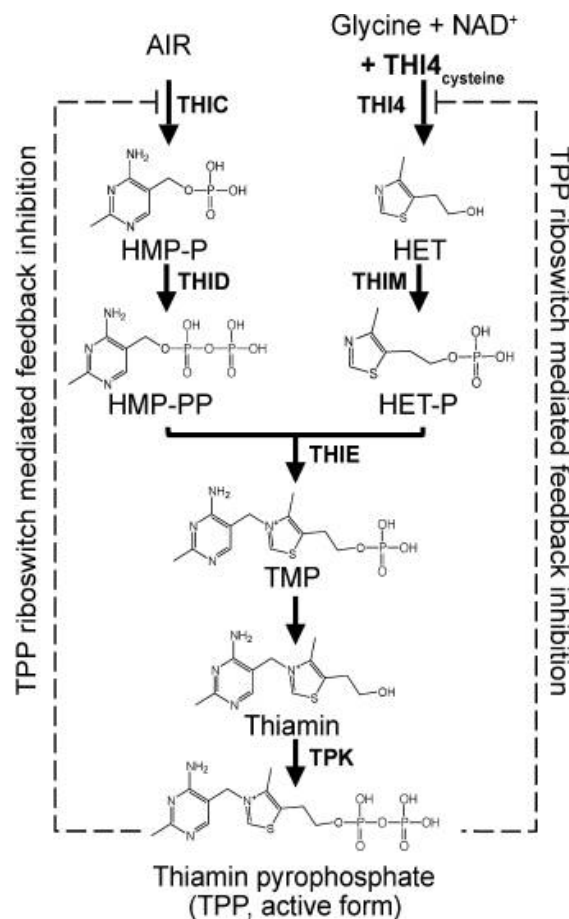


Figure 28. The thiamin biosynthesis pathway in *Chlamydomonas*. As in all organisms, TMP is generated from the condensation of HET-P and HMP-PP by the action of TMP synthase. THI4 catalyzes the formation of the thiazole moiety from NAD⁺, glycine, and the sulfur of a backbone cysteine residue. THIM, which is a salvage enzyme in bacteria, is essential for thiazole production in *Chlamydomonas*. The pyrimidine moiety is biosynthesized from aminoimidazole ribonucleotide (AIR) via the action of THIC and THID. THID and TMP synthase enzyme activities are found in a single, bifunctional enzyme equivalent to THI in higher plants. To generate the active cofactor, TPP, TMP is first dephosphorylated by an unknown phosphatase and then subsequently pyrophosphorylated by thiamin pyrophosphokinase (TPK). Both the THI4 and THIC genes are regulated through a TPP riboswitch (dashed line) (figure from Moulin et al., 2013).

2. TPP riboswitches

In bacteria, fungi, algae, and plants, exogenous THI has been shown to regulate expression of some of the THI biosynthesis genes via binding of mRNA portions called *riboswitches* (Bocobza et al., 2007; Winkler et al., 2002). Riboswitches are basically formed by two elements: an evolutionarily conserved metabolite sensing domain, called aptamer, and an expression platform that carries the gene regulatory signal (Winkler et al., 2002) (Figure 29). Numerous studies have demonstrated that the cofactor form of vitamin B1, TPP, binds directly to the aptamer, inducing a conformational change that interferes with the expression of that specific gene (Winkler et al., 2002; Thore et al., 2006).

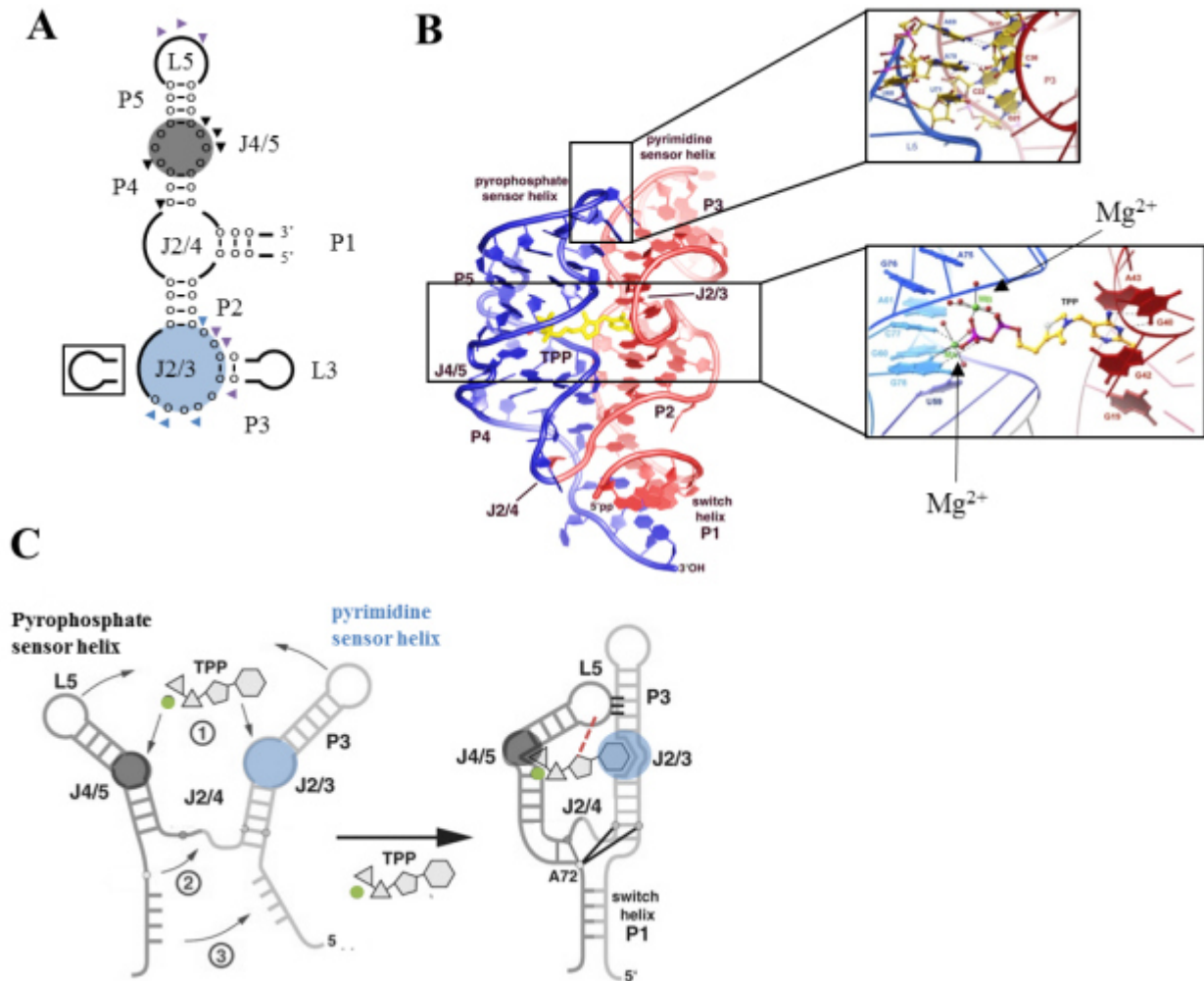


Figure 29. Structure and mechanism of TPP riboswitch. A) Secondary structure of the TPP aptamer with stems (P), loops (L), and junction between stems (J). Locations of pyrimidine binding (blue circle with triangle marks), pyrophosphate binding (black circle with triangle marks), and kissing between L5 and J2/3 (purple triangle marks) are also annotated. B) Crystal V-shaped tertiary structure of TPP-bound aptamer with the amplification of where the aptamer bound TPP components. C) Simplified mechanism to form the tertiary structure. 1 - TPP binds to the pyrimidine and pyrophosphate sensor helices with the assistance of two Mg²⁺ cations (green circle), 2 - J2/4 is formed by base-pairing two helices, 3 - switch helix P1 is formed to stabilise the structure. The thiazole moiety is connected with the aptamer (red dashed line). Figures are adapted from Thore et al. 2006; Thore et al. 2008; Warner et al. 2014.

Several mechanisms for the modulation of gene expression have been described that reflect the diversity of control. For example, in bacteria, riboswitches are found in the 5' untranslated region

(UTR) of the corresponding mRNAs (Mandal et al., 2004), where either transcription termination or translation is affected in the presence of the metabolite (Figure 30).

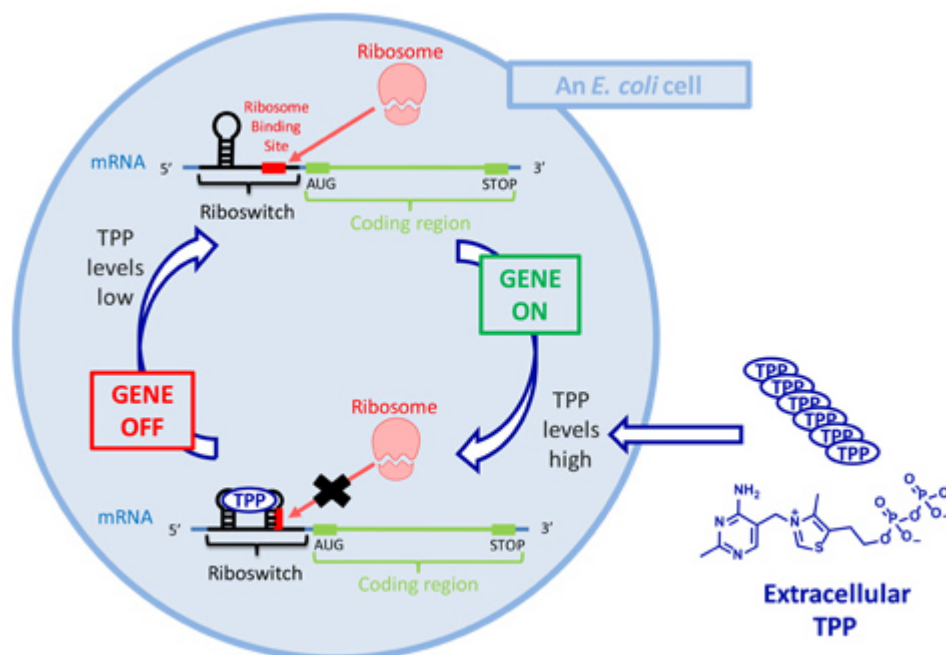


Figure 30. Riboswitch controlled gene expression. In *E. coli* TPP riboswitches suppress the translation of TPP biosynthetic and transport genes in response to TPP binding.

In eukaryotes, in contrast, expression is modulated through alternative splicing. Demonstrated examples of the latter include the fungi, *Aspergillus oryzae* (Kubodera et al., 2003) and *Neurospora crassa* (Cheah et al., 2007); the green alga *Chlamydomonas reinhardtii* (Croft et al., 2007); and the plant *Arabidopsis thaliana* (Bocobza et al., 2007; Wachter et al., 2007; Raschke et al., 2007). Interestingly, the location of the riboswitch varies in these organisms from being in an intron in the 5'-UTR, for example, in ThiA of *Aspergillus* (Kubodera et al., 2003) and THI4 of *Chlamydomonas* (Croft et al., 2007), to being in an internal intron in *Chlamydomonas* THIC (Croft et al., 2007).

3. Cellular effects of THI and TPP

The majority of cellular TPP serves as an essential cofactor for enzymes of the tricarboxylic acid cycle, glycolysis, PPP and branched-chain aminoacid biosynthesis. More than 29 TPP-dependent enzymes have been identified so far including pyruvate dehydrogenase (PDH), transketolase (TK), pyruvate decarboxylase (PDC), 2-oxoglutarate dehydrogenase (2OGDH) (www.expasy.ch). Interestingly, 1-Deoxy-D-Xylulose 5-Phosphate Synthase (DXS) is a HET biosynthetic enzyme and it requires TPP for its enzymatic activity (Jurgenson et al., 2009). They are classified based on their domain architecture although all of them have pyrimidine and pyrophosphate binding domains that interact with TPP to become active cofactor in the enzyme (Costelloe et al., 2008). Phylogenetic analysis of TPP-dependent enzymes revealed that they all evolved from a primitive ancestral TPP-dependent enzyme that had a single domain to bind both of the pyrimidine and pyrophosphate parts of TPP. This underwent dimerization and domain addition to improve catalytic properties (Costelloe et al., 2008) (Figure 31). Fusion of the two ancestral genes in the same or opposite directions resulted in the formation of phosphopyruvate decarboxylase (PPDC) and sulfopyruvate decarboxylase (SPDC) enzymes. All other TPP-dependent enzymes have similar domain architecture to PPDC, but have recruited other add-on domains, like transhydrogenase DIII (TH3) domain to

form pyruvate decarboxylase (PDC) enzymes, transketolase C-terminal (TKC) domain to form transketolase (TK) or DXP synthase (DXS), and pyruvate ferredoxin reductase (PFRD) (Costelloe et al., 2008). In higher plants, TPP is required by plastid enzymes that participate in the Calvin cycle, nitrogen assimilation and signalling (Goyer, 2010).

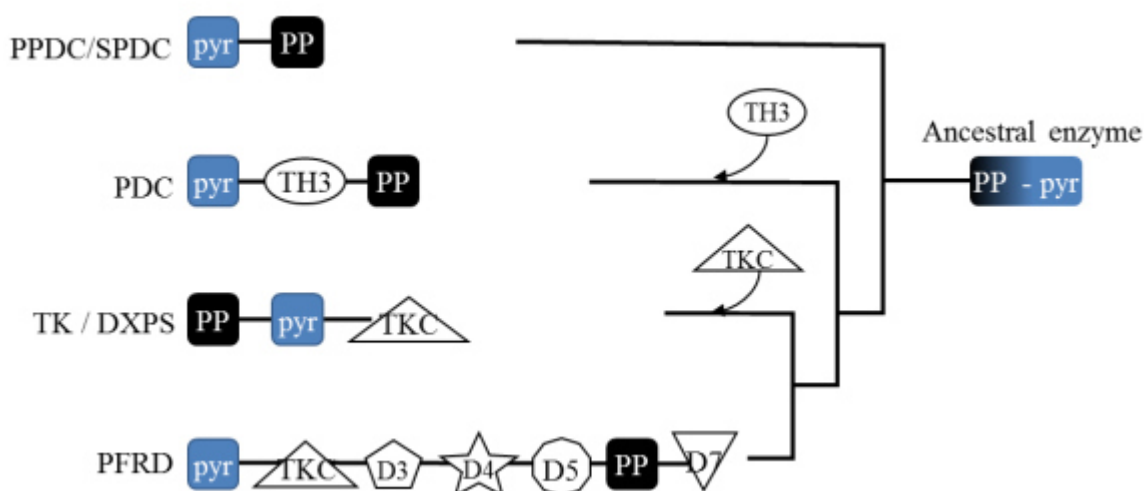


Figure 31. Evolutionary relationship of TPP-dependent enzymes. Pictures were adapted from Costelloe et al. (2008) in which details of all enzymes and domains were described. They were predicted to be evolved from a single-domain enzyme that can bind to both pyrimidine (pyr box) and pyrophosphate groups (PP box) of TPP. TKC (transketolase C-terminal), D3, D4, D5, D6, TH3 (transhydrogenase dIII) are add-on domains (white boxes). PFRD - pyruvate ferredoxin reductase, TK - transketolase, DXPS - DXP synthase, PDC - pyruvate decarboxylase, PPDC - phosphopyruvate decarboxylase, SPDC - sulfopyruvate decarboxylase.

Chemically synthesised thiamine analogues like pyriothiamine (PT), oxythiamine (OT) and other derivatives have been used to provide insight into THI deficiency, the binding activity of TPP-dependent enzymes, as well as the opportunity for drug discovery (Agyei-Owusu and Leeper, 2009).

In order to activate the catalysis of TPP-dependent enzymes, TPP binds and adopts a V-shaped conformation in the active site of the enzyme (Nemeria et al., 2007). Analogues in which the components of TPP (pyrimidine ring, thiazole ring and pyrophosphate groups) have been modified gave rise to negative effects on the activity of the enzymes (Agyei-Owusu and Leeper, 2009). However, there was still some level of flexibility when the binding pocket was maintained, for example, the N-1 residue or the C=C double bond of the pyrimidine ring. Interestingly, modifying the thiazole ring of TPP had a reversible effect and allowed the analogue to bind the enzyme 20,000 times more tightly than TPP (Agyei-Owusu and Leeper, 2009). PT and OT are the two most popular ‘anti-thiamine’ compounds that have been used to study the deficiency of THI. OT has a modified pyrimidine ring in which the NH₂ of the pyrimidine moiety is changed to a carboxyl group, while in PT the thiazole ring is substituted with a pyrimidine ring. Both PT and OT competed with thiamine to serve as substrates of enzymes such as TPK (Liu et al., 2006). Their esters (OTPP and PTPP) also competed with TPP to bind TPP-dependent enzymes such as TK and PDC (Wittorf and Gubler, 1970). They were found to be toxic to most organisms including bacteria, fungi, plants, algae, and animals (Agyei-Owusu and Leeper, 2009).

In many organisms, thiamine and its esters are also able to trigger enzymes to sense, respond and adapt to stresses (Figure 32). Abiotic stresses such as osmotic, salt, oxidative, temperature, water,

and light stresses can cause damage to the main TPP-dependent enzymes such as TK, PDH or DXS. It induces the expression of genes encoding biosynthetic (for example *THI4*, *THI6*, *THIC*, *THI1*, *TPK*) to regenerate the main metabolic pathway. Activity of other TPP-dependent enzymes involved in the Krebs cycle, the PPP and the TCA cycle are induced in order to compensate for the damage, and support adaptive responses by producing protective molecules (Rapala-Kozik et al., 2012). THI can also induce salicylic acid-dependent pathogen-related (PR) gene expression, and systemic acquired resistance via hydrogen peroxide (Tunc-Ozdemir et al., 2009; Ahn et al., 2005). Other factors than THI such as dark exposure, nutrient or vitamin deficiency (Fe, S, and vitamin B₁₂) could also affect the expression of thiamine-related enzymes (Goyer, 2010). THI has been proposed to function as an antioxidant due to its participation in DNA repair in bacteria, yeasts, and plants (Machado et al., 1997; Kowalska and Kozik, 2008; Goyer, 2010).

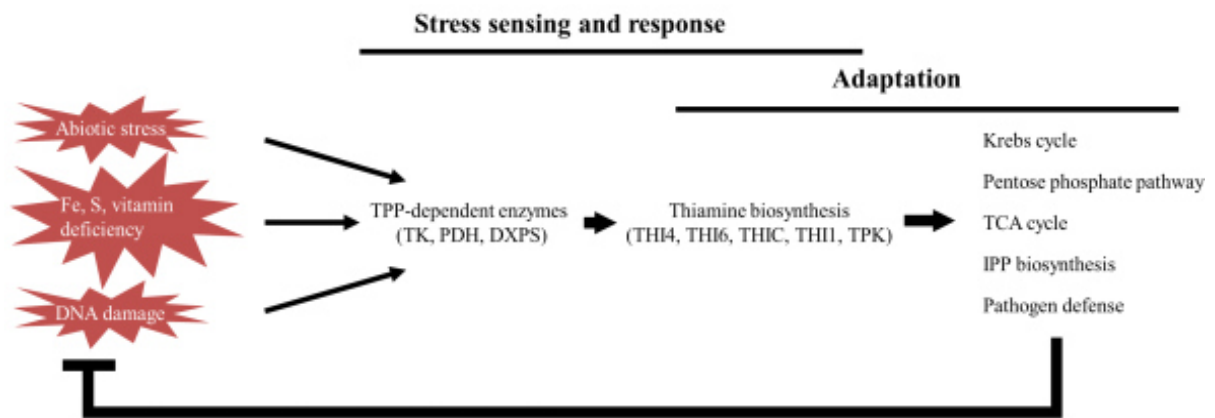


Figure 32. The role of thiamine biosynthesis and its enzymes in sensing and responding damages from abiotic stresses (osmotic stress, high or low temperatures, drought, high or low light, oxidative stress), nutrient and vitamin deficiency, and DNA damage. It triggers the upregulation of gene expression encoding TPP-dependent enzymes. Thiamine biosynthetic genes are also up-regulated to support the metabolism in compensating damages.

Materials and Methods

1. Aim of the study

Chloroplastic transketolase from *Chlamydomonas reinhardtii* (CrTK) is involved in a number of metabolic pathways, like the connection between PPP and glycolysis, the carbon dioxide fixation in the autotrophic organisms and the synthesis of numerous molecules (coenzymes, fatty acids, aminoacids, glutathione and several vitamins).

Actually, contrasting data about the transketolases redox regulation were reported in literature: in fact, there was no clear indication that the TK activity in spinach chloroplasts might be subjected to redox regulatory mechanisms (Teige et al., 1998), although proteomic analysis later suggested that this enzyme could be a potential target of thioredoxins *f* and *m* (Balmer et al., 2003). Furthermore, proteomic surveys performed on cellular extracts from *Arabidopsis thaliana* indicated that TK was able to interact with the cytosolic thioredoxin h3 (Marchand et al., 2004), while no evidence of cytosolic TRX h1-TK interaction has been found in *Chlamydomonas reinhardtii* (Sarkar et al., 2005). These experimental evidences suggest that plant TKs might contain regulatory cysteines and that this regulation likely involves TRXs.

The aim of this study is to get insight into the structural and biochemical properties of the chloroplastic TK from the green microalga *Chlamydomonas reinhardtii* (CrTK). In order to study this key enzyme, we have cloned, over-expressed in *E.coli* and purified CrTK. The TK biochemical features were defined, as well as its redox-sensitivity, while its structural features were determined by X-ray crystallography, circular dichroism and Dynamic Light Scattering (the methods, results and discussion connected to these studies are exposed in the Chapter 1 of the section Materials and Methods, in the Chapter 1 of the section Results and in the Chapter 1 of the section Discussion, respectively).

Furthermore, since the TK cofactor TPP displays a very important role in the activation of the enzyme, the influence of TPP on the transketolase gene expression as been studied *in vivo* on *Chlamydomonas reinhardtii* cultures. The rationale of this question lies in the fact that the TPP, as well as its precursor thiamin, are important regulators of gene expression, since they can bind the TPP riboswitches regions present in the messenger RNA of genes codifying enzymes involved in their own biosynthesis. This post-transcriptional control is able to "sense" the thiamin and TPP levels in the cell, contributing to keep a fine cell homeostasis of these molecules (Moulin et al., 2013; Bocobza and Aharoni., 2014; Duesterberg et al., 2015; Guedich et al., 2016). So does a "crosstalk" exist between the TPP and CrTK gene? In order to answer to this question, the response of the TK gene expression to the treatments with some of the TPP biosynthesis pathway compounds and their analogs has been analyzed. This investigation has been possible thanks to the kind collaboration with Prof. Alison G. Smith, who hosted me in her laboratory in the University of Cambridge (UK) for a four-months period (financially supported by the MarcoPolo Programme of the University of Bologna). The methods, results and discussion are exposed in the Chapter 2 of the section Materials and Methods, in the Chapter 2 of the section Results and in the Chapter 2 of the section Discussion, respectively.

Chapter 1

1. Plasmid Construction for Expression of CrTK and EcE4PDH in *E. coli*

The cDNA-encoding chloroplastic transketolase from *C. reinhardtii* (CrTK) was obtained by PCR using a forward primer introducing an *NdeI* restriction site at the start codon (5'-AACGTGCATATGGCTCAGGCTGCCCCCGCT-3'); and a reverse primer introducing a *BamHI* restriction site downstream of the stop codon (5'-ACCATGGGATCCTTAGTGCTGCAGGGTGGC-3'). CrTK is encoded by the gene at locus Cre02.g080200 and appears to be the only TK in *C. reinhardtii*. CrTK was cloned in a modified pET-3c vector containing additional codons upstream of the *NdeI* site to express a His-tagged protein with seven N-terminal histidines. This modified vector (pET-3c-His) was generated by restriction with *XbaI* and *NdeI* of pET-3c to insert the following sequence: 5'-TCTAGAAATAATTTTGTTTAACTTTAAGAAGGAGATATACAAATGCACCACCACCAC CACCACCATATG-3' (*NdeI* italicized, start codon underlined and seven His codons in bold). The recombinant CrTK contains 692 residues with an estimated molecular weight of 75,169.6 Da; it starts at the N-terminus with the introduced MHHHHHHHM peptide followed by the mature protein sequence (*i.e.* upon removal of the chloroplast targeting sequence, in grey in the Figure 33), beginning with Ala36 (in green in the Figure 33).

The plasmid encoding erythrose-4-phosphate dehydrogenase from *Escherichia coli* (EcE4PDH) was used as in (Rocha et al., 2014).

Below the CrTK and recombinant CrTK (used in this work) sequences (whose alignment was performed using Clustal Omega) and the parameters referred to these proteins are presented, calculated by ExPASy ProtParameters:

CrTK	MQTMLKQRCQPAVGGKQAKAVPAVAPKVGRRARNVVV	QAAPAAAKAAAF	SI	SRDEVEK	CIN	60
CrTKrec	-----MHHHHHHHMQ	QAAPAAAKAAAF	SI	SRDEVEK	CIN	34
	: : : :	*****				
CrTK	AIRFLAIDAINKSKSGHPGMPMGCAFMGYVLWNEVMKYNPKNPDFFNDRDFVLSAGHGSM					120
CrTKrec	AIRFLAIDAINKSKSGHPGMPMGCAFMGYVLWNEVMKYNPKNPDFFNDRDFVLSAGHGSM					94
CrTK	FQYSMMHLTGYSVPLDQIKQFRQWNSLTPGHPEFVTPGVEVTTGPLGQIGICNAVGLAV					180
CrTKrec	FQYSMMHLTGYSVPLDQIKQFRQWNSLTPGHPEFVTPGVEVTTGPLGQIGICNAVGLAV					154
CrTK	AEAHLAARFNKPDVKPIVDHYTYCILGDGCMMEGISENEACSLAGHWGLGKLIALLYDDNKI					240
CrTKrec	AEAHLAARFNKPDVKPIVDHYTYCILGDGCMMEGISENEACSLAGHWGLGKLIALLYDDNKI					214
CrTK	SIDGHTDISFTEDVAKRYEALGWHVIVHVIINGNTDVGDLRAAIAQAKAVKDKPTLIKRVSTL					300
CrTKrec	SIDGHTDISFTEDVAKRYEALGWHVIVHVIINGNTDVGDLRAAIAQAKAVKDKPTLIKRVSTL					274
CrTK	IGYGSFNKADSHDVHGAPLGPDETAATRKNLWNPYGEFEVFPQDVYDVFRGAIKRGAEAEA					360
CrTKrec	IGYGSFNKADSHDVHGAPLGPDETAATRKNLWNPYGEFEVFPQDVYDVFRGAIKRGAEAEA					334
CrTK	NWHKACAEYKARYPKWEAEFEALTSCKLPENWEAALPHFKPEDRGLATRQHSQTMINALA					420
CrTKrec	NWHKACAEYKARYPKWEAEFEALTSCKLPENWEAALPHFKPEDRGLATRQHSQTMINALA					394
CrTK	PALPGLIGGSADLAPSNLTLMKISGDFQKGSYAERNLRFGRV	HAMGAI	CNGIALHKSGL			480
CrTKrec	PALPGLIGGSADLAPSNLTLMKISGDFQKGSYAERNLRFGRV	HAMGAI	CNGIALHKSGL			454
CrTK	IPYCATFYIFTDYMRNAMRMSALSEAGVVVVMTHDSIGLGEDGFTHQPIEHLASFRAMPD					540
CrTKrec	IPYCATFYIFTDYMRNAMRMSALSEAGVVVVMTHDSIGLGEDGFTHQPIEHLASFRAMPD					514
CrTK	MLMIRPAGGNETAGAYKVAIANRKRPTTIALSRQNMNIPNCSEVGVARGAYTIHDTKAG					600
CrTKrec	MLMIRPAGGNETAGAYKVAIANRKRPTTIALSRQNMNIPNCSEVGVARGAYTIHDTKAG					574
CrTK	VKPDVILMGTGSELELATAAAGILEKEGKNVVRVVSFCWELFEEQSAEYKESVLPDVTIA					660
CrTKrec	VKPDVILMGTGSELELATAAAGILEKEGKNVVRVVSFCWELFEEQSAEYKESVLPDVTIA					634
CrTK	RVSVEAATSFGWAKYIGLKGKHVIGIDTFGASAPAPTLYEKFGITVNHVVEAAKATLQH					718
CrTKrec	RVSVEAATSFGWAKYIGLKGKHVIGIDTFGASAPAPTLYEKFGITVNHVVEAAKATLQH					692

Figure 33. Sequence alignment of CrTK in the full-length and recombinant forms. The chloroplast targeting sequence is highlighted in grey. The first residue of the recombinant protein is in green (Ala36). The first residue detected in the CrTK crystal structure is in cyan and corresponds to Ser49 in the full-length CrTK.

Extinction coefficients:

Extinction coefficients are in units of $M^{-1} \text{ cm}^{-1}$, at 280 nm measured in water:

- 1) Ext. Coefficient: 90,02; Abs 0.1% (=1 g/l): 1.198, assuming all pairs of Cys residues form cystines;
- 2) Ext. Coefficient: 89,27; Abs 0.1% (=1 g/l): 1.188, assuming all Cys residues are reduced.

2. Preparation of competent BL21 *Escherichia coli* cells

A liquid BL21 *Escherichia coli* culture was set up taking 20 μL of BL21 strain cells from a glycerine stock (conserved at -80°C) and placing it in a 50 mL falcon with 10 mL of Luria Bertani (LB) [10 g/L tryptone (Sigma), 10 g/L NaCl (Merck), 5 g/L yeast extract (DIFCO Laboratories)]. Bacteria were grown overnight (that means for 16-18 h) at 37°C on a shaking incubator (speed: 70-90 rpm). Subsequently, a subculture was prepared taking 50 μL of overnight culture and placing them in a 50 mL falcon with 20 mL of LB. Subculture bacteria were grown at 37°C on a shaking incubator until the subculture achieved an Optical Density at 600 nm ($O.D._{600\text{nm}}$) between 0.15 and 0.17.

When the right $O.D._{600\text{nm}}$ was suitable, aliquots of 1.5 mL of the subculture were transferred in

centrifuge microtubes (Delchimica) and centrifuged at 8000 rpm, 4° C for 30'. The supernatant was discarded, while the pellet was resuspended in 450 µL of TFB-I solution [30 mM Potassium acetate (Merck); 50 mM Manganese (II) Chloride (Carlo Erba Reagents); 100 mM Rubidium Chloride (Sigma); 10 mM Calcium Chloride (Merck); 15% Glycerine (Carlo Erba Reagents); adjusted to pH 5.8 with 0.2 N acetic acid (Sigma) and filtered with Syringe Driven Filter Unit 0.22 µm (Millex-GS, Millipore)], vortexing for a better result. Microtubes were centrifuged at 3000 rpm at 4° C for 10'. The supernatant is discarded and the pellet is resuspended in 120 µL of TFB-II solution [10 mM MOPS (Sigma); 10 mM Rubidium Chloride; 75 mM Calcium Chloride; 15% Glycerine; adjusted to pH 6.8 with NaOH (Carlo Erba Reagents) and filtered with Syringe Driven Filter Unit 0.22 µm], softly shaking. Microtubes were conserved at -80° C.

3. Transformation of BL21 *Escherichia coli* cells

Tubes with BL21 *Escherichia coli* competent cells were thawed from -80° C; 1 ng/µL of solution with the pet21b-His-TK plasmid (or the plasmid containing the EcE4PDH coding sequence) was placed into the tubes. An incubation in ice for 30' was performed to block the growth of bacterial cells. After this incubation, microtubes were placed at 42° C for 45-60 seconds and then cooled in ice for 2-3 minutes. Subsequently, LB was added to each tube to totally reach 700 µL. Bacteria were grown for 1 h at 37° C on the shaking incubator. Two Petri dishes were prepared: in the first one, 50 µL of bacterial culture were streaked; in the second one, after centrifuging the remaining culture at 13,000 rpm for 3', eliminating the majority of supernatant and resuspending the pellet, ~100 µL of culture were streaked. Bacterial colonies were then grown overnight at 37° C.

4. Extraction of Plasmidic DNA

QIAprep Spin Miniprep Kit (QIAGEN) was used to extract plasmidic DNA to BL21 *Escherichia coli* colonies: a single colony was picked up and transferred in a 50 mL falcon with 10 mL of LB. Bacteria were grown overnight at 37° C on the shaking incubator. After the overnight growth, 4 mL of bacterial culture were placed in a 50 mL falcon and centrifuged at 8000 g at 4° C for 3'. The supernatant was discarded, while the pellet was resuspended in 250 µL of Buffer P1 (containing RNAses) and transferred in a centrifuge microtube. Then 250 µL of Buffer P2 were added in each tube: it is necessary to mix thoroughly by inverting the tube 6-8 times (not vortexing). The lysis reaction proceeded for 5'. Subsequently, 350 µL of Buffer N3 were added in each microtube, mixing immediately by inversion for 6-8 times. Each tube was centrifuged at 13,000 rpm for 10'. The supernatant was applied by decanting to the QIAprep Spin Columns, which were centrifuged at the same speed for 1'. The flow-through was eliminated. Then 750 µL of Buffer PE were added in each column, which was ricentrifuged. The flow-through was discarded again. An additional centrifugation was made to remove residual wash buffer. QIAprep columns were placed in clean 1.5 mL microtube: to elute the DNA, 50 µL of Buffer EB [10 mM Tris-HCl (pH 8.5)] or water were added to the center of each spin column, letting stand for 1' and centrifuging at 13,000 rpm for 1'. Plasmidic DNA concentration was checked to the spectrophotometer ND-1000 (NanoDrop). As shown in Figure 34, DNA was run on an agarose gel (2%). Microtubes with DNA were conserved at -20° C.

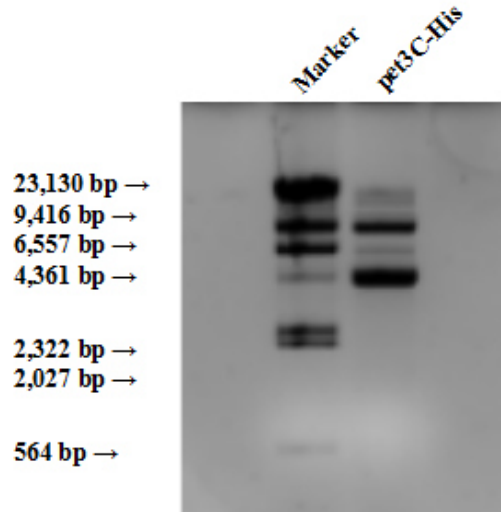


Figure 34. 2% agarose gel performed to verify the presence and the quality of the plasmidic DNA in the *E. coli* transformed colonies.

5. *E. coli* cultures and protein expression induction with IPTG

A single BL21 *E. coli* colony was picked up and transferred in a 50 mL falcon with 10 mL of LB with ampicillin 50 $\mu\text{g}/\text{mL}$. The culture was grown overnight on a shaking incubator at 37° C. 5 mL of this culture was then added to 200 mL of fresh medium and grown on a shaking incubator at 37° C until an O.D._{600 nm} of 1 Abs (Absorbance) was obtained. Subsequently, this culture (the whole volume) was added to 2 L fresh medium. When an O.D._{600 nm} = 0.5 Abs was achieved, the induction of the protein expression was performed, using 0.2 mM isopropyl β -D-1-thio-galactopyranoside (IPTG) (Duchefa) (for both the CrTK and the EcE4PDH). This culture grew overnight on the shaking incubator (temperature for CrTK = 25°C; temperature for EcE4PDH = 30°C; in the Figure 35, the SDS-PAGE run after the expression study for the CrTK).

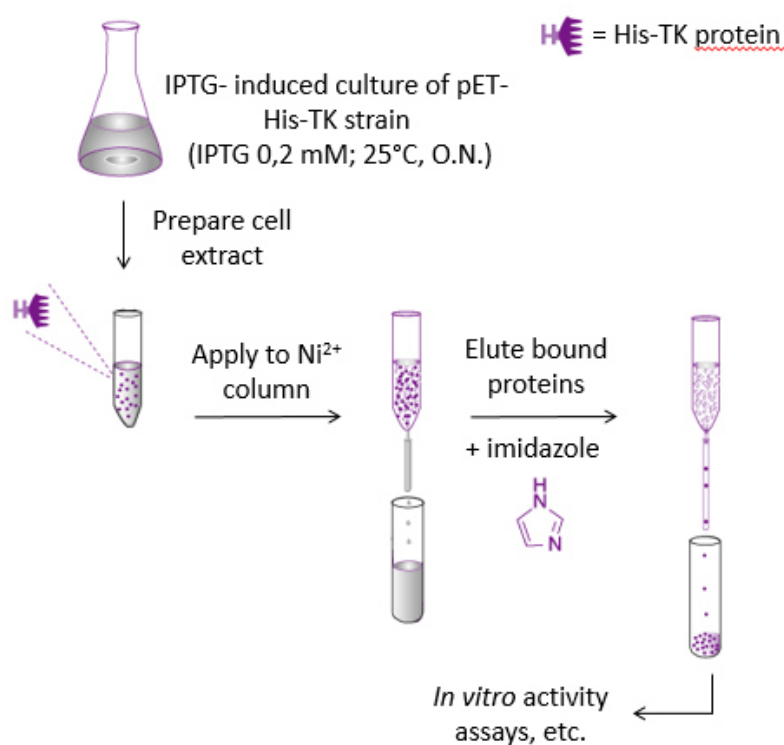


Figure 36. Scheme of the CrTK purification steps.

If necessary, fractions containing pure protein were concentrated by ultrafiltration using Centricons (Amicon, 10 KDa cut-off). The amount of CrTK was determined spectrophotometrically using a molar extinction coefficient at 280 nm of 89,27 M⁻¹cm⁻¹, while for the EcE4PDH a molar extinction coefficient of 32,43 M⁻¹cm⁻¹, was considered.

7. SDS-PAGE (Sodium Dodecil Sulphate-Protein Acrylamide Gel Electrophoresis)

To check for the protein quality or to obtain a concentration profile of the purified protein fractions, a SDS-PAGE was performed. A 12,5% acrylamide running gel (1,5 mm thick) was prepared according to the following instructions:

	<i>Running gel (10ml)</i>	<i>Stacking gel (2.5ml)</i>
Water	3.179 mL	1.455 mL
1.5 M Tris-HCl (pH 8.8)	2.5 mL	/
0.5 M Tris-HCl (pH 6.8)	/	625 µL
10% SDS (Sigma)	100 µL	25 µL
30 % Acrylamide/Bis-Acrylamide (37:1)	4.166 mL	375 µL
20% APS (Merck)	50 µL	15 µL
TEMED (Sigma)	20 µL	5 µL

The low-molecular weight marker (Amersham, Code: 17044601), 40 µL of Sample Buffer (negative control) and 40 µL of sample were loaded. All the samples were prepared in 40 µL with: 8 µL of Sample Buffer 5X (300 mM Tris-HCl (pH 6.8), 10% SDS, 12.5% methanol, 0.125% bromophenol blue, 50% glycerol). The gel was run for 90' at 110 V.

After completing the run, the gel was put in the Staining Solution [50% ethanol (Sigma), 10% acetic acid (Sigma), 0.25% Coomassie Brilliant Blue R-250 (Biorad)] for 2 h to allow the protein band(s) visualisation. When the protein band(s) was/were visible, the gel was put in Destaining Solution [25% ethanol (Sigma), 8% acetic acid (Sigma)]. The destaining procedure can be performed overnight or for at least 3 h. After this last step, the gel was put in MilliQ water and/or scanned (in the Figure 37, gels representing the CrTK elution profile and the profile of the purification steps for the EcE4PDH are shown).

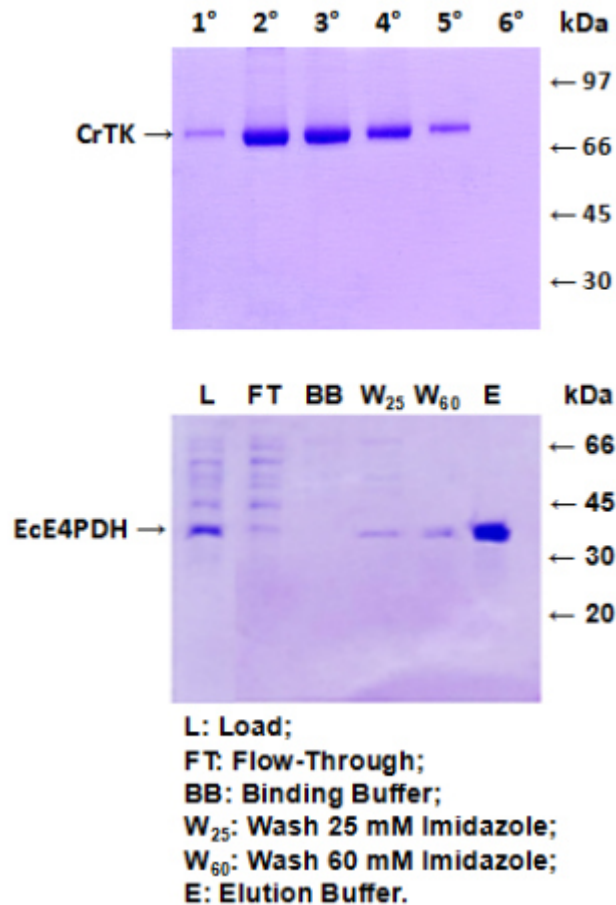


Figure 37. CrTK elution profile (above) and the profile of the purification steps for the EcE4PDH (below). On the right, the molecular weights in KDalton.

8. CrTK Molecular Mass Determination through Gel Filtration

Analytical gel filtration of apo-CrTK was performed on a Superdex 200 10/300 GL column connected to an ÄKTA Purifier system (GE Healthcare). The column was calibrated with standard proteins as described in (Sparla et al., 2005). The protein was eluted at a flow rate of $0.5 \text{ ml}^{-1} \text{ min}^{-1}$ with 50 mM Tris-HCl (pH 7.5) containing 150 mM NaCl and 1 mM EDTA. The AtGAPC1 was used as control protein for this measurement. A SDS-PAGE was run after the gel filtration to check the molecular weight and the purity of CrTK (Figure 38).



Figure 38. SDS-PAGE performed after gel filtration; the numbers on the lanes indicate the numbers of the different fractions collected during the gel filtration. To the right, the molecular weight in KDalton.

9. CrTK analysis through Dynamic Light Scattering (DLS)

DLS experiments were performed employing a Malvern Nano ZS instrument equipped with a 633-nm laser diode. Samples consisted of 500 μL of apo- and holo-CrTK (at a concentration of 1 mg/mL) in 50 mM Tris-HCl (pH 7.9) supplemented or not with TPP and Mg^{2+} . Protein samples were set up in disposable polystyrene cuvettes of 1 cm optical path length, using water as a solvent. The width of DLS hydrodynamic diameter distribution was indicated by the polydispersity index. In the case of a monomodal distribution (Gaussian) calculated by means of cumulant analysis, polydispersity index = $(\sigma/Z_{\text{avg}})^2$, where σ is the width of the distribution and Z_{avg} is the average diameter of the protein population, respectively.

10. Absorption and CD spectroscopy

10.1 Binding studies with thiamine pyrophosphate (TPP)

Stock solutions of CrTK in both reduced and oxidized forms were prepared at an approximate concentration of 9 mg/mL in concentrated Tris buffer [50 mM (pH 7.9), containing 1 mM EDTA]. CrTK samples (500 μL) were prepared by diluting stock solutions 1:20 (v/v) with concentrated Tris buffer, MgCl_2 (100 mM in water) and water in order to obtain an aqueous solution with the following composition: 5 mM Tris (pH 7.9), 0.1 mM EDTA, 2 mM MgCl_2 (referred to hereafter as diluted buffer). CrTK samples were then analyzed by UV and CD spectroscopy in the 400–250 nm spectral range, using a Hellma (Milan, Italy) 115B-QS micro cell with a 1 cm path length on a Jasco (Tokyo, Japan) J-810 spectropolarimeter with the following settings: 20 nm/min scanning speed, 2 sec data integration time, 2 nm spectral bandwidth, 3 accumulations. The concentration was determined

experimentally for each individual sample by means of Lambert-Beer law based on the absorbance at 280 nm (A₂₈₀). Molar extinction coefficients at 280 nm for the reduced ($\epsilon_{280\text{nm}} \text{CrTK}_{\text{red}} = 89270 \text{ M}^{-1} \text{ cm}^{-1}$ assuming that all cysteine residues are reduced) and oxidized ($\epsilon_{280\text{nm}} \text{CrTK}_{\text{ox}} = 90020 \text{ M}^{-1} \text{ cm}^{-1}$ assuming that all cysteine residues are involved in disulfide bonds) forms of apo-CrTK were derived from the equation developed by Pace et al., (1995):

$$\epsilon_{280\text{nm}} = 5500 \cdot N_{\text{W}} + 1490 \cdot N_{\text{Y}} + 125 \cdot N_{\text{C-C}}$$

where N_{W} is the number of tryptophan residues (10 in CrTK), N_{Y} is the number of tyrosine residues (23 in CrTK) and $N_{\text{C-C}}$ is the number of disulfide bonds. Once the experimental concentration of apo-CrTK in the sample was assessed, the binding of TPP to CrTK in both reduced and oxidized forms was monitored by means of UV and CD spectroscopy. 5 μL aliquots of a stock solution of thiamine pyrophosphate (500 μM TPP in dilute buffer), up to a maximum addition of 50 μL , were sequentially added to 400 μL of the apo-CrTK sample directly inside the micro cell; for the reduced form of CrTK, the remaining 100 μL of sample were used for secondary structure estimations (see next subsection). Concentrations were then corrected by the final volume of sample after addition of TPP; using this protocol, different molar ratios ($[\text{TPP}]/[\text{CrTK}]$) ranging from 0.87 to 10.23 were obtained for holo-CrTK samples, depending on the initial apo-CrTK concentration. All UV and CD spectra, including blank measurements on diluted buffer, were subtracted of the contribution of air in order to reduce baseline drift; all samples were then blank-corrected. The onset of induced CD (ICD) signals upon binding of TPP to CrTK was finally evaluated by subtracting the spectra of apo-CrTK from the spectra of holo-CrTK samples. Three independent experiments on different days were carried out on both the reduced and oxidized forms of CrTK, yielding reproducible results.

10.2 Secondary structure estimation for CrTK in its reduced form

For the estimation of the secondary structure of CrTK in its reduced form, 100 μL of apo-CrTK at a known concentration (see previous subsection) were diluted 1:3 (v/v) with diluted buffer; the resulting solution was divided in two different samples of 150 μL . The first sample was directly analyzed to estimate the secondary structure of apo-CrTK, while the second sample was mixed with a small aliquot of the 500 μM stock solution of TPP, in order to analyze the secondary structure of holo-CrTK. A $[\text{TPP}]/[\text{CrTK}]$ ratio of around 3 was used for the purpose: the final concentrations of CrTK and TPP in the sample were corrected by the final volume of sample after addition of TPP. UV and CD spectra in the 260–190 nm spectral range were measured using a Hellma (Milan, Italy) 100-QS micro cell with a 0.05 cm path length on a Jasco (Tokyo, Japan) J-810 spectropolarimeter with the following settings: 20 nm/min scanning speed, 2 s data integration time, 2 nm spectral bandwidth, 3 accumulations. Spectra were then blank-corrected and converted to molar units per residue; the contribution of TPP to the UV spectrum of holo-CrTK was negligible in the experimental conditions used for the analysis. The estimation of secondary structure was finally performed on the CD spectra of CrTK in molar units per residue using a locally modified version of the CDPPro software: the CONTIN/LL algorithm was used in combination with the SP175 reference dataset, and the resulting values of secondary structure content were converted to percent values (Provenker and Glokner, 1981).

11. Mass Spectrometry

Enzymatic digestion of CrTK, both reduced and oxidized, was performed with Trypsin with two different protocols: a) 30 μL of the reduced form (7 mg/mL) was treated with 55 mM iodoacetamide (IAM) for 40 min at room temperature, in the dark; afterwards, it was incubated at 37°C overnight after the addition of 1 μL of trypsin (1 $\mu\text{g}/\mu\text{L}$). The digestion reaction was stopped by diluting the sample 1:50 with 0.1% formic acid (v/v). b) 15 μL of the oxidized form of the protein (8.25 mg/mL) was directly incubated with 1 μL of trypsin (1 $\mu\text{g}/\mu\text{L}$), at 37°C, overnight. The digestion reaction was

stopped by diluting the sample 1:50 with 0.1% formic acid (v/v). LC-ESI-MSMS transketolase peptides analysis was carried out by using a nano-LC Agilent 1100 Series (Walbronn, Germany). Analyses were performed on a C18 (150 mm × 75 µm; 3.5 µm) column. Mobile phases A [water/acetonitrile/formic acid, 99:1:0.1 (v/v/v)] and B [acetonitrile/water/formic acid, 98:2:0.1 (v/v/v)] were used to develop a gradient. The solvent gradient was set as follows: 25% – 38% B, 60 min; 38% – 80% B, 1 min; 80% B, 1 min; 80% – 25% B, 5 min. System was equipped with an auto-sampler and the injection volume was 10 µL. The column was equilibrated with the mobile phase composition of the starting conditions for 10 min before the next injection. Mass spectrometry analysis was performed on the Q-ToF (Micromass, Manchester, UK) with nano-Z-spray ion source. The ESI-QToF source temperature was set at 120°C, the capillary voltage at 3.3 kV, and the cone voltage at 35 V. Peptide ions within a m/z 400-1700 survey scan mass range were analysed for subsequent fragmentation. 2⁺, 3⁺ and 4⁺ charged ions exceeding a threshold abundance (TIC value 10 counts/sec), were selected for MS/MS analyses. From a single survey scan 5 ions were selected for subsequent fragmentation. Scan returned to mass survey mode when the ion intensity fell below 5 counts/sec or after 8 sec. Scan time was 1 sec for the parent ion and 1 sec for the MS/MS ions. Collision energy was selected using charge state recognition.

12. Crystallization and Data Collection

Apo- and holo- (containing 0.25 mM TPP and 2 mM MgCl₂ and reconstituted as described before) CrTK were concentrated to 4.5 mg ml⁻¹ in 50 mM Tris-HCl (pH 7.9) containing 1 mM EDTA and crystallized by the hanging drop vapor diffusion method at 293 K. The Structure screen 1 from Molecular Dimensions and the Crystallization Extension kit for Proteins from Sigma Aldrich (Jancarik and Kim, 1991) were used as starting screening. A protein solution aliquot of 2 µL was mixed to an equal volume of reservoir, and the prepared drop was equilibrated against 800 µl of reservoir. Small crystals and crystalline aggregates grew from various reservoirs of the Extension kit (i.e. 22, 30, 37 and 38). The crystallization conditions were optimized and the best crystals grew from reservoir containing 10 % w/v PEG 6K, 5 % v/v MPD and 0.1 M MES pH 6.5-7.0 or HEPES pH 7.0-8.0. Crystals were fished from the crystallization drop, briefly soaked in a cryo solution containing 12 % w/v PEG 6K and 15 % v/v MPD, and then frozen in liquid nitrogen. Diffraction images were recorded at 100 K using a synchrotron radiation at Elettra (Trieste, beam line XRD) for the holo form and at the European Synchrotron Radiation Facility (Grenoble, beam line ID30B) for the apo form. The data were processed using XDS (Kabsch, 2010) and scaled with SCALA (Evans, 2006). The correct space group was determined with POINTLESS (Evans, 2006) and confirmed in the structure solution stage.

12.1 Structure Solution and Refinement

The CrTK holo-structure was solved by molecular replacement using the program MOLREP from CCP4 package (Vagin and Teplyakov, 2010) selecting the data from the highest resolution polymorph (see Table 3 in Results). The coordinates of TK from *Zea mays* (PDB code 1ITZ; Gerhardt et al., 2003), deprived of TPP, Mg²⁺ and water molecules, were used as search probe. Initial stages of the refinement were performed with CNS1.3 (Brunger et al., 1998) selecting 5% of reflections for Rfree. The manual rebuilding was performed with Coot (Emsley and Cowtan, 2004). The electron density map clearly showed the position of TPP and Mg ion, which were inserted into the model. Water molecules were automatically added and, after a visual inspection, they were conserved in the model only if contoured at 1.0 σ on the (2Fo – Fc) map and if they fell into an appropriate hydrogen bonding environment. In the final stages of the refinement performed with REFMAC 5.5.0109 (Murshudov et al., 1997), alternate conformations, if visible, were inserted. The

structure of the holo form without TPP, Mg^{2+} and waters, was used as probe to solve the apo structure by molecular replacement. The refinement was performed as described above.

12.2 Accession numbers

The atomic coordinates and structure factors of CrTK_{TPP/Mg} and CrTK_{apo} structures have been deposited in the Protein Data Bank with the accession numbers 5ND5 and 5ND6.

13. Choice of the CrTK-EcE4PDH activity assay and assay description

The standard TK activity assay needs two supplemental enzymes to be performed [triose phosphate isomerase (TPI) and glycerol 3-phosphate dehydrogenase (G3PD)] and the phosphate sugars xilulose 5-phosphate (Xu5P) and ribose 5-phosphate (R5P) (Figure 39). Unfortunately, these types of sugars are no more commercially available due to their prohibitive cost.

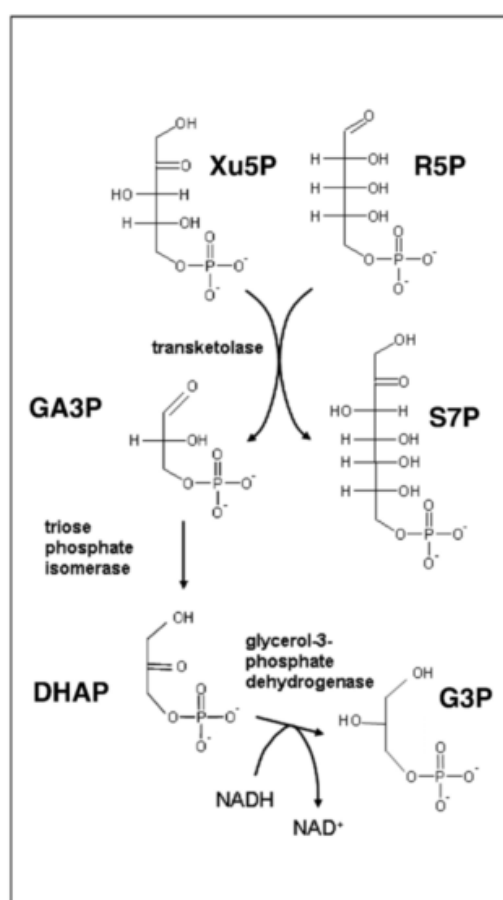


Figure 39. Standard TK activity assay.

For this reason, a number of research groups recently focused their attention on the creation of a cheaper assay: many assays have been set up, among which an amperometric one (Touisni et al., 2014), a UV-visible assay in which the transketolase was immobilized on a metal layer (Touisni et al., 2013) and a pH-based high-throughput method (Yi et al., 2012). For our purposes a coupled assay, where the transketolase activity is measured thanks to the functioning of the enzyme erithrose 4-phosphate dehydrogenase was chosen (Naula et al., 2008, see Figure 40).

The catalytic activity of CrTK was detected spectrophotometrically in a mixture containing 50 mM Tris-HCl (pH 7.9), 0.1 mM TPP, 2.5 mM β -NAD, 15 mM $MgCl_2$, 5 mM $CaCl_2$, 2 mM DL-G3P, 12

mM F6P, 2.7 μ M EcE4PDH. The reaction was started by the addition of CrTK. Activity was calculated from the increase in absorbance at 340 nm (*i.e.*, NADH production) with a Jasco V-550 UV/VIS spectrophotometer. Care was taken to ensure that at these concentrations of substrates, EcE4PDH and CrTK, the rate of NADH production was depending only from the CrTK activity.

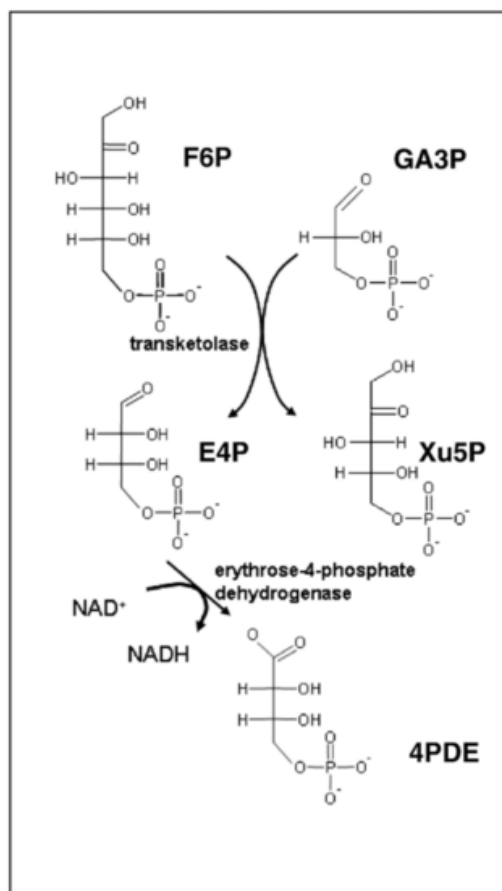


Figure 40. Coupled TK-E4PDH activity assay (adapted by Naula et al., 2008).

14. Activity Measurement for EcE4PDH

The EcE4PDH activity was measured through a spectrophotometric assay, in a reaction mix with 40 mM triethanolamine (pH 8.9), 0.2 mM EDTA, 2.5 mM β -NAD, 3 mM erythrose-4-phosphate (E4P) and 10 μ g EcE4PDH. The assay was started by adding EcE4PDH. Activity was calculated from the increase in absorbance at 340 nm (*i.e.*, NADH production) with a Jasco V-550 UV/VIS spectrophotometer.

15. Reconstitution of the CrTK

Before activity assays, CrTK samples in the apo-form (hereafter CrTK_{apo}) were desalted using NAP5 columns (GE Healthcare) pre-equilibrated with 50 mM Tris-HCl (pH 7.9). CrTK_{apo} (2.9 mg mL⁻¹) was then incubated at 25 °C for variable times (5-300 min) in the presence of 0.7 mM TPP supplemented or not with different concentrations of MgCl₂ ranging from 0.05 to 8 mM (hereafter CrTK_{TPP/Mg} and CrTK_{TPP}, respectively).

16. Treatment with NEM (Alkylation) of CrTK_{TPP}

0.41 mg/mL of CrTK_{TPP} were incubated with the alkylating agent NEM, at concentrations varying from 0 to 500 μ M for 15 minutes at 25°C. Activity of treated CrTK_{TPP} samples was monitored adding it to the reaction mix and recording the Abs at 340 nm as explained above. The inhibition kinetics was also monitored following the activity of the alkylated CrTK_{TPP} for 30 minutes (taking points to 2, 10, 20 and 30 minutes).

17. Treatment with DTNB of CrTK_{TPP}

The number of free thiols in wild-type, glutathionylated and oxidized CrTK_{TPP} was determined spectrophotometrically using 5,5-dithiobis-2-nitrobenzoic acid [DTNB (Zaffagnini et al., 2008)]. CrTK (0.41 mg/mL) was incubated with different concentrations of the alkylating agent DTNB (20, 50 and 200 μ M) for 20 minutes, at 25°C, in 50 mM Tris-HCl (pH 7.9), 1 mM EDTA (the solution without the protein represents the blank). The absorbance at 412 nm was determined. A molar extinction coefficient $\epsilon_{412\text{nm}} = 14,150 \text{ M}^{-1}\text{cm}^{-1}$ for the TNB⁻ anion was used to calculate the number of titrated sulfhydryl groups per monomer under non-denaturing conditions, using as general formula:

$$N_{SH} = \frac{A}{\epsilon \cdot l \cdot C}$$

where the N_{SH} is the number of free thiols that reacted with DTNB; A is the absorbance at 412 nm detected at fixed time (normally 30-45 minutes after DTNB addition); ϵ is the extinction molar coefficient of the TNB⁻, l is the optical length, and C is the enzyme concentration.

An aliquote of all the treated samples of CrTK_{TPP} was tested for the reversibility of the alkylation, adding 30 mM tricarboxyethylphosphine (TCEP, Getz et al., 1999). This reversibility test was performed just for the DTNB-treated protein and not for the NEM-treated ones since this last leads to an irreversible type of alkylation.

18. Treatment with CuCl₂ and Activity Recovery of CrTK_{TPP}

0.41 mg/mL of CrTK_{TPP} was treated with CuCl₂, a specific agent shown to be responsible for disulfide bond formation (Rehder and Borges, 2010). Incubations of 20 minutes with 50 and 250 μ M were set up. After measuring the treated CrTK_{TPP} activity, aliquotes of the CuCl₂-treated proteins were added with 30 mM TCEP to test the reaction reversibility. The inhibition kinetics of the treated enzymes were followed for 45 minutes (taking points to 2, 10, 20, 30 and 45 minutes).

19. Treatment with oxidized DTT and Activity Recovery of CrTK_{TPP}

Inactivation treatments were performed on samples of 0.41 mg/mL CrTK_{TPP} reconstituted under different conditions, by incubations for 180 minutes at 25°C in buffer 50 mM Tris-HCl (pH 7.9), 0.1 mM TPP, 50 mM trans-4,5-dihydroxy-1,2-dithiane (DTTox). The reversibility of the oxidation treatment was assessed by measuring the enzymatic activity after incubation of oxidized CrTK_{TPP} samples for 15 minutes in the presence of 30 mM TCEP.

20. BIO-GSSG Western Blot on CrTK_{TPP}

CrTK_{TPP} was incubated in presence of 0.5, 2 and 5 mM biotinylated GSSG (Bio-GSSG), freshly made as described in (Zaffagnini et al., 2012a). After incubation at 25°C for 30 minutes, half of the sample was transferred into a tube in the presence of 100 mM iodoacetamide (IAM) and 20 mM N-ethylmaleimide (NEM), while the second half was treated with 60 mM reduced DTT and further incubated at 25°C for additional 30 min. Control samples were pre-treated with 100 mM IAM and 20 mM NEM (1 h at 25 C in the dark) followed by a second incubation of 30 min with 2 mM Bio-GSSG. After incubations, each aliquot was further divided and loaded on two 15% poly-acrylamide gels under denaturing conditions. At the end of the run, one gel was Coomassie stained while the second gel was blotted onto a nitrocellulose membrane. Membrane was stained with Red Ponceau, blocked with skimmed milk powder and then incubated overnight at 4°C in the presence of anti-biotin antibodies (Sigma) diluted 1:10,000. The membrane was thoroughly washed prior incubation for additional 3 h at room temperature in the presence of a 1:2000 dilution of the peroxidase-conjugated secondary antibodies. Blot was revealed by chemi-luminescence according to the standard procedure.

21. Treatment with H₂O₂ of CrTK_{TPP}

A 30 minutes-treatment on the 0.41 mg/mL CrTK_{TPP} was performed with 1 mM hydrogen peroxide (H₂O₂, Sigma) dissolved in buffer 50 mM Tris-HCl (pH 7.9).

22. Assays for determining temperature and pH optimum

Different aliquotes of CrTK_{TPP} and CrTK_{TPP/Mg} were incubated for 30 minutes at temperatures ranging from 20 to 60°C prior to activity assay. The activity of CrTK_{TPP} as a function of pH was evaluated by changing the pH of the activity assay buffer (from 6.0 to 9.0 pH units). To disentangle the pH effect on the CrTK_{TPP} activity from the pH effect on the EcE4PDH activity, this experiment was performed even for the EcE4PDH as described above.

Data regarding the temperature dependence have been fitted by an arbitrary sigmoidal function using the Origin 6.1 software package.

23. Determination of Kinetic Parameters

Activity of CrTK_{TPP} as a function of the F6P, TPP and Mg²⁺ concentration, in presence of saturating concentration of the other substrates and excess of EcE4PDH, were fitted by the Michaelis-Menten equation using the Origin 6.1 software package. When the amount of protein was comparable with the concentration of Mg²⁺, a quadratic function has been use to fit the data.

Chapter 2

1. Strain, medium and treatments of *Chlamydomonas* cultures

The *C. reinhardtii* strain used in all the experiments was the wild type 12 (WT12). 10 mL cultures volume were set for every treatment by a 1/60 dilution of a saturated culture. WT12 was cultured in TAP medium (see below for its composition) at 24 °C at a white light intensity of 60 $\mu\text{mol m}^{-2} \text{s}^{-1}$ for 7 days.

Chemical	Stock Concentration	Final Concentration
Tris-HCl (pH 7.0)	-	2.42 g/L
TAP salts	15 g/L NH_4Cl ; 4 g/L $\text{MgSO}_4 \cdot 7\text{H}_2\text{O}$; 2 g/L $\text{CaCl}_2 \cdot 2\text{H}_2\text{O}$	25 mL/L
Phosphate solution	288 g/L K_2HPO_4 ; 144 g/L KH_2PO_4	0.375 mL/L
Hutner's trace elements	-	1 mL/L
Glacial acetic acid	-	1 mL/L

The “Hutner's trace elements” stock solutions present the following composition :

- 1) 25 mM Na_2EDTA ;
- 2) 28 μM $(\text{NH}_4)_2\text{Mo}_2\text{O}_4$;
- 3) 2 mM CuCl_2 and 2 mM EDTA;
- 4) 2.5 mM ZnSO_4 and 2.75 mM EDTA;
- 5) 6 mM MnCl_2 and 6 mM EDTA;
- 6) 20 mM FeCl_3 , 22 mM EDTA and 22 mM Na_2CO_3 .

1 ml of each stock solution was added for each L of culture media.

Treatments were performed at a final concentration:

1. Thiamin (THI, Sigma) at 0.1, 1 and 10 μM ;
2. Hydroxy-ethyl-thiazole (HET, Sigma) at 0.1, 1 and 10 μM ;
3. Missing the hydroxymethylpyrimidine (HMP): (a) 10 μM 2-hydroxymethylpyrimidine (2HXMP, Sigma) and (b) HET and pyrithiamin (PYR, Sigma) at 0.1, 1 and 10 μM were used (Figure 41);
4. as stressors, (a) H_2O_2 (Sigma) at 1 mM for 90 minutes after 7 days of growth and (b) High light intensity, corresponding to 300 $\mu\text{mol m}^{-2} \text{s}^{-1}$ (5-times the normal light intensity), for 7 days were used.

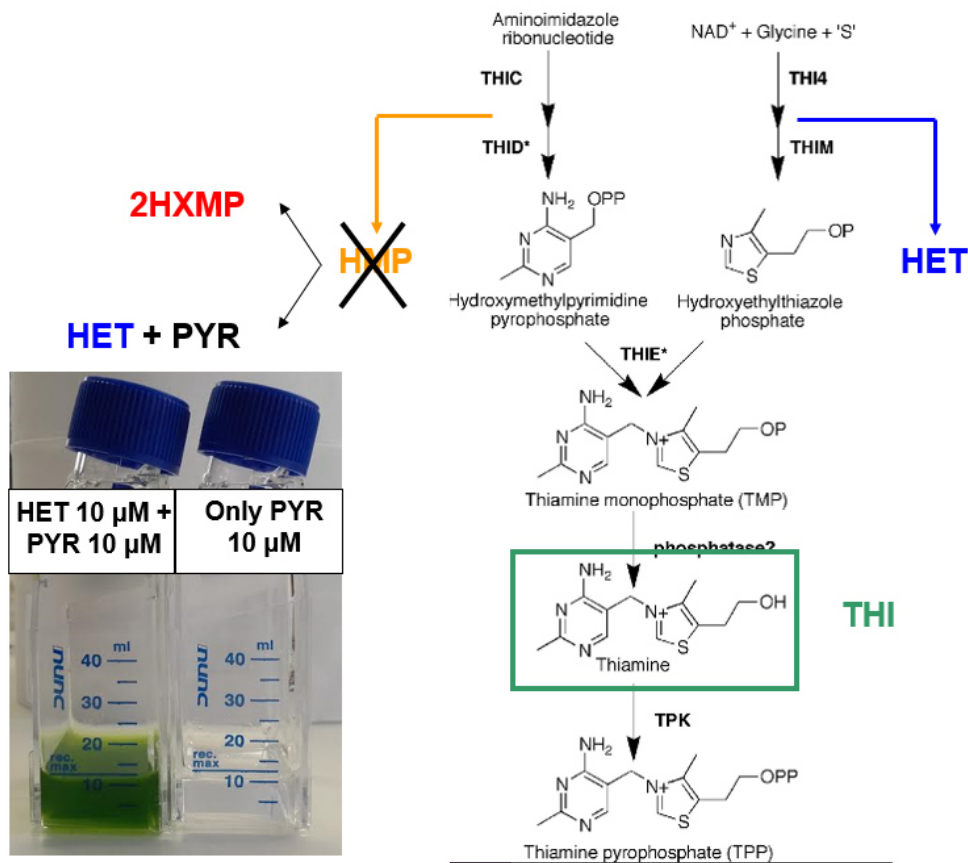


Figure 41. Treatments performed on the *Chlamydomonas* cultures. To note, the treatment with the sole PYR is toxic for cells (flask on the right - no growth), while the addition of HET to the PYR medium allows algae to grow (flask on the left - normal saturated culture).

2. RNA Extraction from *Chlamydomonas reinhardtii*, using the RNAeasy Mini Kit (QIAGEN)

Chlamydomonas cells (WT12 strain) were grown and the culture was harvested at 2,000 g for 10 minutes at 22°C. The cells were broken, vortexing them for a minute with acid-washed glass beads (with a diameter between 425 and 600 μ m, Sigma) in Buffer RLT and β -mercaptoethanol (dilution 1:100 in the Buffer RLT). The lysate was transferred in a “purple” column and centrifuged for 2 minutes at 17,000 g; the supernatant was transferred in a new tube without disturbing the pellet. After an addition of 0.5 volumes of 96-100% ethanol (Sigma), the mixture was moved in a “pink” column and centrifuged for 15 seconds at 8,000 g; the flow-through was discarded. 700 μ L of Buffer RW1 were added in the column and centrifuged for 15 seconds at 8,000 g; the flow-through was discarded. Then 500 μ L of Buffer RPE were added to the column and centrifuged for 15 seconds at 8,000 g; the flow-through was discarded. After repeating this last step (centrifuging for just 2 minutes), the pink column was moved in a new microcentrifuge tube; 40 μ L of RNase-free water were added and centrifuged for 1 minute at 8,000 g for the RNA elution. Finally, RNA concentration was checked using the Nanodrop (considering the ratio 260/280 - it should be around 1.8 for the DNA and around 2.0 for the RNA - and the ratio 260/230 - commonly in the range of 2.0-2.2 for RNA containing samples).

3. DNase treatment of RNA samples, using TURBO DNA-free kit (Ambion)

5 μ L of Buffer 10X, 2 μ L of TURBO DNase and 3 μ L of RNase-free water were added to the 40 μ L RNA sample (for a final volume corresponding to 50 μ L). After an incubation of 30 minutes at

37°C, the reaction was blocked adding 5 µL of Inactivation Buffer and incubating it for 5 minutes at r.t., occasionally mixing. The mixture was centrifuged for 90 seconds at 10,000 g and the supernatant (that contains the RNA) was moved in a new tube. Finally, the RNA concentration was checked again (it is possible that, after the DNase treatment, the RNA concentration is slightly decreased). The RNA was run on a 2% agarose gel to check its purity.

4. cDNA synthesis, using SuperScript III First-Strand Synthesis System for RT-PCR (Invitrogen)

A mix with 2.5 µg of DNase-treated RNA, 1 µL of random examers (Initial concentration: 50 ng/µL), 1 µL of dNTPs (Initial concentration: 10 mM) and nuclease-free water up to 10 µL was prepared. This mixture was incubated for 5 minutes at 65°C and put on ice for (at least) a minute. Then the “cDNA synthesis mix” was prepared (10 µL/each RNA sample: 2 µL of RT Buffer 10X, 4 µL of MgCl₂ with an initial concentration of 25 mM, 1 µL of RNase OUT with an initial concentration of 40 U/µL and 1 µL of SuperScript III RT, having initial concentration of 200 U/µL) and added to each RNA sample. The samples were incubated for 10 minutes at 25°C, then for 50 minutes at 50°C and finally for 5 minutes at 85°C. 1 µL of RNase H was added in each tube and incubated for 20 minutes at 37°C. DNA concentration was determined at the Nanodrop and the DNA quality was checked with a 2% agarose gel.

5. Gene sequences and primer design

All the genes' sequences were found on the data banks Ensembl Plants or Phytozome, while all the primers (Table 1) were designed using Snapgene and ordered by Sigma-Aldrich.

For all the experiments, THI4 has been used as positive control gene. THI4 codifies for the hydroxyethylthiazole (HET) synthase. This gene was used as positive control since its behavior in presence of TPP biosynthesis pathway compounds has been previously characterized in Moulin et al. (2013).

GENE	FORWARD PRIMER localization on the target gene	REVERSE PRIMER localization on the target gene
RACK1 (GBLP)	EXON 2 5'-CGCTCGGAGTCCAACACTACG-3'	EXON 3 5'-GTGTTCCACAGCTTGATGGTCTTG-3'
ACTIN	EXON 7 5'-AAATCGTGCGCGACATCAAG-3'	EXON 8 5'-GAAGGTGGTGTTCGTGGATGC-3'
TRK1	EXON1 5'-GTCGATCTCTCGCGATGAGG-3'	EXON 2 5'-CGGAAGTCTTGATCTGGTC-3'
APX1	EXON 5'-GCAGTTGTTACAAGCGTCATACTG-3'	EXON 5'-GTCGTAGGTGCCGGAATCG-3'
THI4s	EXON 1 5'-AAGACCCTCACCACCGGAA-3'	EXON 1 5'-TCAGTGACATGCCCGAATGA-3'

Table 1. List of the primers that were used in the qRT-PCR/PCR analysis (in RED, the housekeeping genes; in BLACK, the target genes; in LIGHT-BLUE, the control genes).

6. Polymerase Chain Reaction - PCR, using BioTaq (Bioline)

A “Master Mix” was prepared per each sample with 2 μL of NH_4 Reaction Buffer 10X, 0.8 μL of MgCl_2 (Initial concentration: 50 mM), 0.5 μL of dNTPs (Initial concentration: 10 mM), 0.8 μL of forward primer (Initial concentration: 100 μM), 0.8 μL of reverse primer (Initial concentration: 100 μM), 0.6 μL of DMSO (pure), 13.5 μL of nuclease-free water and 0.5 μL of Biotaq (5 U/ μL) (total volume: 19.5 μL). 0.5 μL of DNA were added to each tube (final volume: 20 μL). The PCR was run following the next steps:

- 1) *Initial phase - denaturation: 98°C for 3 minutes; 98°C for 10 seconds;*
- 2) *Annealing: 55°C for 30 seconds (for 35 cycles);*
- 3) *Extension: 72°C for 30 seconds; 72°C for 10 seconds;*
- 4) *End: 4°C forever.*

Finally, a 2% agarose gel was run to check for the length of the amplicons.

Semiquantitative PCR: The semiquantitative PCR was performed following the same protocol written above, but doing 25 cycles instead of 35 cycles.

Gradient PCR: Following the same steps described above, a gradient PCR can be set, establishing, per each sample, a specific annealing temperature (*e.g.*: from 58°C to 65°C).

7. Agarose gel electrophoresis

2% agarose gels were prepared melting agarose (Sigma) in Tris-Acetate-EDTA (TAE) buffer [40 mM Tris, 20 mM acetate, 1 mM EDTA (all Sigma products)] and then adding 0.3 mg/mL ethidium bromide (Initial concentration: 10 mg/mL, Sigma).

6 μL of ladder (marker) were loaded - if DNA: Hyperladder 100 bp (Bioline), if RNA: Hyperladder 1 Kbp (Bioline) in each gel. All the samples were loaded with Loading Buffer 5X (Bioline) - 4 μL of RNA + 1 μL of Loading Buffer 5X or 20 μL of DNA (after PCR) + 5 μL of Loading Buffer 5X.

The gel was run for 45 minutes at 100 V before being imaged.

8. Real Time PCR - or quantitative PCR (qPCR), using the SYBR Green JumpStart Taq Ready Mix (Sigma)

The cDNA samples were diluted to a final concentration corresponding to ~ 100 ng/ μL . 20 μL of “Working Solution 25X” (solution with the couple of primers) was prepared, with 1.25 μL of Forward primer (Initial concentration: 100 μM ; Final concentration: 6.25 μM), 1.25 μL of Reverse primer (Initial concentration: 100 μM ; Final concentration: 6.25 μM) and 17.5 μL of nuclease-free water. Then 25 μL of the “Master Mix” was prepared per each sample, with 12.5 μL of SYBR Green JumpStart Taq Ready Mix, 1 μL of “Working Solution 25X”, 1 μL of diluted cDNA and 10.5 μL of nuclease-free water. The qPCR was run following the next steps: 5 minutes, at 95°C - initial activation step (denaturation); 20 seconds, at 95°C - denaturation; 20 seconds, at 55°C and 30 seconds, at 72°C- annealing, extension and read fluorescence; final (optional) step at 4°C - only if the products will be run on a gel. The results were analyzed with the comparative method, using RACK1 and ACTIN as housekeeping genes, and the significance of all the data was calculated using the Student’s T-TEST (the two-tailed one, third type - also called heteroscedastic type). The significance of a result was based on the Reliable Change Index (RCI), where: p value ≤ 0.05 : *; p value < 0.01 : **; p value < 0.001 : ***.

Results

Chapter 1

1. Quaternary structure of apo- and holo-forms of CrTK

The quaternary structure of transketolases varies among different organisms (monomeric or oligomeric - Lindqvist et al., 1992; Gerhardt et al., 2003). In order to investigate the structure composition of CrTK, different analysis were set up: (I) SDS-PAGE, (II) LC-ESI-MS, (III) gel filtration experiments and (IV) DLS measurements. All these investigations were performed on the apo-form of CrTK.

The SDS-PAGE (imaged in Materials and Methods - Figure 37) showed that the monomer of the CrTK possesses a molecular weight around 75 KDa. This was then confirmed through mass spectrometry, which determined that the molecular weight of the CrTK monomer is exactly 75170 Da (Figure 42), in excellent agreement with what expected from the primary sequence of the recombinant CrTK used in this work (See Figure 33 in Materials and Methods). Analyzing the protein by size-exclusion chromatography (Figure 43), a single symmetric peak with an apparent molecular mass of 156 KDa appeared concomitantly with the CrTK elution, suggesting an homodimeric state for the protein in solution. The dimericity of CrTK in solution was further confirmed by DLS measurements (Table 2), that reported a hydrodynamic radius of 5.1 ± 0.1 nm, corresponding to an apparent molecular mass of 151.6 ± 7.4 KDa. DLS analysis was also exploited to evaluate the effect of the cofactors (*i.e.* TPP and Mg^{2+}) on the CrTK structure (Table 2). CrTK incubated with the sole TPP (called hereafter CrTK_{TPP}) showed a very similar hydrodynamic radius (5.0 ± 0.2 nm) and molecular weight (146.1 ± 14 KDa). Only in the case of the CrTK reconstituted with both the TPP and the Mg^{2+} (called hereafter CrTK_{TPP/Mg}) these two parameters seemed to be slightly higher: in fact, the resulted hydrodynamic radius was 5.6 ± 0.2 nm, corresponding to a molecular mass of 191.5 ± 17.8 KDa. To exclude the formation of any kind of aggregates in solution, this last experiment was repeated using a smaller concentrations of CrTK, TPP and Mg^{2+} , but keeping the same ratios among all these components: even in this last case, the hydrodynamic radius and the molecular mass of the CrTK_{TPP/Mg} resulted larger (respectively, 5.4 ± 0.8 nm and 175.4 ± 54.8 KDa) than the values reported for apo-CrTK and CrTK_{TPP}.

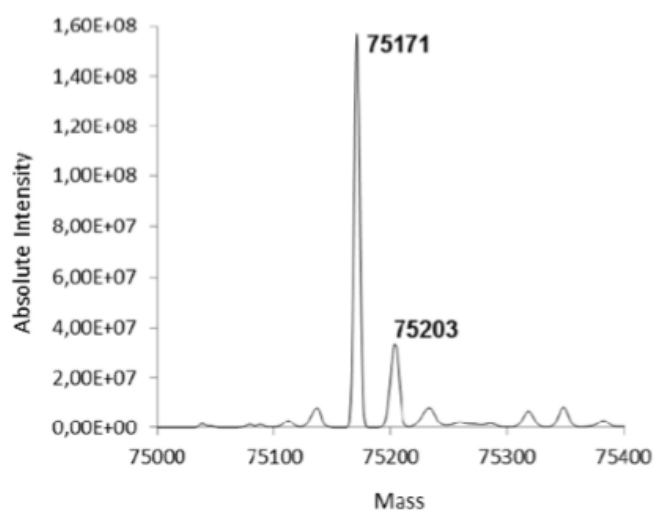


Figure 42. Deconvoluted ESI mass spectrum of the Apo-CrTK derived from the LC-ESI-MS analysis. The most intense signal was attributed to the unmodified CrTK form (m/z values for $[M + H]^+$ of 75,171) in agreement with the theoretical molecular weight of recombinant CrTK. The second peak, in terms of intensity (m/z values for $[M + H]^+$ of 75,203), showed a mass increment of 32 Da, which could be attributed to the oxidation of two methionines.

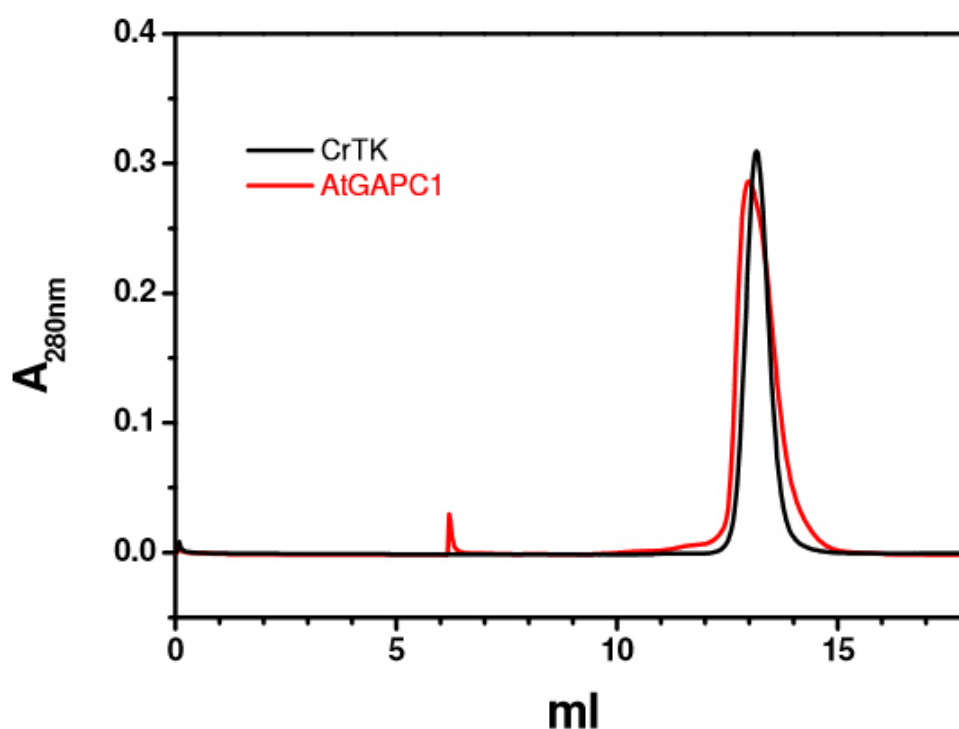


Figure 43. Gel filtration chromatography. To evaluate the molecular mass of the enzyme, CrTK solution (12 μ M) was loaded on a Superdex 200 column and eluted in buffer 50 mM Tris-HCl (pH 7.5), 150 mM KCl and 1 mM EDTA. The elution profile of CrTK (black line) was superimposed to the elution profile of the well-known tetrameric enzyme AtGAPC1 (160 kDa, red line). Since the molecular mass of the CrTK monomer is 75 kDa, this result indicates that the apo-CrTK is a homodimer.

CrTK (mg/mL)	TPP (mM)	Mg ²⁺ (mM)	Rh (nm)	M.W. (KDa)
3.65	\	\	5.1 \pm 0.1	151.6 \pm 7.4
2.9	0.7	\	5.0 \pm 0.2	146.1 \pm 14.0
2.9	0.7	8	5.6 \pm 0.2	191.5 \pm 17.8
0.5	0.12	1.3	5.4 \pm 0.8	175.4 \pm 54.8

Table 2. Dynamic Light Scattering (DLS) analysis on apo-CrTK, CrTK_{TPP} and CrTK_{TPP/Mg} (the last one, at two different concentrations of protein, TPP and Mg²⁺, but with the same ratios among the components). Rh = hydrodynamic radius.

2. Crystal structure of CrTK_{apo} and CrTK_{TPP/Mg}

The crystallization of CrTK_{apo} and CrTK_{TPP/Mg} (Table 3) led to the production, for both the forms, of different polymorphs, belonging to C2 or P1 space groups. A crystal for each form was selected for the final structure determination, considering the resolution and the data quality. Although differing for unit cell dimensions, crystals of CrTK and CrTK_{TPP/Mg} both belong to the C2 space group and show a similar Matthews coefficient (2.32 and 2.42, respectively) and solvent content (47.1 % and 49.2 %, respectively).

	CrTK _{TPP/Mg}	CrTK _{apo}
<i>Data collection</i>		
Unit cell (Å)	201.49, 75.93, 103.76, 90.00, 109.99, 90.00	165.21, 74.31, 133.72, 90.00, 119.30, 90.00
Space group	C2	C2
Resolution range* (Å)	97.52 - 1.74 (1.82-1.74)	116.60 – 1.58 (1.64 – 1.58)
Unique reflections	114961	193102
Completeness* (%)	76.2 (64.6)	98.1 (97.9)
R _{merge} *	0.053 (0.240)	0.049 (0.567)
I/σ(I)	11.9 (1.7)	12.7 (1.9)
Multiplicity	2.1	3.3
<i>Refinement</i>		
Resolution range* (Å)	97.52- 1.74 (1.78-1.74)	116.61 – 1.58 (1.62 – 1.58)
Reflection used	109213 (6421)	180084 (13980)
R _i /R _{free} *	15.9/19.9 (21.3/25.4)	15.9/19.2 (30.4/31.8)
rmsd from ideality (Å, °)	0.02, 2.04	0.021, 1.97
<i>N° atoms</i>		
Non-hydrogen atoms	10815	11118
Protein atoms	10223	10219
Solvent molecules	538	841
Hetero atoms	54	58
<i>B value (Å²)</i>		
Mean	17.7	26.2
Wilson plot	25.7	28.8
Protein atoms	17.5	26.1
Hetero atoms [§]	16.1	47.4
Solvent molecules	22.27	30.7
<i>Ramachandran plot (%)</i>		
Most favoured	97.7	97.1
Allowed	2.3	2.2
Disallowed	0.0	0.7

*The values in parenthesis refers to the last resolution shell;

§ The hetero atoms are 2 TPP molecules and 2 Mg²⁺ in CrTK_{TPP/Mg} and 1EDO (etilen glicole) molecule in CrTK_{apo}.

Table 3. Data collection and refinement statistics for CrTK_{apo} and CrTK_{TPP/Mg} structure.

In both crystals, the asymmetric unit contains two protein chains related by a non-crystallographic two fold axis and forming a physiological V-shaped homodimer (Figure 44). For each monomer, 683 amino acids are detectable. In both the forms, the electron density map starts with residue Ser49, while the last C-terminal residue (*i.e.* His718) can be modeled only in one subunit of CrTK. To avoid misinterpretation with previous studies (Zaffagnini et al., 2012a; Michelet et al., 2013), amino acids are numbered following the full-length enzyme sequence (mature enzyme plus chloroplast transit peptide, UniProt Identifier : A8IAN1).

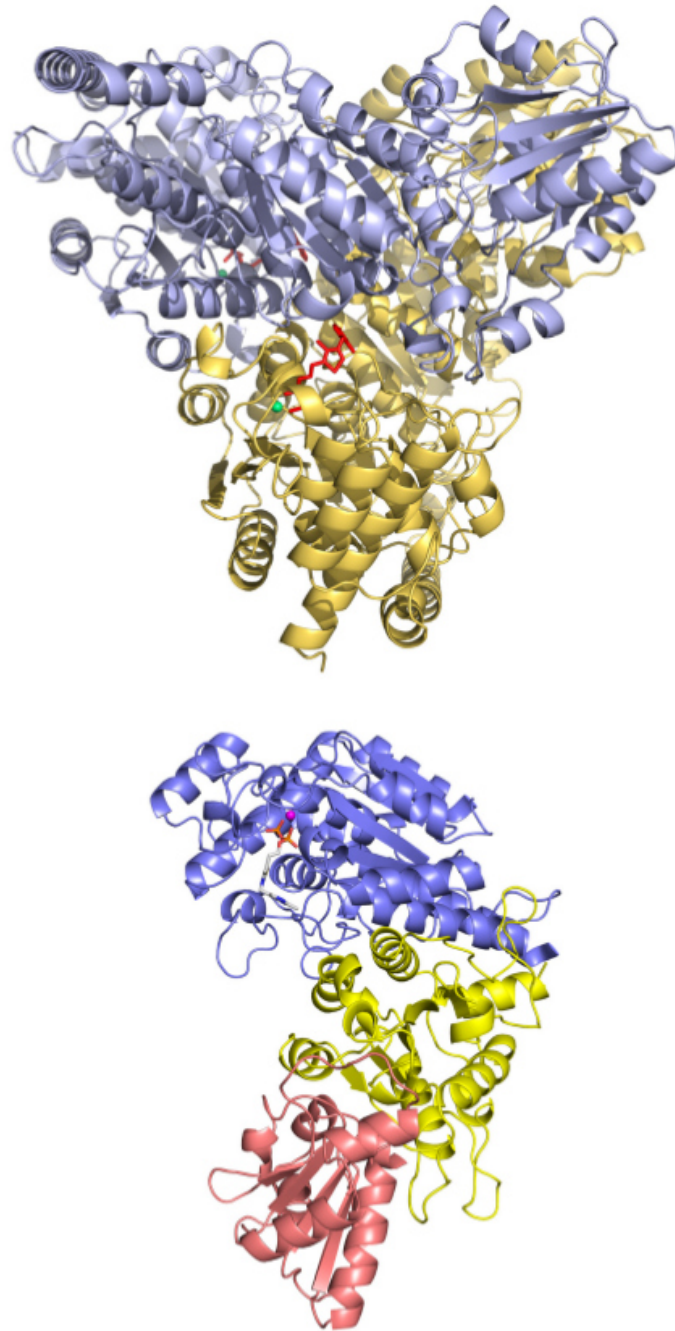


Figure 44. Ribbon representation of CrTK structure. Above: View of the V-shaped dimer including the cofactor and the Mg^{2+} ion. The two monomers are differently colored. Below: View of the single monomer including the TPP and the Mg^{2+} . The three domains are the N-terminal domain (in light blue), the middle domain (in yellow) and the C-terminal domain (in salmon).

In both the structures, the TPP (in red) is represented as sticks and the Mg^{2+} (in green) is represented as sphere. The figure was prepared with Pymol (The PyMOL Molecular Graphics System, Version 1.5.0.5 Schrödinger, LLC).

As previously reported for other TK structures (Lindqvist et al., 1992; Gerhardt et al., 2003), each CrTK monomer is composed of three consecutive α/β domains, all containing a central five stranded β -sheet. The N-terminal domain (residues 49-372) folds in a parallel β -sheet composed of strands β 1, β 2, β 3, β 6 and β 7 surrounded by several α -helices (α 1- α 12). It binds the Mg^{2+} ion and the pyrophosphate moiety of TPP, therefore it is called PP domain (Figure 44, light blue). The middle

domain (residues 373-582) is also composed by a parallel β -sheet (β 9- β 13) embedded in several helices from α 13 to α 18. This domain binds the cofactor pyrimidine ring of the adjacent monomer and is called Pyr domain (Figure 44, yellow). The C-terminal domain (residues 583-718) is the smallest domain and it folds in a mixed β -sheet with four parallel strands (β 16- β 19, one antiparallel strand (β 15), and several α -helices (α 19 to α 25). This domain is not involved either in dimer interface or in the cofactor binding (Figure 44, salmon). The CrTK structure possesses long α -helix regions, but it also contains several short 3_{10} and π helices connecting diverse secondary structural elements.

3. CrTK in comparison with other TK structures

The tridimensional structure of TK from *Zea mays* (PDB code 1ITZ; Gerhardt et al., 2003) was the only TK structure from a photosynthetic organism present in PDB. CrTK shares with this protein a sequence identity of about 65%. Superimposition of C α atoms, based on secondary structural matching, results in a Root Mean Square Deviation (RMSD) of 0.864 Å on 1320 aligned residues (whole dimer) and 0.821 on 664 aligned residues (single monomer), indicating that the TK structure is highly conserved between the two organisms. While the internal β -sheets of N-terminal and middle domains are well superimposed, some deviations can be observed in correspondence of the solvent exposed helices α 12 and α 13 and the C-terminal domain. Moreover, the N- and the C-terminal domains of the two structures superimpose using a least square fit, with RMSD of 2.881 Å (323 C α atoms) and 1.040 Å (133 C α atoms), respectively, while the middle domains with a lower RMSD of 0.764 Å. This indicates a slight different bending angle between the two enzymes.

In the case of the yeast enzyme (PDB code 1TRK; Lindqvist et al., 1992), the sequence identity with CrTK is about 53%. The RMSD from the superimposition of C α atoms increases to 1.179 Å on 1293 aligned residues (whole dimer) and 1.208 Å on 623 aligned residues (single monomer) respect to the previous comparison. Also in this case, deviations are observed in correspondence of some exposed regions, in particular in the region including helices α 10, α 11, α 12 and α 13.

4. CrTK_{TPP/Mg} structure reveals a number of interactions between TPP, Mg²⁺ and active site residues

In the CrTK_{TPP/Mg}, each subunit binds one TPP and one Mg²⁺ ion in the active site cleft located at the dimer interface. The TPP and the Mg²⁺ are set in place by hydrogen bonds, involving residues of both subunits, and by water molecules (Figure 45 and Table 4).

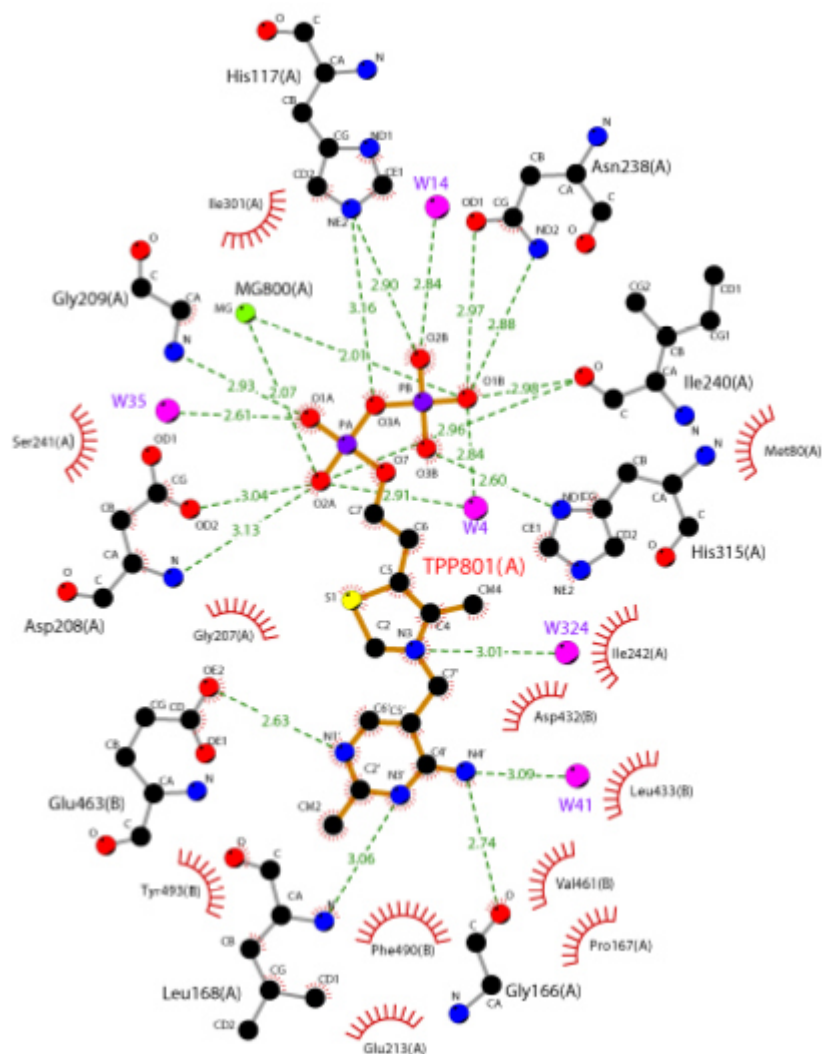


Figure 45. Bi-dimensional diagram of interactions between TPP and CrTK residues. Protein residues, TPP, Mg^{2+} and waters are shown in ball-and-stick representation. Hydrogen bonds are shown as green dotted lines and their length is indicated in Å, while the spoked arcs represent protein residues making non-bonded contacts with the ligand. Atoms colors: black (C), blue (N), red (O), yellow (S) and purple (P). The image was prepared by using the software Ligplot+ v1.4.5 (Wallace et al., 1996).

Cofactor atoms	Protein residue or Mg ion or Water molecule atoms	Chain (cofactor/residue)	Distance (Å)	Chain (cofactor/residue)	Distance (Å)
O1B	Asn238 ND2	A/A	2.88	B/B	2.76
	Asn238 OD1	A/A	2.97	B/B	2.09
	Ile240 O	A/A	2.98	B/B	2.94
	Mg800 MG	A/A	2.01	B/B	2.03
	W4 O	A/W	2.84	/	/
	W216 O	/	/	B/W	2.91
O2B	His117 NE2	A/A	2.90	A/A	2.89
	W14 O	A/W	2.84	/	/
	W217 O	/	/	B/W	3.10
	W421 O	/	/	BW/	3.12
O3B	His315 ND1	A/A	2.60	B/B	2.54
O3A	His117 NE2	A/A	3.16	B/B	3.13
O1A	Gly209 N	A/A	2.93	B/B	2.92
	W35 O	A/W	2.61	/	/
	W128 O	/	/	B/W	2.66
O2A	Mg800 MG	A/A	2.07	B/B	2.08
	W4 O	A/W	2.91	/	/
	W216 O	/	/	B/W	3.02
	Ile240 O	A/A	2.96	B/B	2.98
	Asp208 OD2	A/A	3.04	B/B	2.97
	Asp208 N	A/A	3.13	B/B	3.21
N3	W324 O	A/W	3.01	/	/
N4'	Gly166 O	A/A	2.74	B/B	2.75
	TPP801 C2	A/A	3.18	B/B	
	W41 O	A/W	3.09	/	/
	W334 O	/	/	B/W	3.23
N3'	Leu168 N	A/A	3.06	B/B	3.12
N1'	Glu463 OE2	A/B	2.63	B/A	2.70
MG	Asp208 OD2	A/A	2.08	B/B	1.99
	Asn238 OD1	A/A	2.2	B/B	2.19
	Ile240 O	A/A	2.07	B/B	2.11
	W4 O	A/W	2.13	/	/
	W216 O	/	/	B/W	2.15
	TPP801 O1B	A/A	2.01	B/B	2.03
	TPP801 O2A	A/A	2.07	B/B	2.08

Table 4. Intermolecular interactions and distances between cofactors, protein residues and water molecules. The distance cut-off was set to 3.2 Å.

The phosphate groups of the TPP pyrophosphate moiety are stabilized by the N-terminal domain of one subunit, while the pyrimidine and the thiazolium rings interact with the middle domain residues of the other subunit (Figure 46). Both rings are stabilized in the active site mainly by hydrophobic interactions: the thiazolium ring interacts with the side chains of Leu168 and Ile242 of the same subunit and Leu433 of the adjacent subunit, while the pyrimidine ring is stacked between Leu168 of

the same subunit and Phe490 of the adjacent subunit (Figure 46). Moreover, the hydrophobic cavity is also completed by Pro167, Val461, Leu433, Phe487 and Tyr493 from the two subunits. The N1 nitrogen atom of the pyrimidine ring is hydrogen bonded to the carboxyl oxygen OE2 of the strictly conserved residue Glu463 [Figure 46, and Table 4 (Kern et al., 1997; Nauton et al., 2016)]. This interaction is fundamental to promote the TPP activation by stabilizing the 4'-imino-1',4'-dihydropyrimidine tautomer of the cofactor. In addition, the N4 atom of the pyrimidine ring forms an intramolecular interaction with the C2 carbon of the thiazolium ring (Figure 46 and Table 4) which favor the V-like conformation of TPP after binding and the C2 deprotonation required for catalysis (Gerhardt et al., 2003; Pletcher and Sax, 1972).

Mg²⁺ shows an octahedral coordination with six oxygen atoms, belonging to the pyrophosphate groups of TPP (O1B and O2A), the carboxylic group of Asp208 (OD2), the amide group of Asn238 (OD1), the main chain carbonyl group of Ile240 and a water molecule (Figure 46). This last molecule (W4 in chain A and W216 in chain B) is in turn stabilized by the two metal ligands Asp208 and Asn238, the carbonyl group of Asp236 and another water molecule (W5 in chain A and W419 in chain B).

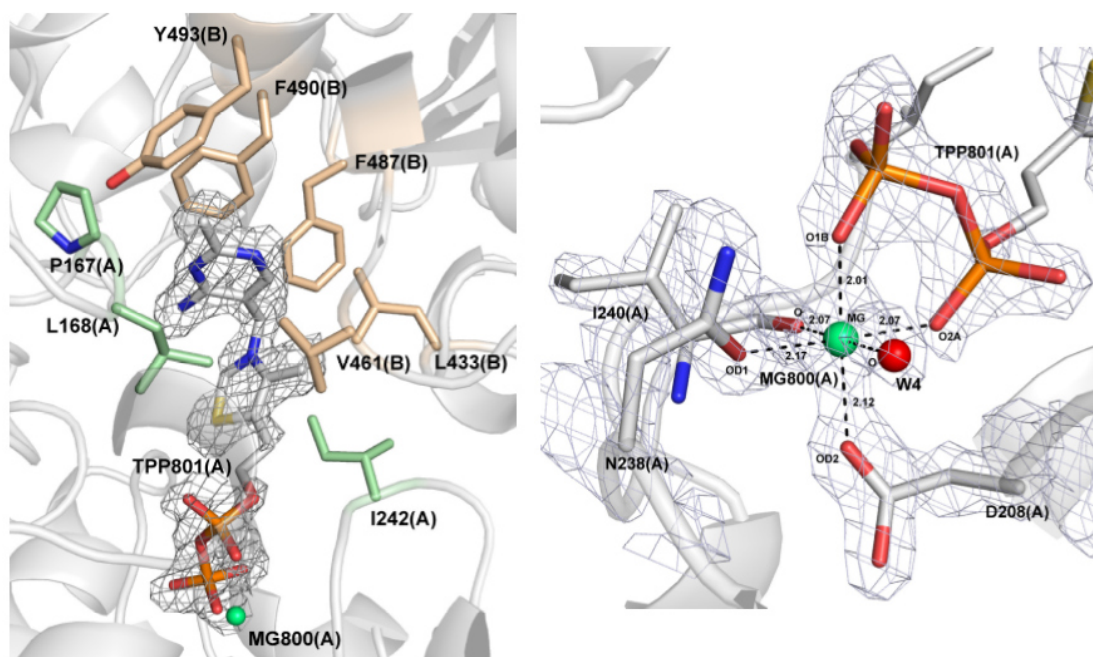


Figure 46. Hydrophobic interactions of TPP and coordination site of Mg²⁺ ion. Left: Protein residues shown in sticks of both subunits (A in light-green, B in pale brown) stabilizing by hydrophobic interactions the pyrimidine and the thiazolium rings of TPP. Right: The Mg²⁺ ion shows an octahedral coordination with six oxygen atoms as electron donors. Mg²⁺ ion is represented as sphere, the ligands as ball-and-stick. Atoms colors: grey (C), blue (N), red (O) and orange (P).

5. Comparison between CrTK_{apo} and CrTK_{TPP/Mg} structures

In the CrTK_{apo}, no electron density for both TPP and Mg²⁺ was observed. By superimposing C α atoms of CrTK and CrTK_{TPP/Mg} monomers (chains A and B) and dimers, RMSD of 0.343 Å and 0.399 Å (on 667 and 668 superimposed atoms) and 0.422 Å (on 1335 superimposed atoms) were observed, respectively. Despite the high similarity between these two forms, in the CrTK two regions

ranging between residues 239-247 and 433-437 are completely deprived of electron density, indicating that these regions are likely disordered and flexible (Figure 47-A). In CrTK_{TPP/Mg} structure, both regions are involved in TPP and Mg²⁺ binding (Figure 47-B); the main chain carbonyl group of Ile240 and pyrophosphate O1B atom of the TPP participate in the coordination of Mg²⁺ ion (Figure 47 and Table 4) while the side chains of Ile242 and Leu433 stabilize by hydrophobic interaction the TPP aromatic rings. CrTK structure shows that TPP is replaced by several water molecules located in the region of phosphate groups (W214, 450, 526, 557 and 751 in chain A and W366, 493 and 643 in chain B) and pyrimidine ring (W284, 496 and 559 in chain A and W172, 300 and 530 in chain B), whereas the Mg²⁺ ion site is empty (Figure 47-C). These water molecules contribute, mainly by hydrogen bonds, to the stabilization of active site residues lying almost in the same position in the CrTK_{TPP/Mg} structure, except for the two protein portions mentioned above. Both the protein regions found to be disordered in CrTK structure are also involved in dimer interface in CrTK_{TPP/Mg} structure. Indeed, Ser241, Ile242 and Asp243 of one subunit interact with the carboxylate group of Asp432, the main chain of Ala434 and the amino group of Arg458 of the other subunit (Figure 47-D). The absence of TPP probably induces a disorder in the region from residues 239 to 247, causing the impairment or eventually the loss of the hydrogen bonds formed with residues 433-437 of the other subunit. In consequence, also this second region more exposed to the solvent becomes flexible and disordered. To further investigate whether the presence/absence of TPP/Mg²⁺ (*i.e.* absence/presence of disordered regions) influences the protein stability, the thermal-induced denaturations of CrTK and CrTK_{TPP/Mg} were investigated. Protein activities have been measured after 30 minutes-exposure to increasing temperature ranging from 20 °C to 60 °C. As shown in Figure 48, CrTK had a T₅₀ (temperature causing 50% inactivation) of around 37°C, while this value was shifted to ~45 °C for CrTK_{TPP/Mg}. This indicated that the presence of TPP/Mg²⁺ in the active site stabilized the enzyme when exposed to high temperatures, suggesting that a significant decrease of the disorder/flexibility is due to TPP and Mg²⁺ binding.

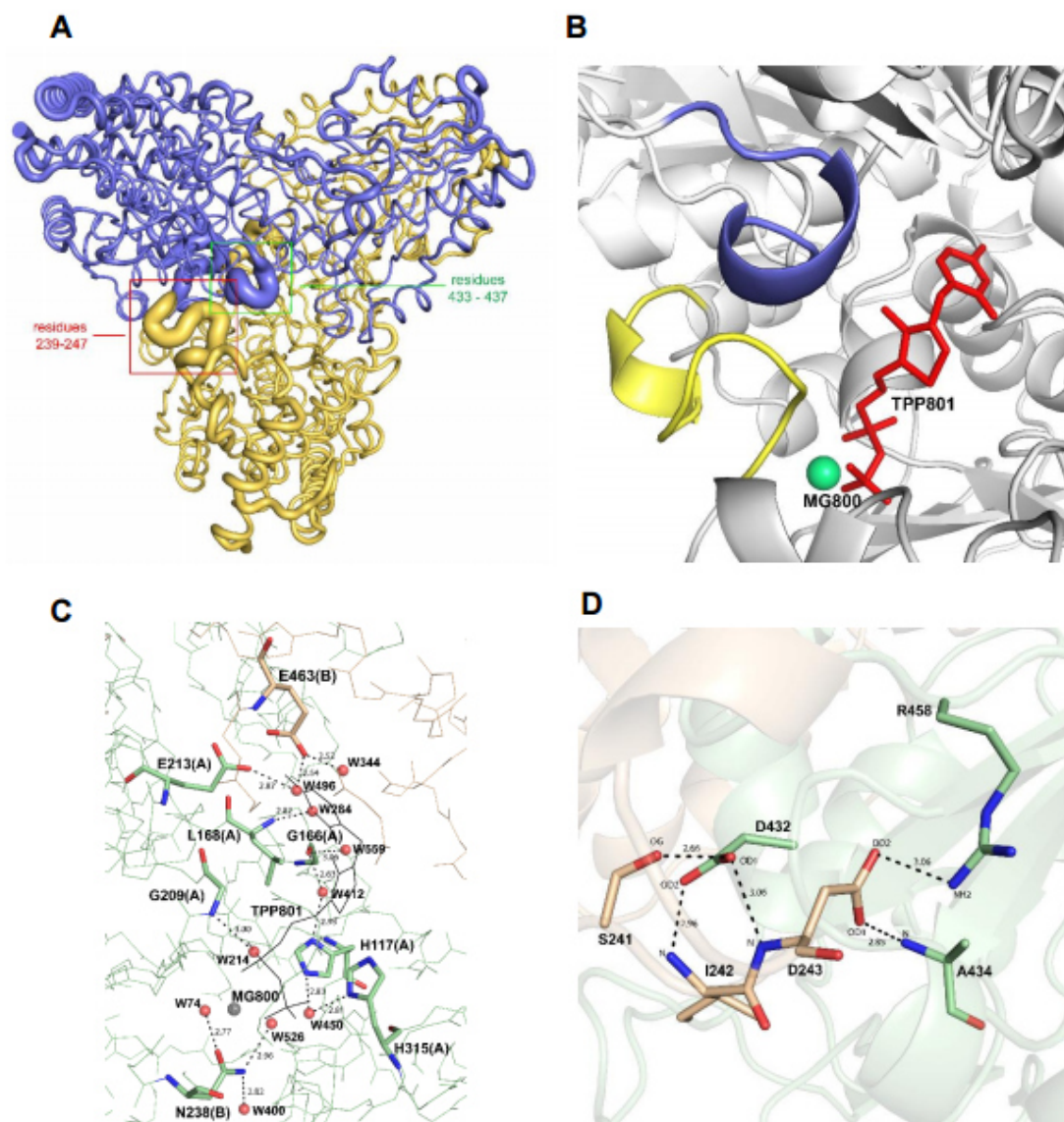


Figure 47. Comparison between CrTK and CrTK_{TPP/Mg} structures. A) Representation of the CrTK dimer structure. The thickness is correlated to the atom thermal factor (B). The highlighted protein regions (239 - 247 and 433 - 437) are disordered and flexible. B) CrTK_{TPP/Mg} structure reveals that the same protein regions have an ordered conformation and interact with TPP and Mg ion. C) CrTK active site structure showing that several water molecules occupy the position of TPP in CrTK_{TPP/Mg} structure (represented by thin lines in grey) and stabilize catalytic residues by hydrogen bonds. D) Dimer interface in CrTK_{TPP/Mg} structure showing the interactions between the residues belonging to regions 239 - 247 and 433 - 437, disordered in CrTK structure. The figure was prepared by Pymol (The PyMOL Molecular Graphics System, Version 1.5.0.5 Schrödinger, LLC).

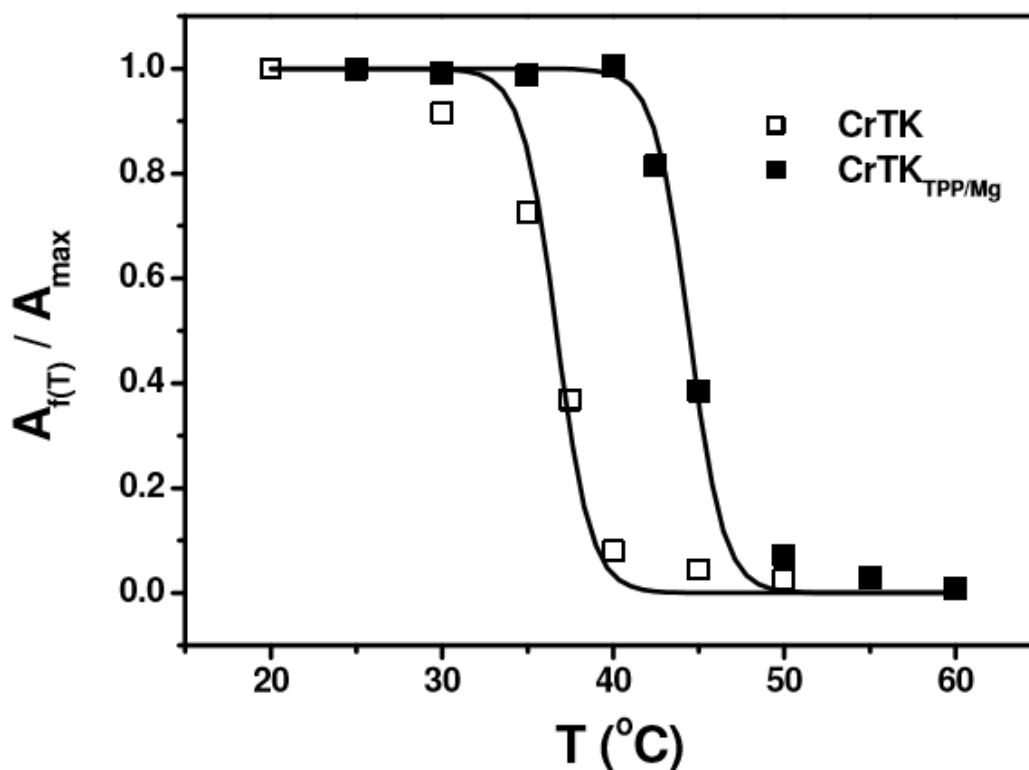


Figure 48. Thermal stability of CrTK and CrTK_{TPP/Mg}. CrTK samples incubated for 3 h in the absence (CrTK, open squares) or presence (CrTK_{TPP/Mg}, filled squares) of 8 mM MgCl₂, 0.7 mM TPP, were exposed for 30 min to temperature ranging from 25 to 60 °C. The residual activity was measured as described in Materials and Methods. Data were normalized to the maximal activity of the control (i.e. samples incubated at 25 °C).

6. pH optimum

6.1 Determination of the pH optimum for the EcE4PDH

Since all the spectrophotometric activity assays were performed using the EcE4PDH (erithrose 4-phosphate dehydrogenase from *E. coli*) as coupled enzyme, the pH to which this enzyme had the highest activity was measured in function of the pH, determining its pH optimum in a range from 6.0 to 9.0 pH units. As shown in the Figure 49, the EcE4PDH exhibited its maximal activity when the pH is around 8.0.

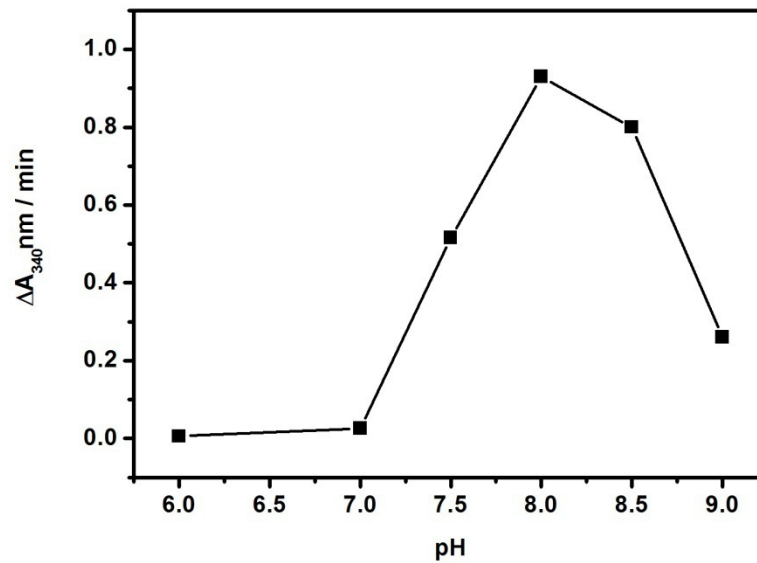


Figure 49. Activity of EcE4PDH as a function of pH. The assay was performed in buffer 50 mM Tris at the indicated pH, 15 mM MgCl₂, 5 mM CaCl₂, 3 mM Erithrose 4-phospate, 2.5 mM β-NAD. The reaction was started by adding 10 μg/ml of EcE4PDH.

6.2 Comparison between CrTK and EcE4PDH pH dependence

The CrTK pH dependence was established incubating a number of aliquotes of protein at different pHs (from 6.0 to 9.0 pH units): as represented in the Figure 50, the CrTK pH optimum is set around 8.0 pH units, concordingly with the pH value (ranging from 7.9 to 8.0) existing in the chloroplasts' stroma upon illumination, when the Calvin cycle enzymes are active, and with the pH optimum of other transketolases belonging to other organisms (see Table 5, <http://www.brenda-enzymes.org/>). Despite these observations, the CrTK possesses the same pH optimum of the EcE4PDH (Figure 49). This could mean that, while the influence of the pH on the CrTK was measured, a strong contribute was due to the EcE4PDH pH dependence (which is an obviously unsuppressible factor, since we always use this coupled assay to measure the CrTK activity).

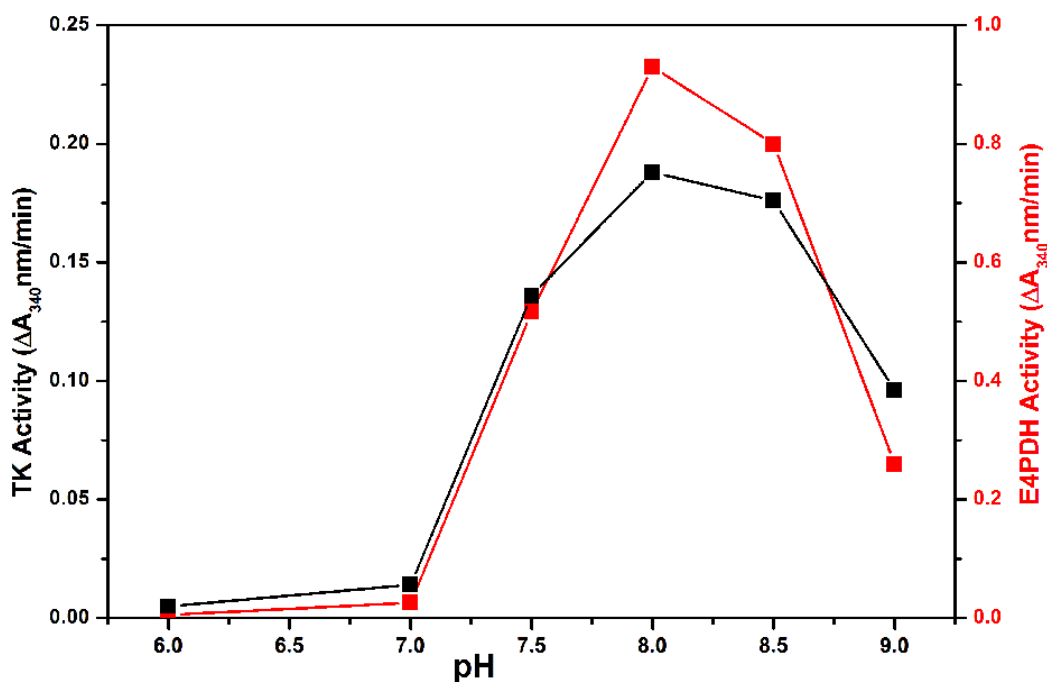


Figure 50. Dependence of CrTK and EcE4PDH activities from the pH levels.

Organism	pH optimum
<i>Escherichia coli</i>	7.0
<i>Candida utilis</i> (yeast)	7.8
<i>Spinacia Oleracea</i>	7.5-7.6
<i>Homo sapiens</i>	7.6-8.0

Table 5. pH optimum of transketolases from diverse other organisms (from <http://www.brenda-enzymes.org/>).

7. Magnesium and TPP role in the reconstitution of the fully active CrTK

The reconstitution of the holo TKs isolated from different organisms always showed a strong dependence from their divalent cation (Mg^{2+} or Ca^{2+}) and TPP (Heinrich et al., 1972; Jung et al., 1988; Sprenger et al., 1995). Since the crystallization showed that the purified CrTK is in its apo-form (during the purification, the TPP and Mg^{2+} are lost), reconstitution of the holo-enzyme is absolutely necessary to study its activity. For this reason, samples of apo-CrTK were incubated at 25°C containing 50 mM Tris-HCl (pH 7.9), 0.7 mM TPP and 8 mM $MgCl_2$. As the Figure 51 shows, the reconstitution of the CrTK is a very slow process, which can be considered complete about after 3 hours of incubation with both the cofactors TPP and Mg^{2+} .

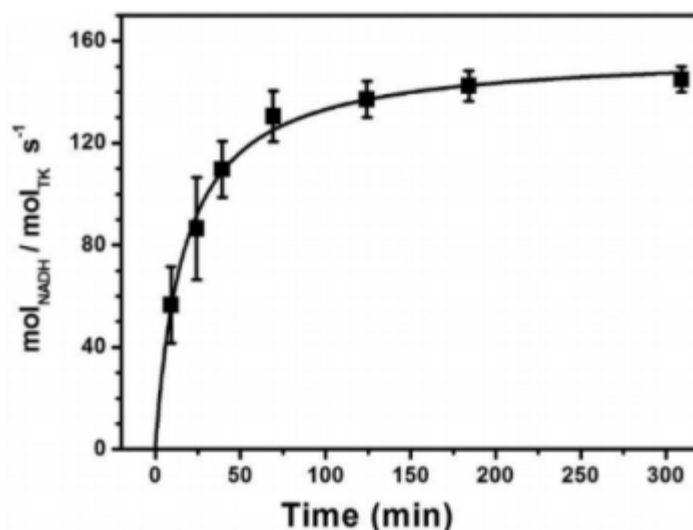


Figure 51. Reconstitution of CrTK needs about three hours to be completed.

In addition, the process of reconstitution was finely studied varying a number of parameters, among which the Mg^{2+} content.

Therefore, the CrTK catalytic activity was analyzed in presence of different Mg^{2+} concentrations in the reconstitution step, in presence of saturating TPP. Samples of apo-CrTK were incubated at 25°C in a buffer containing 50 mM Tris-HCl (pH 7.9), 0.7 mM TPP and diverse $MgCl_2$ concentrations, ranging from 0 to 8 mM. After 3 hours, the activity was evaluated with the coupled assay described in Materials and Methods. As shown in Figure 52, the activity of $CrTK_{TPP/Mg}$ was strictly dependent upon Mg^{2+} content, and the enzyme reaches its full activation when $Mg^{2+} \geq 1$ mM (~ 150 - 160 mol_{NADH}/mol_{TK} s⁻¹). By contrast, the activity of the $CrTK_{TPP}$ was 40 mol_{NADH}/mol_{TK} s⁻¹ (Figure 52, white square), a value four times lower compared to the $CrTK_{TPP/Mg}$. In agreement with the studies in the yeast TK (Eganand Sable, 1981), when $CrTK_{TPP}$ is not pre-incubated in the presence of Mg^{2+} , the enzyme exhibits a reduced activity even if exposed to saturating concentrations of this cation during the activity assays.

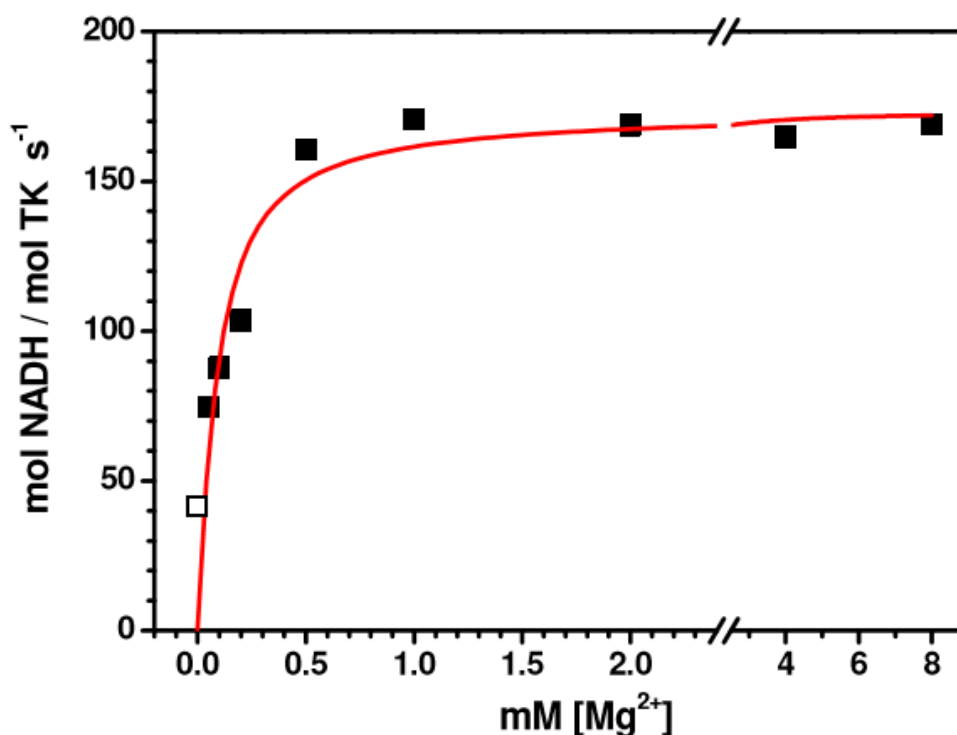


Figure 52. Reconstitution of the CrTK_{TPP/Mg} active enzyme. Activities of CrTK samples reconstituted with saturating TPP and different [Mg²⁺] was determined following the procedure described in Materials and Methods. The reaction was started with the addition of enzyme to a final concentration of 20 nM. From the experimental data a half-maximal saturation concentration value of ~70 μ M for Mg²⁺ could be estimated. The empty symbol is referred to CrTK_{TPP} (absence of Mg²⁺), corresponding to 40 mol_{NADH}/mol_{TK} s⁻¹.

Since the coupled assay used to measure the CrTK activity implied the use of an high content of Mg²⁺ and Ca²⁺ (Naula et al., 2008), the dependence of CrTK_{TPP} and CrTK_{TPP/Mg} activity was determined as a function of the Mg²⁺ concentration in an assay buffer deprived of Ca²⁺ ions. As shown in Figure 53 (black squares), CrTK_{TPP/Mg} is not responsive to variable amount of Mg²⁺ in the assay buffer, presenting 90% of maximal activity even in the absence of Mg²⁺. Diversely, CrTK_{TPP} displays a strong sensitivity to Mg²⁺ in the assay buffer, with a half maximal saturation concentration of ~130 μ M Mg²⁺ (Figure 53, white squares). The activity of CrTK_{TPP} measured in the buffer deprived of Mg²⁺ (Figure 53, first white square) accounts for almost 10% of the maximal activity reached at saturating Mg²⁺ concentration (*i.e.* standard assay conditions). As reported by (Heinrich et al., 1972), we cannot exclude the presence of contaminants cations in the assay buffer due to the additions of substrates, or that the enzyme retains some activity in absence of divalent cations. However, when we compared the activities of CrTK_{TPP} and CrTK_{TPP/Mg} in assay conditions deprived of Mg²⁺, the CrTK_{TPP} activity is extremely low, being only 3% of the activity measured for CrTK_{TPP/Mg}.

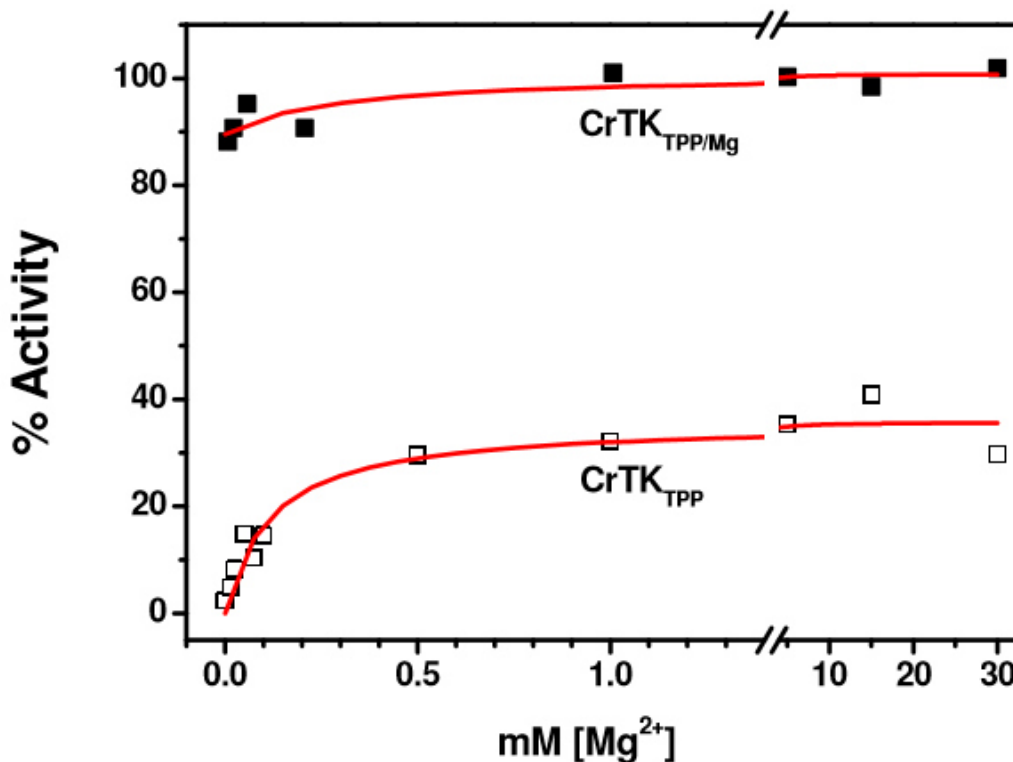


Figure 53. Activity of CrTK_{TPP} and CrTK_{TPP/Mg} as a function of Mg²⁺ concentration in the assay buffer. The enzyme at a concentration of 2.9 mg/ml was reconstituted for 3 hours in 50 mM Tris-HCl (pH 7.9), 0.7 mM TPP, with (black squares) or without (white squares) 8 mM Mg²⁺. Activity was determined in the following assay conditions: 50 mM Tris-HCl (pH 7.9), 2.5 mM βNAD, 12 mM F6P, 2 mM DL-G3P, 0.1 mM TPP, 2.7 μM EcE4PDH and variable amount of MgCl₂. The reaction was started with the addition of CrTK. The activities as a function of the [Mg²⁺] concentration in the assay buffer have been normalized to the maximal activity (130 mol_{NADH}/mol_{TK} s⁻¹) measured for CrTK_{TPP/Mg}.

Summarizing, these results indicate that the presence of Mg²⁺ during the reconstitution phase is fundamental for CrTK activity and that its presence, together with TPP (CrTK_{TPP/Mg}), is necessary for an optimal enzymatic catalysis (Egan and Sable, 1981). Indeed, the only presence of TPP (CrTK_{TPP}) is not enough to reach the maximal activity.

8. Mg²⁺ is required for the formation of a TPP-induced absorption band

As already explained in the Introduction, there is a wide literature, mainly on the yeast TK, reporting the formation of a catalytically active enzyme accompanied by the arise of a positive band in the absorption spectrum in the range 285-360 nm (Kochetov, 1982; Wikner et al., 1994), attributed to the presence of TPP and the divalent cations Mg²⁺ or Ca²⁺. The appearance of the absorption band has been attributed to the conversion of the amino tautomeric form of the TPP aminopyrimidine ring into its imino tautomeric partner. In the yeast TK, this latter tautomeric form is stabilized by interactions of the TPP aminopyrimidine ring with residues Glu418 and Phe445 (Kovina et al., 2002). The structure of the CrTK_{TPP/Mg} showed that Glu463 and Phe490 are structural homologues of the yeast enzyme residues Glu418 and Phe445, respectively (Figure 54).

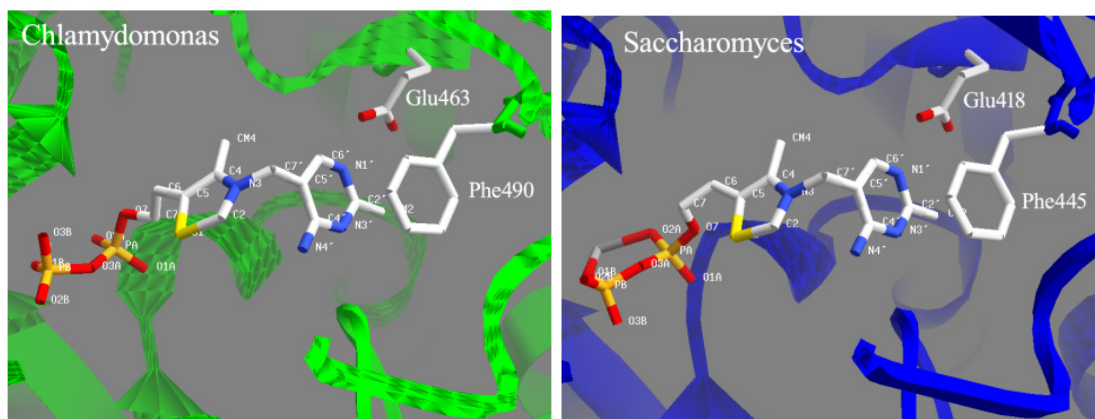


Figure 54. Comparison between the residues stabilizing the imino-form of the TPP aminopyrimidine ring in CrTK and ScTK.

Basing on the comparison with the yeast TK, the formation of a wide TPP-induced absorption band was observed also for CrTK_{TPP/Mg} (see the zoomed graph of the Figure 55).

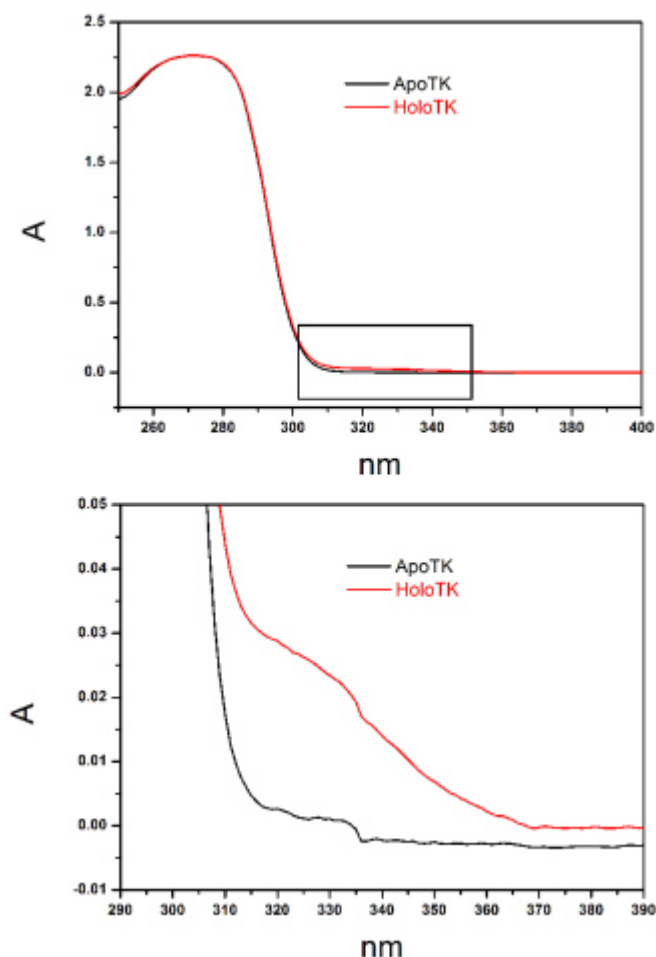


Figure 55. Absorption bands of apo- and holo-CrTK. Upper panel: absorption bands of both the proteins have a pick at 280 nm; lower panel: magnification of the 290-390 spectral region showing the arise of a band at 320 nm in the holo-enzyme.

The time evolution of this wide absorption band upon addition of TPP was observed in a 12.5 μ M

apo-CrTK sample resuspended in 50 mM Tris (pH 7.9), 2.4 mM MgCl₂ (Figure 56-A). To follow the kinetic of this TPP-induced band, the absorbance values at 320 nm were plotted as function of time in Figure 56-B. In line with the experiments performed on the yeast TK (Kochetov, 1982), the TPP-induced band did not appear in absence of Mg²⁺ (CrTK_{TPP}) (Figure 56-B, white squares), while, after adding this cation to the sample (CrTK_{TPP/Mg}), the band started to rise (Figure 56-B, black squares). Furthermore, the enzymatic activity was monitored before and after the addition of the Mg²⁺ (times are indicated in Figure 56-B): the addition of Mg²⁺ led to a quick increase in the enzyme activity, which reaches a plateau value after about 3 hours (in agreement with what reported above). Differently, the TPP-induced band associated with these activity measurements did not reach a saturating absorption value.

To sum up, these results suggested that the formation of the holo-enzymatic structure strongly depends on the presence of Mg²⁺ and not just on the TPP binding and that the increase in the TPP-induced absorption band is parallel by the increase of the catalytic activity.

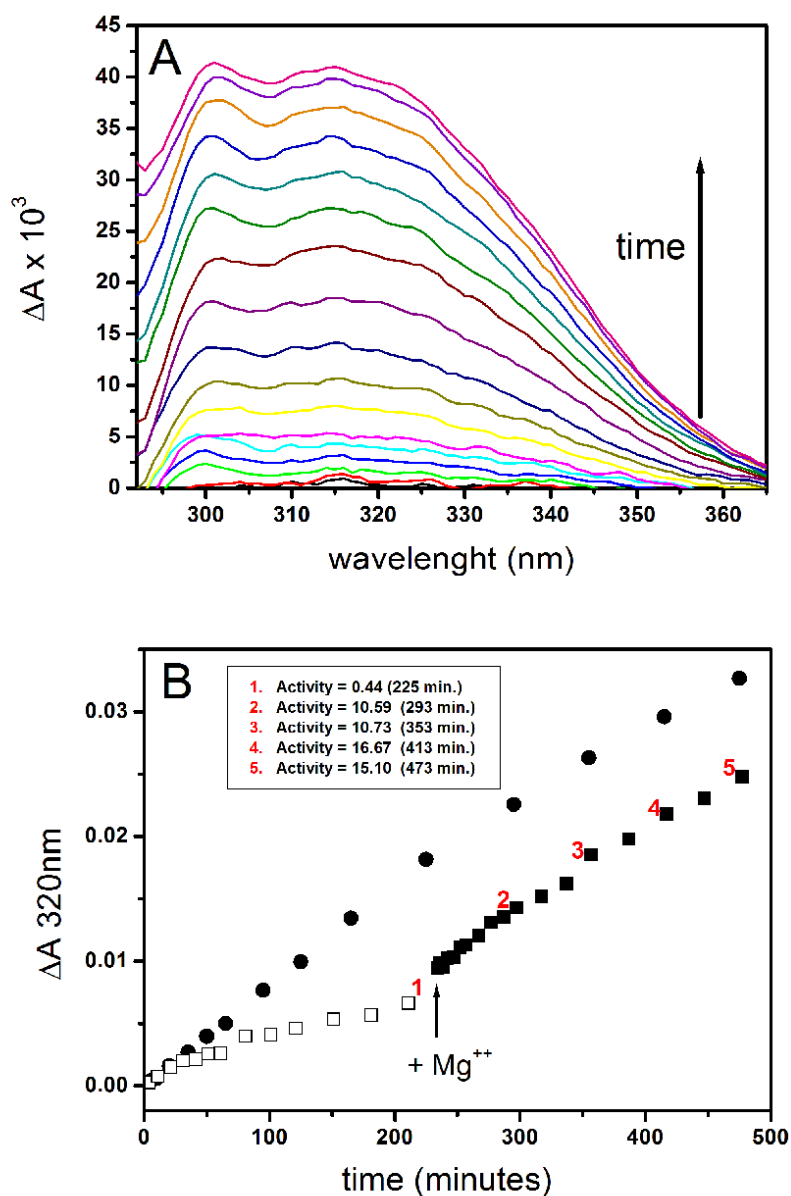


Figure 56. Formation of the CrTK TPP-induced absorption band. **A.** Time evolution of the TPP-induced absorption band in a 12.5 μM CrTK samples resuspended in buffer 50 mM Tris (pH 7.9), 2.4 mM MgCl_2 . At time 0 (zero), 220 μM TPP were added to the sample; the spectrum recorded immediately after the TPP addition has been subtracted to the spectra recorded at longer times to correct for the TPP and CrTK absorption. **B.** Time evolution of the TPP-induced absorption band followed at 320nm. At time 0 (zero), 220 μM TPP were added to the samples. Black circles: absorption at 320 nm ($\Delta A_{320\text{nm}}$) from the spectra presented in panel A; white squares: $\Delta A_{320\text{nm}}$ of a 12.5 μM CrTK sample without Mg^{2+} ; black squares: absorption of the latter samples upon addition of 2.2 mM MgCl_2 . The numbers in red are associated to the enzymatic activity detected in samples picked up at the indicated time.

9. CD spectra of the CrTK_{TPP} and CrTK_{TPP/Mg}

To confirm if the reconstitution of the CrTK_{TPP/Mg} is accomplished by major changes in the protein secondary structure, CD spectroscopy was performed on CrTK_{Mg} samples incubated in the presence or in the absence of TPP. Spectra were recorded in the 190-240 nm region on CrTK samples (1.7 μ M) suspended in buffer 5 mM Tris (pH 7.9), 2.5 mM MgCl₂ with (CrTK_{TPP/Mg}) or without (CrTK_{Mg}) addition of TPP. The secondary structure analysis was reported in the Table 6 (see Material and Methods for details), compared with the crystal structure of the CrTK_{TPP/Mg}.

	crystal	Cr-TK	
		apo	holo
Regular helix	26.8	30.1	29.7
Distorted helix	17.7	17.7	17.5
Regular strand	6.5	7.6	8.0
Distorted strand	5.4	5.3	5.5
Turn	19.4	16.5	16.6
Unordered	24.2	22.8	22.7
Total	100.0	100.0	100.0
RMSD	-	0.075	0.074
NRMSD	-	0.014	0.014

Table 6. Predicted contents of secondary structures in the apo- and holo-CrTK (The estimation of secondary structure was finally performed on the CD spectra of CrTK in molar units per residue using a locally modified version of the CDPro software: the CONTIN/LL algorithm was used in combination with the SP175 reference dataset, and the resulting values of secondary structure content were converted to percent values).

10. Effect of DTTox on the CrTK activity

Several enzymes of the CB cycle are regulated by the reversible oxidation of disulfide bonds, a process linked to the light-dark cycle through the TRX system (Michelet et al., 2013). CrTK enumerates twelve cysteines mainly distributed in the PP and Pyr domains (Cys58, 84, 173, 204, 210, 220 and 366 in the PP domain; Cys386, 470, 484 and 582 in the Pyr domain) and only the Cys638 located in the C-terminal domain. Among them, only cysteine residues at position 84, 210, 220, 386, 470, 638 are conserved in photosynthetic organisms (Michelet et al., 2013). Such a large number of cysteine residues makes CrTK a putative target of redox regulation through disulfide bond formation. To test the effect of oxidative conditions on the activity of CrTK, CrTK_{TPP} and CrTK_{TPP/Mg} were treated with DTTox. After 3h incubation, the activity of CrTK_{TPP/Mg} was almost unaffected, retaining more than 90% of the control (not oxidized) enzyme (Figure 57, left bars). Thus, the oxidation induced by DTTox did not substantially influence the catalytic activity of fully reconstituted enzyme. Although its activity was 4-fold lower compared to the CrTK_{TPP/Mg}, CrTK_{TPP} was strongly inhibited when exposed to 50 mM DTTox, retaining from 20 to 30% of its control activity (Figure 57, central bars). A similar result was observed for the CrTK, being 80% inactivated following incubation in presence of 50 mM DTTox (Figure 57, right bars).

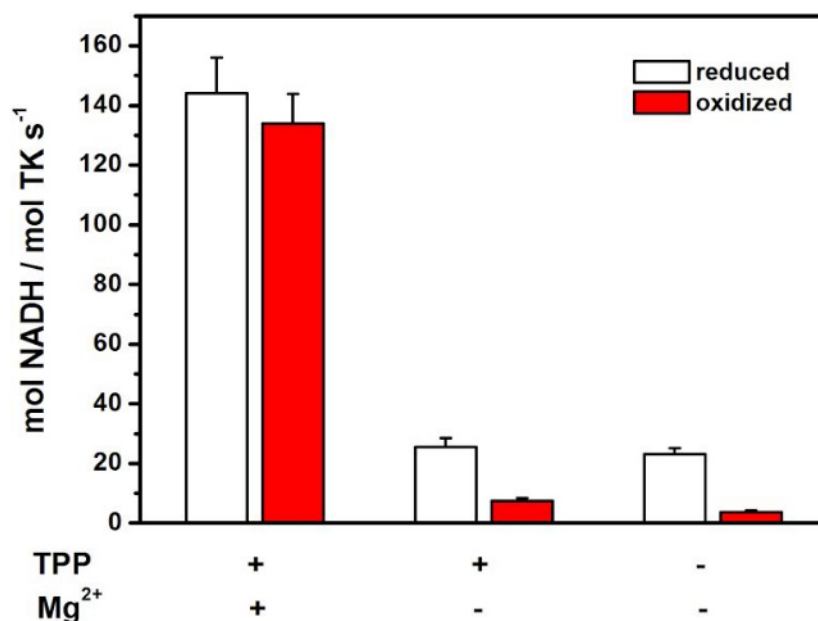


Figure 57. Oxidation of CrTK samples. After incubation, each sample was divided in two aliquots and diluted seven-fold in 50 mM Tris-HCl (pH 7.9), in the presence (red bars) or absence (white bars) of 50 mM DTTox. The residual activity was measured after 3 h following the procedure described in Materials and Methods. Data represent the mean percentage \pm SD ($n = 3$).

Besides, the incubation of inhibited CrTK_{TPP} with the strong reducing agent TCEP (30 mM) completely restored the activity, indicating that enzyme inhibition is due to reversible modifications such as the presence of disulfide bond(s) (Figure 58).

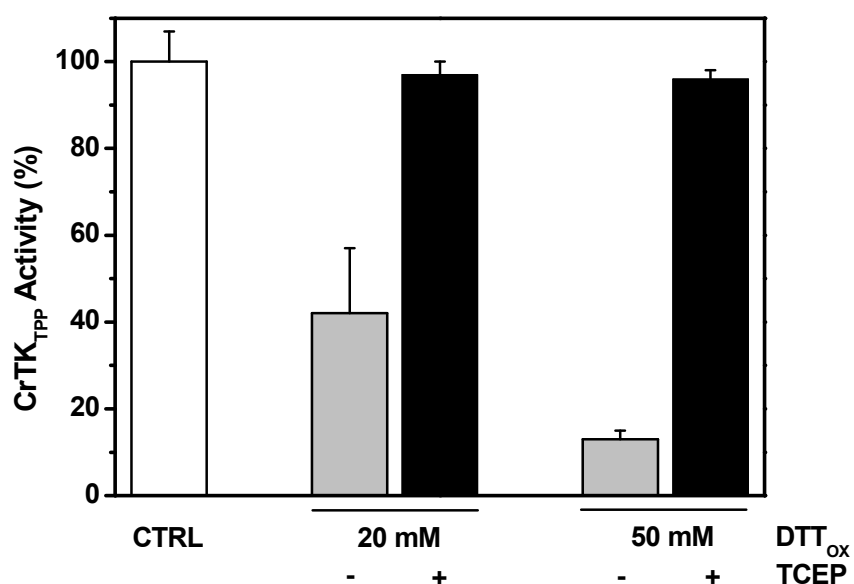


Figure 58. Reversibility of CrTK_{TPP} oxidation. CrTK_{TPP} samples were incubated for 3 h with 20 or 50 mM DTTox (grey bars). The reversibility of CrTK_{TPP} inactivation was assessed by incubation for 15 min in the presence of 30 mM TCEP (black bars). Data represent the mean percentage \pm SD ($n = 3$).

To better investigate the influence of the Mg²⁺ on the DTTox-induced inactivation of the enzyme, reduced and oxidized CrTK_{TPP} were incubated with variable concentrations of Mg²⁺. By plotting the

ratios between oxidized and control activities as a function of the Mg^{2+} content, it was evident that a decrease of the Mg^{2+} amount in the reconstitution buffer was simultaneous to an increased sensitivity of the enzyme to the oxidizing conditions (Figure 59).

Taken together, these results indicated that only the CrTK and CrTK_{TPP} forms are prone to the oxidation-induced inhibition, and suggested that the Mg^{2+} concentration can modulate the amount of enzyme that is sensitive to oxidative modifications.

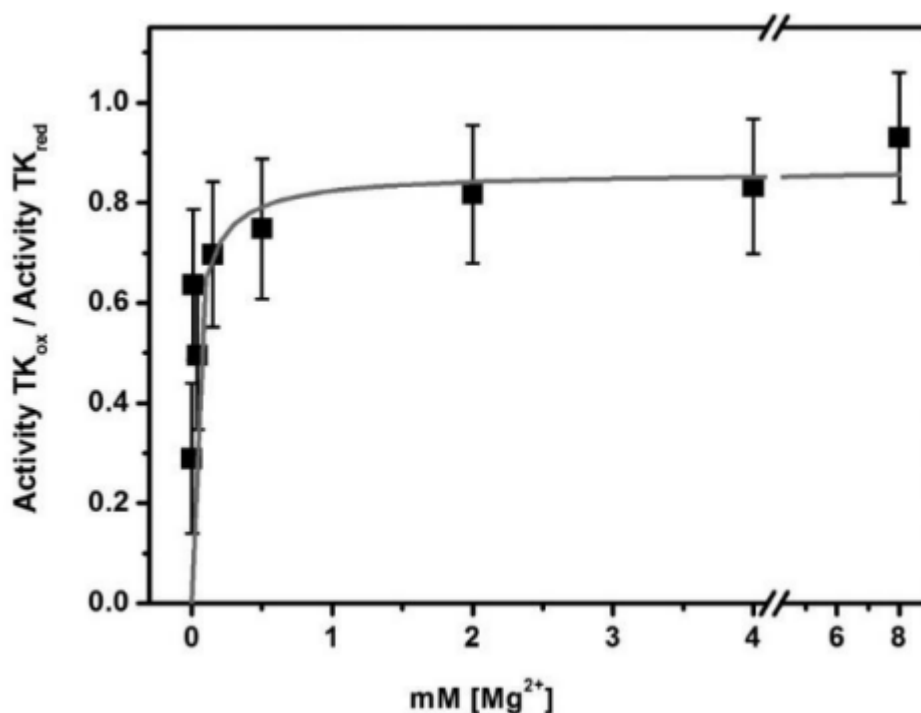


Figure 59. Activity ratio of oxidized/reduced CrTK as a function of $[Mg^{2+}]$. The enzyme was reconstituted for 3 h in 50 mM Tris-HCl (pH 7.9), 0.7 mM TPP, and variable $[Mg^{2+}]$. At the end of the incubation, each sample was divided in two aliquots, diluted seven times in 50 mM Tris-HCl (pH 7.9) with or without 50 mM DTTox. After additional incubation (3h) the residual activity was assayed following the procedure described in Materials and Methods. The reaction was started with the addition of CrTK to a final concentration of 20 nM. The ratio between the activity of the oxidized and reduced (control) sample are plotted as a function of the $[Mg^{2+}]$. Data represent the mean percentage of two replicates ($n = 2$).

11. Effects of oxidation with $CuCl_2$ on the CrTK_{TPP} activity

A further oxidating treatment of CrTK_{TPP} was performed with the copper chloride ($CuCl_2$), an agent known to induce the formation of disulfide bonds (Rehder and Borges, 2010). As shown in the Figure 60, the action of the $CuCl_2$ caused a decrease of the CrTK_{TPP} activity, dependent from the concentration and the time of incubation.

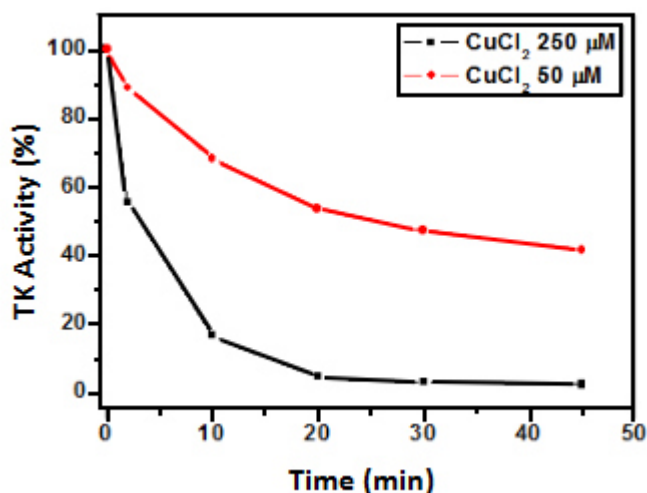


Figure 60. CuCl_2 -induced inhibition of CrTK.

It was also shown that, after a incubation of 20 minutes of the oxidized CrTK_{TPP} with 30 mM TCEP, a very good recovery of the enzymatic activity occurred in the CuCl_2 -treated samples (Figure 61), like previously observed for the reactivation of the DTT_{OX} oxidized CrTK_{TPP} .

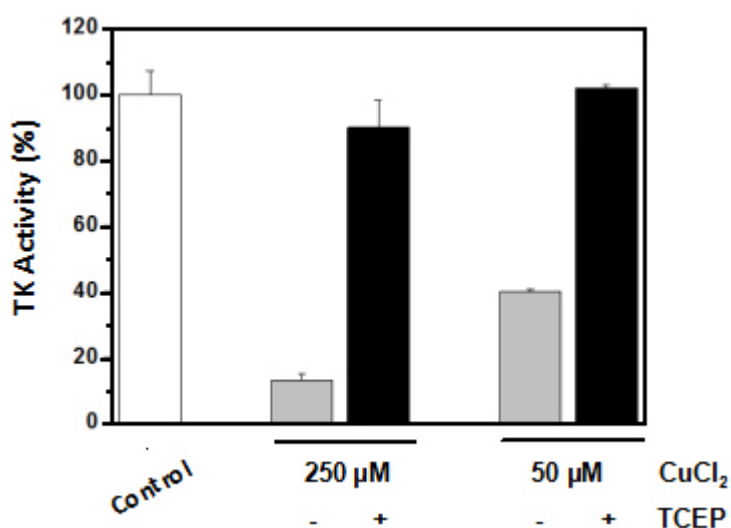


Figure 61. Effects of the CuCl_2 treatment (grey columns) on the CrTK_{TPP} activity (control: white column) and recovery upon TCEP incubation ($[\text{TCEP}] = 30 \text{ mM}$) of the inhibited enzyme (black columns).

12. Induced Circular Dichroism (ICD) spectra of $\text{CrTK}_{\text{TPP/Mg}}$

Besides the formation of the band of absorption in the near UV region, the binding between TPP and TK gives rise to a peculiar Induced Circular Dichroism (ICD) signal, observed across a variety of TPP-dependent enzymes (Wikner et al., 1994; Kovina et al., 2004; Kochetov and Solovjeva, 2014).

ICD spectra derive from the perturbations to the symmetry and electronic structure of a non-chiral ligand (*i.e.* TPP) interacting with a chiral guest (Allenmark, 2003; Tedesco and Bertucci, 2015); in the case of TPP, these perturbations are due to the stabilization of the 4'-imino-1',4'-dihydropyrimidine tautomer and to the selection of a V-like conformation upon binding, dictated by the optimal mutual orientation of the thiazole and pyrimidine rings for the

effective deprotonation at C₂ (Schellenberger, 1982) and well conserved across TPP-dependent enzymes (Friedemann and Breitkopf, 1994; Schellenberger, 1998).

CrTK_{TPP/Mg} also displayed a bisignate ICD signal in the 250–350 nm range, with a positive band centered at 280 nm and a negative band centered at 320 nm; the profile is very similar to those reported for other TKs (Wikner et al., 1994; Kovina et al., 2004) (Figure 62-A). When CrTK_{TPP/Mg} was treated with excess of Na₂EDTA, Mg²⁺ got strongly involved in complexation with the chelating agent, causing the complete disappearance of the ICD signal (Figure 62-B): this clearly showed that Mg²⁺ is necessary for the effective formation of the CrTK_{TPP/Mg} in the catalytically active configuration.

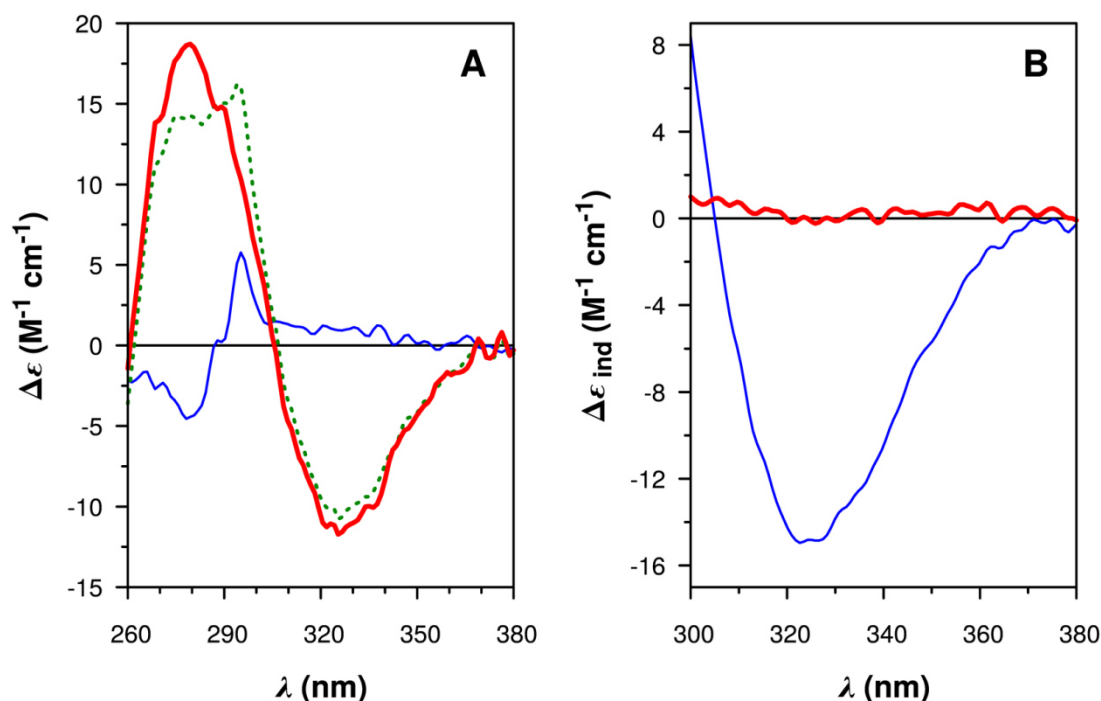


Figure 62. CD spectra for the apo and holo CrTK. (A) CD spectra for apo-CrTK (6.3 μ M; thin line) and holo-CrTK_{TPP/Mg} (5.6 μ M, [TPP] = 55.6 μ M; dotted line); the resulting ICD signal for the binding of TPP to CrTK is shown (bold line). Solvent: 5 mM Tris-HCl (pH 7.9) with 0.1 mM Na₂EDTA and 2 mM MgCl₂; pathlength: 1 cm. (B) ICD spectra for the binding of TPP to CrTK before (thin line) and after (bold line) addition of 8 mM Na₂EDTA ([CrTK] = 18.6 μ M, [TPP] = 220 μ M). Solvent: 5 mM Tris-HCl (pH 7.9) with 2.5 mM MgCl₂; pathlength: 1 cm.

13. CD study of the TPP binding in the reduced and oxidized CrTK_{TPP} forms

The CD analysis was used to compare the TPP binding in the reduced and oxidized form of the CrTK_{TPP}. Figure 63 shows the ICD signals time evolution of the reduced (upper panel) and oxidized (lower panel) CrTK_{TPP} upon addition of 12 molar excess of TPP in a 5 mM Tris buffer (pH 7.9) supplemented with 2.5 mM MgCl₂. The magnitude of the ICD signal reaches a maximum saturation after three hours only in the reduced CrTK_{TPP} sample, confirming what observed for the slow reconstitution of the enzyme activity. On the contrary, the ICD signal related to the oxidized CrTK_{TPP} sample rises slower and do not saturate even after 24 hours. To better appreciate this difference, the ICD values of both the reduced and oxidized enzymes at 325 nm were plotted in a secondary graph as a function of time (Figure 64).

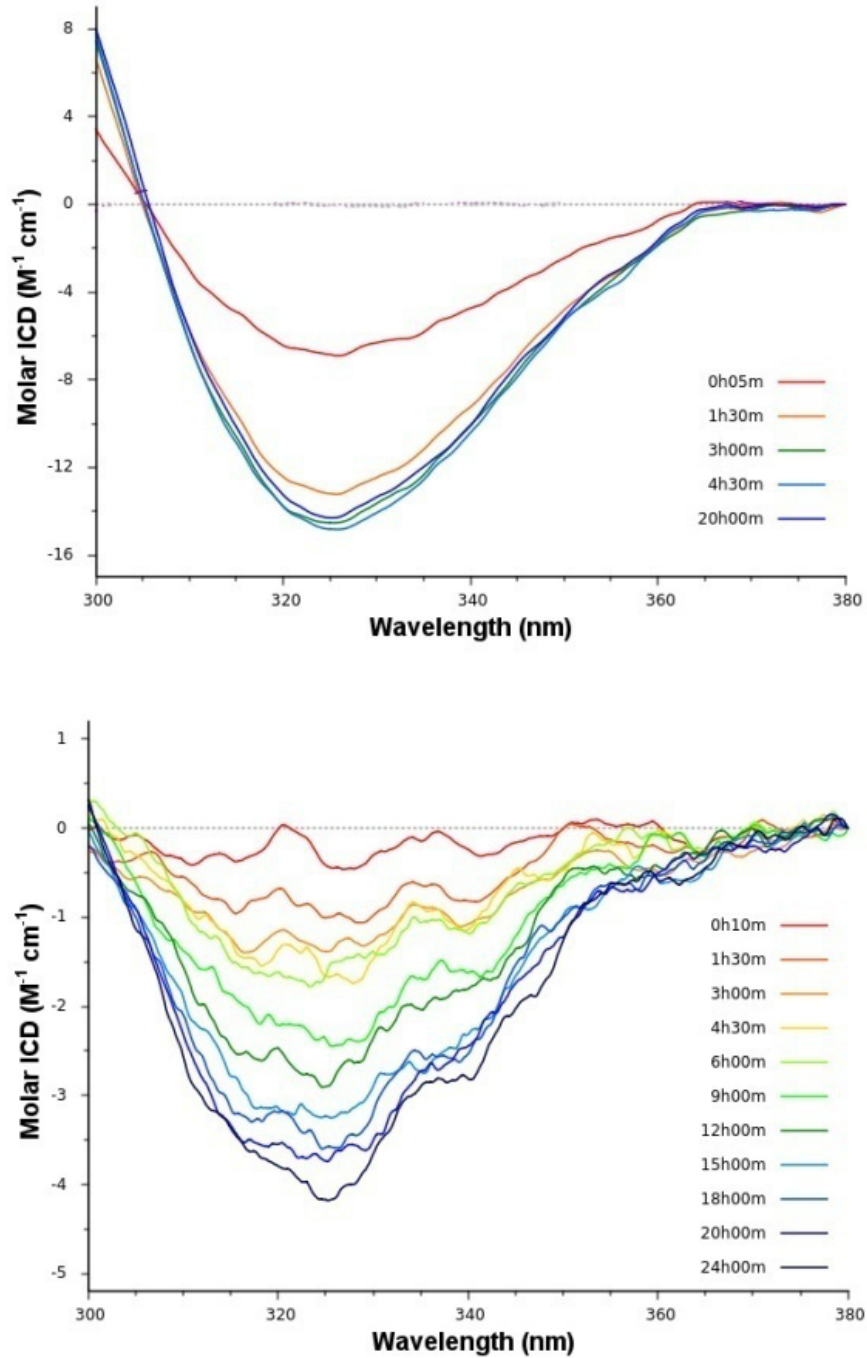


Figure 63. Time evolution of the TPP-induced CD band. ICD spectra for the binding kinetic of TPP (220 μM) to 17.8 μM reduced CrTK (upper panel) and to 12.5 μM oxidized CrTK (lower panel) monitored at different times after TPP addition. ICD values are expressed in molar units based on the total CrTK concentration. Solvent: 5 mM Tris-HCl (pH 7.9) with 2.5 mM MgCl_2 .

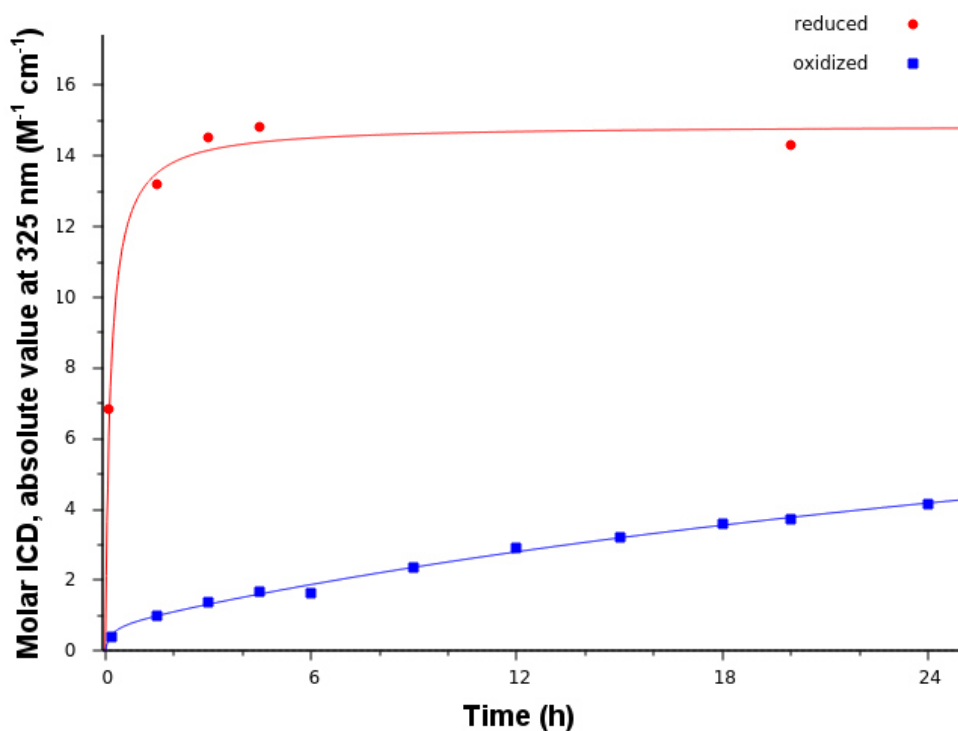


Figure 64. Time evolution of the 325 nm ICD molar absorption of the reduced (red) and oxidized (blue) CrTK_{TPP}. Data from the spectra presented in Figure 63.

This indicates that, upon oxidation of the CrTK, the insertion and/or correct orientation of the TPP into the active site is perturbed.

14. Affinity constant (K_m) for the F6P in the reduced and oxidized CrTK_{TPP}

We obtained the affinity constant for F6P of the reduced and oxidized CrTK_{TPP} adding in the reaction mix diverse amounts of the donor substrate. The oxidized CrTK sample was obtained upon incubation of the protein reconstituted in the absence of MgCl₂ as previously described in Materials and Methods. Activity was measured after removal of the added DTT_{ox} by desalting with a sephadex column. As shown in Figure 65, we observed that the affinity constant for the reduced CrTK_{TPP} is very similar to that of the oxidized CrTK_{TPP} (F6P K_m for the CrTK_{red} = 1.5 mM; F6P K_m for the CrTK_{ox} = 1.7 mM). In addition, we can observe that the maximal activity of the reduced CrTK_{TPP} is basically one third than the activity of the oxidized CrTK_{TPP}, accordingly with what previously observed.

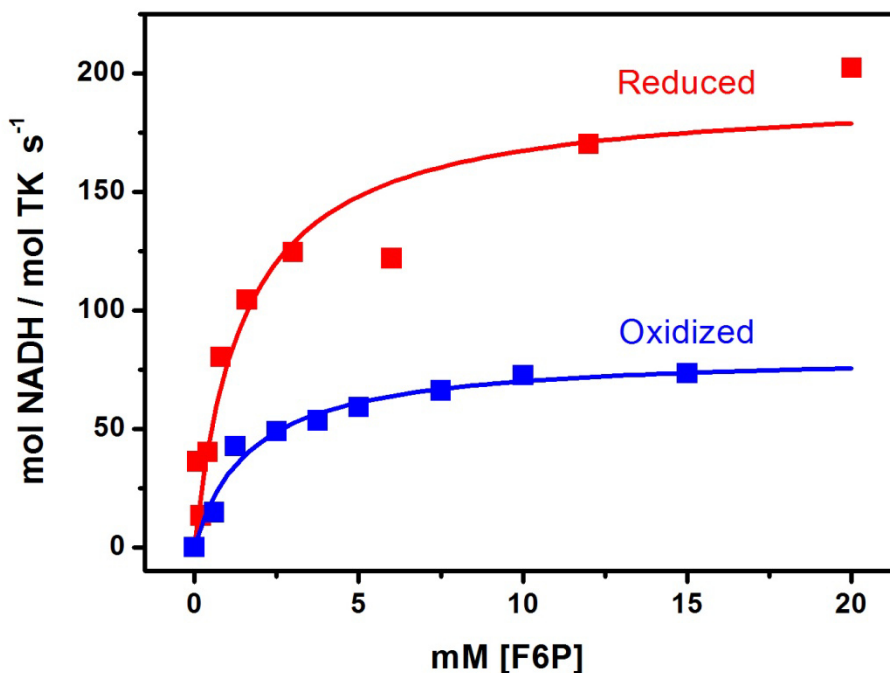


Figure 65. Determination of the affinity constant for F6P of reduced and oxidized CrTK_{TPP}. Activity was determined in buffer containing 50 mM Tris-HCl (pH 7.9), 15 mM MgCl₂, 5 mM CaCl₂, 2.5 mM β-NAD, 2 mM DL-G3P, 0.1 mM TPP, 5.4 μM EcE4PDH and variable amount of F6P (0.1-15 mM). Reaction was started by the addition of CrTK (10 nM). In red: reduced CrTK_{TPP}; in blue: oxidized CrTK_{TPP}. Data represent the mean of three replicates (n = 3).

Furthermore, we can compare the obtained K_m for the F6P with the constants present on the Brenda Database for other TKs, noticing the high similarity among all the described constant values (Table 7).

Organism	K _m F6P (mM)
Escherichia coli	1.1
Saccharomyces cerevisiae	1.8
Spinacia Oleracea	3.2
Homo Sapiens	7.0

Table 7. K_m for the F6P of transketolases from different organisms from BRENDA database (<http://www.brenda-enzymes.org>).

15. Effect of NEM-induced irreversible alkylation on the CrTK_{TPP}

To test the effect of the alkylation on the enzyme activity, the CrTK_{TPP} was treated for 20 minutes with different concentrations of N-ethylmaleimide (NEM), an alkylating agent that specifically binds cysteine residues. Observing the Figure 66, it is clear that the CrTK_{TPP} activity was found to be strongly influenced by the NEM action, since a concentration-dependent (on the left) and a

time-dependent (on the right) decrease in the enzymatic activity were observed, indicating that the accessible cysteine residues are important for the enzyme function.

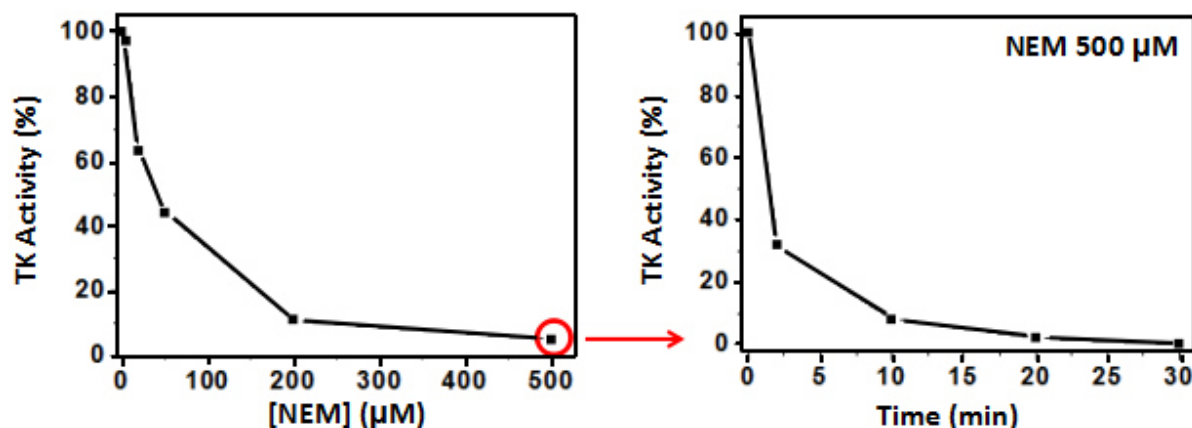


Figure 66. Effects of the NEM-induced alkylation on the CrTK activity. On the left: CrTK activity dependence on the NEM concentration; on the right: time-dependent inhibition of CrTK activity.

16. Glutathionylation of the CrTK_{TPP} by BIO-GSSG

To verify whether CrTK_{TPP} could contain cysteines subjected to glutathionylation, a Western Blot analysis was performed: the protein was differentially alkylated with a mixture of IAM (iodoacetamide) and NEM, treated with biotinylated glutathione (BIO-GSSG) and reduced with DTTred (Zaffagnini et al., 2012a). As shown in the Figure 67, when the enzyme is alkylated, no biotinylated bands could be detected by western blot analysis. The bands are clearly present in not pre-alkylated samples, while the signal disappeared upon treatment with the reducing agent DTTred. This experiment suggests that one or more cysteine residues could be target of glutathionylation in the CrTK_{TPP}. This agrees with what reported in a proteomic study that indicated Cys84 as a target of glutathionylation in CrTK (Zaffagnini et al., 2012a).

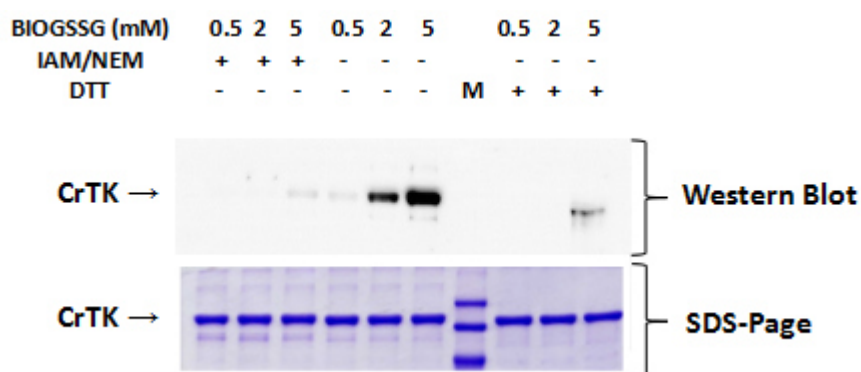


Figure 67. Western Blot (above) and SDS-PAGE (below) after the BIO-GSSG treatment of the CrTK.

17. Effect of DTNB -induced reversible alkylation on the CrTK_{TPP}

It is well-known that the NEM represents an irreversible type of alkylating agent, meaning that it irreversibly binds cysteine residues. In contrast, other alkylating substances, like the

di-thio.nitro-benzoic acid (DTNB), are able to perform a different kind of alkylation which can be reversed.

The theory indicates that the disulfide bridge present in the DTNB molecule is broken after the formation of a mixed disulfide bridge with the free thiol cysteine residues and a 2-nitro-5-thiobenzoate (TNB⁻) is released. At neutral and alkaline pH the TNB⁻ ionizes to the TNB²⁻ dianion (see Figure 68). It is possible to follow this reaction since the TNB²⁻ ion assumes a typical yellow coloration.

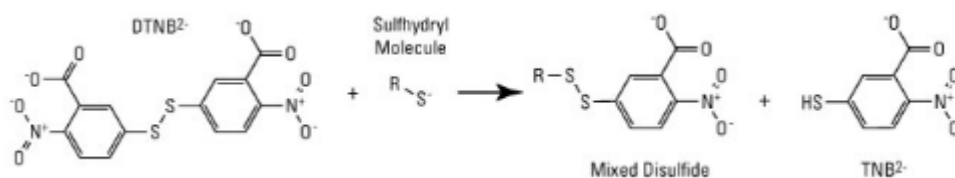


Figure 68. Cleavage of the DTNB molecule to give TNB⁻ (not shown in the picture), which then ionizes to TNB²⁻ in water solutions.

As shown in Figure 69, the DNTB treatment led to a concentration-dependent inhibition of the CrTK_{TPP} activity. In addition to this, it was observed that, after a 20 minutes-incubation with TCEP of the DTNB-treated samples, an almost complete recovery of the enzymatic activity occurred independently from the DTNB concentration.

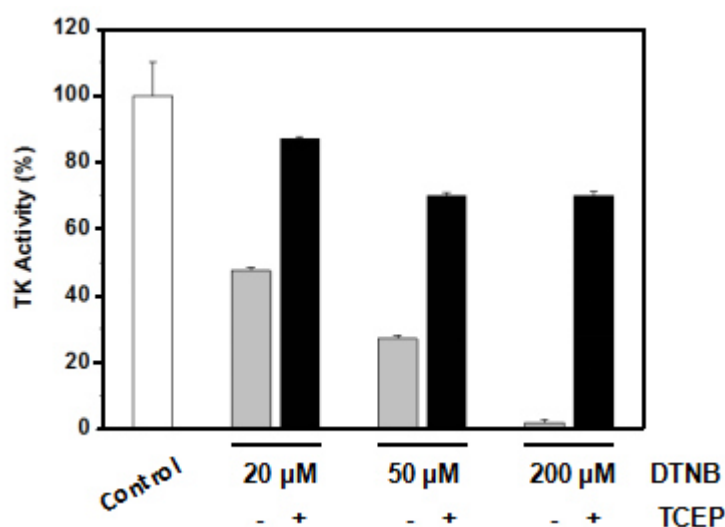


Figure 69. Effects of the DTNB treatment (grey columns) on the CrTK activity (control: white column) and recovery upon 30 mM TCEP incubation of the inhibited enzyme (black columns).

18. Titration of CrTK_{TPP} free thiols with DTNB

The DTNB, also known as Ellman's reagent, is widely used to evaluate the number of free thiol residues on a target protein. The TNB⁻ produced by the reaction of DTNB with the thiols could be detected spectrophotometrically at 412 nm. So it was exploited to quantify the number of free thiols present in CrTK_{TPP} samples after oxidation with 50 mM DTTox or in glutathionylation with 5 mM GSSG (Figure 70). The following formula has been used to calculate the number of free thiols:

$N_{SH} = (A / \epsilon \cdot l) / C$, where the N_{SH} is the number of free thiols that reacted with DTNB; A is the absorbance at 412 nm detected at fixed time (normally 30-45 minutes after DTNB addition); ϵ is the extinction molar coefficient of the TNB⁻ (corresponding to 14,150 M⁻¹ cm⁻¹); l is the optical length,

and C is the enzyme concentration.

After subtracting the blank absorbance (*i.e.* a DTNB solution deprived of protein), the following results were obtained:

Not-treated CrTK_{TPP} = 13.94 free SH/TK monomer (≈ 14)

CrTK_{TPP} + DTT_{OX} = 9.97 free SH/TK monomer (≈ 10)

CrTK_{TPP} + GSSG = 8.2 free SH/TK monomer (≈ 8)

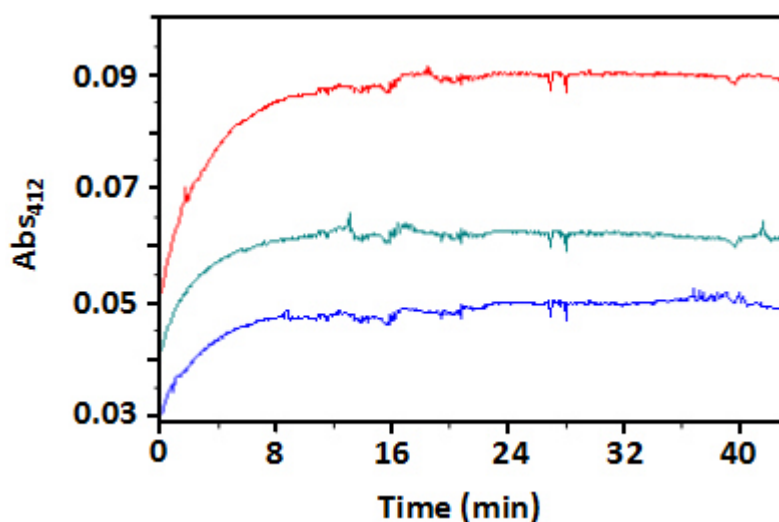


Figure 70. Thiol titration of not-treated CrTK_{TPP}, oxidized CrTK_{TPP} and glutathionylated CrTK_{TPP}; performed in a quartz cuvette (0.2 cm) with 200 μ M DTNB, followed for 45 minutes. Reaction was started by the addition of CrTK_{TPP} (2.5 μ M). Red line: not-treated CrTK_{TPP}; green line: oxidized CrTK_{TPP}; blue line: glutathionylated CrTK_{TPP}.

19. Mass spectrometry on CrTK_{TPP}

The thiol titration showed that, upon oxidation, the number of free thiols decreases from 14 to 10 (see precedent paragraph). Despite the total number of cysteine residue in the recombinant CrTK used in this work is 12, this difference suggests that one or more disulfide bridges can be formed. Inspection of the CrTK_{TPP} structure showed that a couple of cysteine residues, Cys470 and Cys484 are at suitable distance for making a disulfide bond without invoking large conformational changes of the protein structure. A sample of 7 mg/mL CrTK_{TPP}, pre-treated with iodoacetamide, was incubated overnight in the presence of 1 μ g trypsin and analyzed by LC-ESI-MSMS.

Analysing the reduced form of CrTK_{TPP}, two peptides are expected: PEP 463-477 (highlighted in salmon in Figure 71) and PEP 478-495 (highlighted in green in Figure 71) with MW of 1621 and 2217 Dalton, respectively.

470 480 490 500
[...]**VREHAMGAIC** **NGIALHK**SGL **IPYCATFYIF** **TDYMRNAMRM** [...]

Figure 71. Transketolase region containing the Cys470 and Cys484 supposed to be involved in a disulfide bridge formation.

If a disulfide bridge between Cys470 and Cys484 is formed upon oxidation of CrTK_{TPP}, a new

peptide of MW equal to 3722 Dalton is expected (PEP X, Figure 72).

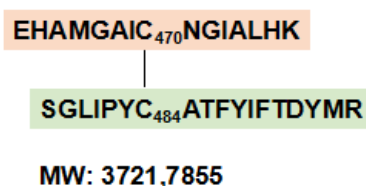


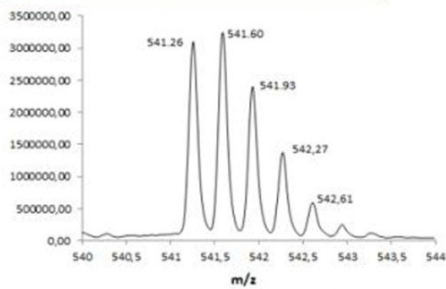
Figure 72. PEP X composition and its molecular weight.

19.1 LC-ESI-MS-MS analysis on reduced CrTK_{TPP}

The expected m/z values of the PEP 463-477 and PEP 478-495 are reported in Figure 73. Peptide ions within a m/z 400-1700 survey scan mass range were analysed for subsequent fragmentation. 2^+ , 3^+ and 4^+ charged ions exceeding a threshold abundance (TIC value 10 counts/sec), were selected for MS/MS analyses. The signals of the PEP 463-477 $(M+3H)^{3+}$ 541 and of the PEP 478-495 $(M+2H)^{2+}$ 1109 ions found during the LC-MS analysis are shown in Figure 73. The theoretic m/z values of PEP 463-477 and PEP 478-495 after fragmentation of the 541 and 1109 ions, during the LC-MSMS analysis, are reported in the bottom tables of Figure 73. Recorded signals, matching with the theoretic values of the fragmentation spectrum, clearly showed that mass spectrometry analysis on the CrTK_{TPP} reduced form found the expected peptides in the protein region containing the 470 and 484 cysteine residues.

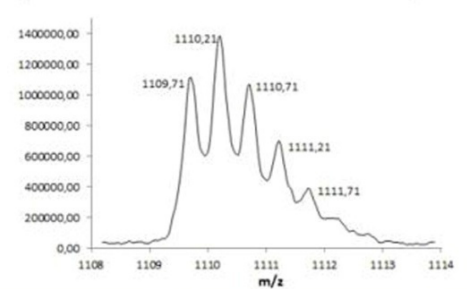
PEP 463-477

Mass (m/z)	
(M)	1620.76504
(M+H) ⁺	1621.77287
(M+2H) ²⁺	811.39037
(M+3H) ³⁺	541.26287
(M+4H) ⁴⁺	406.19912



PEP 478-495

Mass (m/z)	
(M)	2217.00606
(M+H) ⁺	2218.01389
(M+2H) ²⁺	1109.51088
(M+3H) ³⁺	740.00988
(M+4H) ⁴⁺	555.25937



Seq		B	Y	
E	1	130.05046	1621.77287	15
H	2	267.10937	1492.73028	14
A	3	338.14649	1355.67137	13
M	4	469.18697	1284.63425	12
G	5	526.20844	1153.59377	11
A	6	597.24555	1096.57230	10
I	7	710.32961	1025.53519	9
C	8	870.33880	912.45113	8
N	9	984.38173	752.44194	7
G	10	1041.40319	638.39901	6
I	11	1154.48725	581.37755	5
A	12	1225.52437	468.29394	4
L	13	1338.60843	397.25637	3
H	14	1475.66734	284.17231	2
K	15	1603.76231	147.11340	1

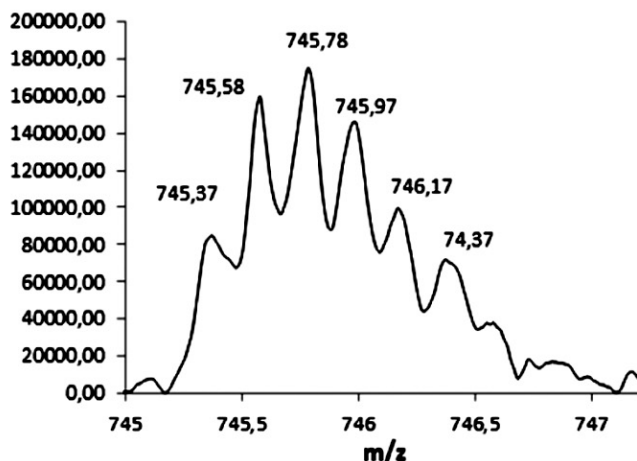
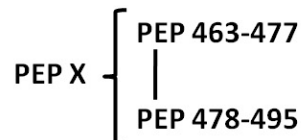
Seq		B	Y	
S	1	88.03990	2218.01389	18
G	2	145.06136	2130.98186	17
L	3	258.14543	2073.96040	16
I	4	371.22949	1960.87633	15
P	5	468.28225	1847.79227	14
Y	6	631.34558	1750.73950	13
C	7	791.35477	1587.67618	12
A	8	862.39188	1427.66699	11
T	9	963.43956	1356.62988	10
F	10	1110.50797	1255.58220	9
Y	11	1273.57130	1108.51379	8
I	12	1386.65536	945.45046	7
F	13	1533.72378	832.36639	6
T	14	1634.77146	685.29798	5
D	15	1749.79840	584.25030	4
Y	16	1912.86173	469.22336	3
M	17	2043.90221	306.16003	2
R	18	2200.00332	175.11955	1

Figure 73. Mass spectrometry analysis of apo-CrTK. The 463-477 and 478-495 peptides m/z values are presented in the upper left and upper right tables, respectively. Signals corresponding to the PEP 463-477 (M+3H)³⁺ 541 and of the PEP 478-495 (M+2H)²⁺ 1109 ions found during the LC-MS analysis are shown on the left and right spectra, respectively. The expected m/z values of PEP 463-477 and PEP 478-495 after fragmentation of the 541 and 1109 ions, during the LC-MSMS analysis, are reported in the left and right bottom tables, respectively. Recorded signals matching with the theoretic values of the fragmentation spectrum are highlighted in the tables.

19.2 LC-ESI-MSMS analysis on oxidized CrTK_{TPP}

The mass spectrum of a CrTK_{TPP} sample oxidized by incubation with 50 mM DTT_{ox} for 3 hours was analyzed. Upon removal of the DTT_{ox} by desalting, the oxidized CrTK_{TPP} sample was digested overnight with trypsin. LC-MS analysis revealed the presence of the PEP X (M+4H)⁴⁺ and PEP X (M+5H)⁵⁺ ions (m/z of 931.25 and 745.23, respectively) in the spectrum, expected if the Cys470-Cys484 disulfide bridge was formed in the oxidized sample.

LC-MSMS fragmentation of the PEP X (M+5H)⁵⁺ 745 ion is presented in Figure 74, lower tables. Detected m/z signals indicated the presence of the TFYIFTDYM peptide sequence of PEP 478-495 in the (M+5H)⁵⁺ 745 PEP X ion. These results clearly indicated that oxidation of CrTK_{TPP} with DTT_{ox} induced the formation of a Cys470-Cys484 disulfide bridge. However, we can not exclude the presence of other disulfide bridges formed upon oxidation of CrTK_{TPP} not covered by this kind of mass spectrometry analysis.



Mass (m/z)	
(M)	3721.78
(M+H) ⁺	3722.78
(M+2H) ²⁺	1861.89
(M+3H) ³⁺	1241.35
(M+4H) ⁴⁺	931.25
(M+5H) ⁵⁺	745.23

Seq	B	Y
E	1	130,05046
H	2	267,10937
A	3	338,14649
M	4	469,18697
G	5	526,20844
A	6	597,24555
I	7	710,32961
C	8	813,33880
N	9	927,38173
G	10	984,40319
I	11	1097,48725
A	12	1168,52437
L	13	1281,60843
H	14	1418,66734
K	15	1546,76231

Seq	B	y
S	1	88,03990
G	2	145,06136
L	3	258,14543
I	4	371,22949
P	5	468,28225
Y	6	631,34558
C	7	734,35477
A	8	805,39188
T	9	906,43956
F	10	1053,50797
Y	11	1216,57130
I	12	1329,65536
F	13	1476,72378
T	14	1577,77146
D	15	1692,79840
Y	16	1855,86173
M	17	1986,90221
R	18	2143,00332

Figure 74. Mass spectrometry analysis of oxidized apo-CrTK. The theoretic m/z values of PEP X ions are presented in the upper right table. Signal corresponding to the PEP X (M+5H)⁵⁺ 745 ion found during the LC-MS analysis are shown on the left spectrum. Some of the expected m/z values of PEP X 745 ion fragmentation during the LC-MSMS analysis are reported in the right bottom table, with recorded signals matching the theoretic values of the fragmentation spectrum highlighted.

Chapter 2

Since the CrTK cofactor TPP displays a very important role in the transketolases, both from the structural and the functional point of view, the effects of the cofactor on the transketolase gene expression were investigated. The rationale of this question lies in the fact that the TPP, as well as its precursor, the thiamin, are important regulators of the gene expression, since they can bind the so called TPP riboswitches, that, as explained in the Introduction, are able to “sense” the thiamin and TPP levels in the cell, contributing to a fine cell homeostasis of these molecules (Moulin et al., 2013; Bocobza et al., 2014; Duesterberg et al., 2015; Guedich et al., 2016). In order to investigate if a "crosstalk" exists between the TPP and CrTK gene, the response of the TRK1 gene expression to the treatments with some of the TPP biosynthesis pathway intermediates in *Chlamydomonas reinhardtii* cultures has been analyzed. This investigation has been conducted in collaboration with the group of Prof. Alison G. Smith, at the University of Cambridge (UK) – Department of Plant Sciences.

1. Influence of intermediates of the TPP biosynthetic pathway on the TRK1 gene expression levels

THI (thiamine), HET (hydroxyethylthiazole) and HET/PYR (hydroxyethylthiazole + pyriothiamine) at the growing concentrations of 0.1, 1 and 10 μM were used to treat the WT12 *Chlamydomonas* cultures following the procedure described in Materials and Methods. Experiments of qRT-PCR showed that, in all the cases, the transketolase gene (TRK1) expression was significantly decreased when the growth medium was supplemented with the highest concentration (10 μM) of THI, HET and HET/PYR (Figure 75). Control gene expression level (*i.e.* *Chlamydomonas* cultures grown in TAP medium without additions) has been normalized to 1, indicated by a dotted line in the Figure 75. The expression levels of the THI4 gene (coding for the hydroxyethylthiazole synthase - HET-S) were measured simultaneously with the TRK1 gene expression, since its behavior in presence of compounds belonging to the TPP biosynthetic pathway is known. In fact, THI4 was found to contain a TPP riboswitch that can bind the thiamine and its intermediates, leading to a decrease in the gene expression when these molecules are present in the growth medium (Moulin et al., 2013).

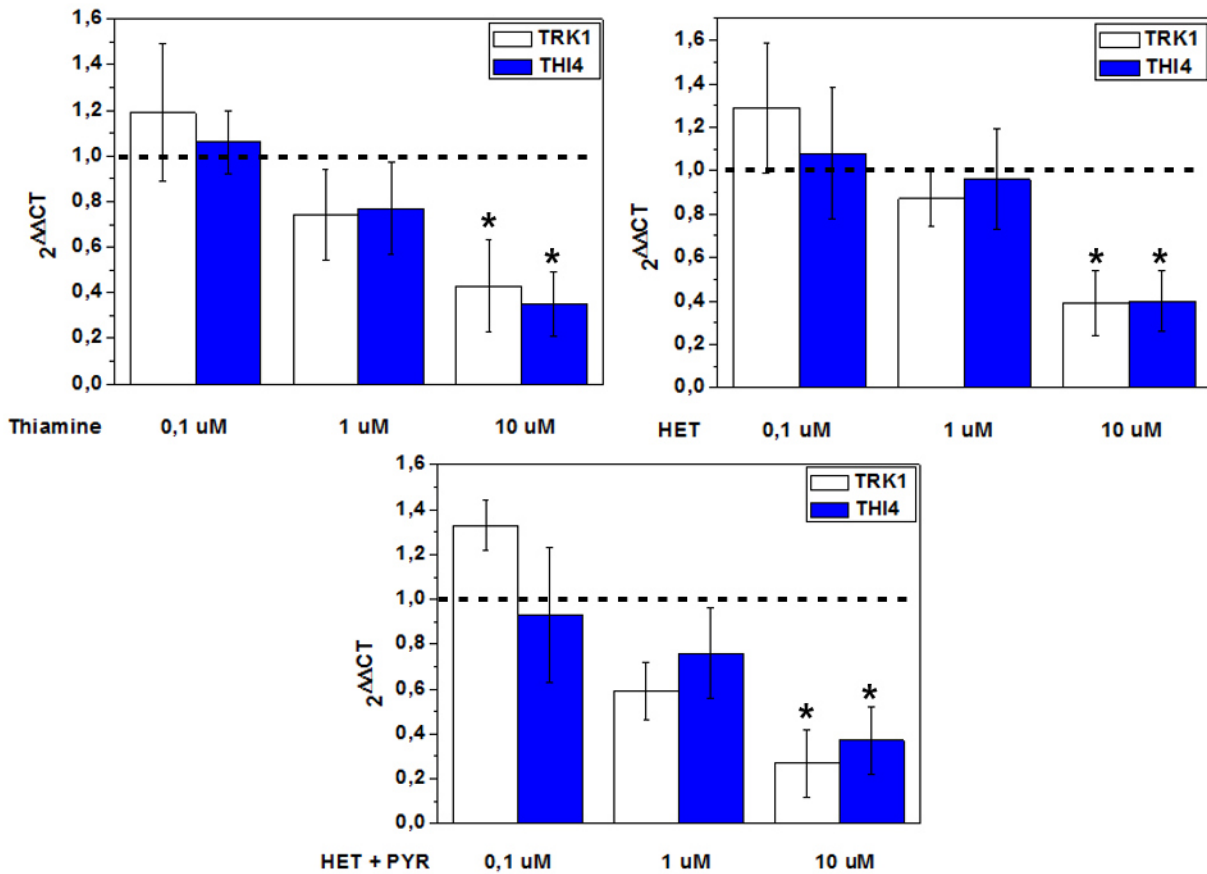


Figure 75. TRK1 (white columns) vs THI4 (blue columns) gene expression levels. The $2^{\Delta\Delta CT}$ was measured following the qRT-PCR procedure described in Materials and Methods. Data represent the mean percentage \pm SD ($n = 6$). Significance of all the data was calculated using the Student's T-TEST (the two-tailed one, third type - or eteroscedastic type). The significance of a result was based on the Reliable Change Index (RCI), where:* indicates p value ≤ 0.05 .

This result confirmed the semiquantitative PCR previously performed on the TRK1 cDNA obtained from the diversely treated cultures: as shown in the agarose gel in the Figure 76 (left, white arrows), the bands had lower intensities when the concentration of the compounds present in the growing culture media corresponded to 10 μ M. An exception to this behavior was noticed for the sample treated with the same concentration of 2HXMP (grey arrow in the Figure 76): in fact, its band intensity was evidently brighter than the bands corresponding to the other treatments (see the last lane of the gel), suggesting that the TRK1 could not modify its expression upon this treatment. The qPCR confirmed this hypothesis, showing no changes in the TRK1 gene expression and even in the THI4 gene expression levels (Figure 76, right). We can just notice that, for all the analyzed samples, the TRK1 gene expression levels exactly followed the trend of the THI4 expression levels (See the Discussion for more details).

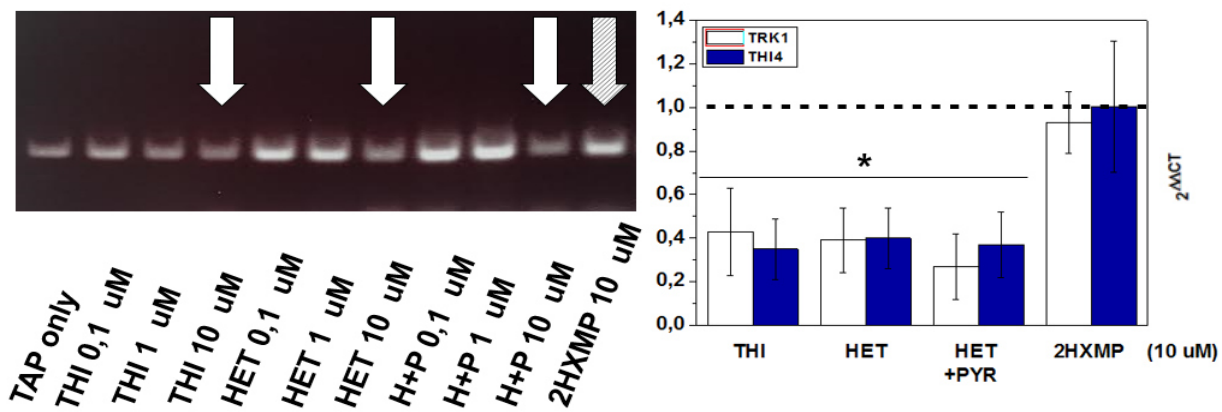


Figure 76. Left: Semi-quantitative PCR showing the TRK1 cDNA from the WT12 *Chlamydomonas* cultures treated with: only TAP, THI (0,1, 1 and 10 μM), HET (0,1, 1 and 10 μM), HET+PYR (0,1, 1 and 10 μM) and 2HXMP (10 μM). Right: qRT-PCR comparing the TRK1 and THI4 gene expression in all the treated samples, showing that the 2HXMP did not modify the expression of these genes. The dotted line represents the level of the control gene expression, i.e. the not-treated culture.

2. Influence of stress agents on TRK1 gene expression

The literature indicated that the transketolase gene expression seemed to be influenced by oxidative stress conditions in numerous organisms, but with different results. For instance, in all the species of *Candida*, the transketolase expression was found to be upregulated, in contrast with *Saccharomyces*, where it was found to be downregulated (Ralser et al., 2009). The difference between *Saccharomyces* and *Candida* in the transketolase gene expression may be associated with the higher dependence of the latter species on the oxygen metabolism and, thus, higher generation of oxygen radicals (Wolak et al., 2015).

Trying to understand what is the response of the TRK1 gene expression under oxidative stress conditions in the cultures of WT12 *Chlamydomonas*, two stress agents were selected:

- 1) hydrogen peroxide (H_2O_2), at a concentration of 1 mM, for 1.5 hours (after 7 days of algal cell growth);
- 2) and a high light intensity, corresponding to $300 \mu\text{mol sec}^{-2} \text{m}^{-1}$, 5-6 times the light intensity normally used to grow these *Chlamydomonas* cells (in the Figure 77, it is possible to appreciate the different coloration - i.e. chlorotic phenotype - of the cultures exposed to these diverse light conditions).

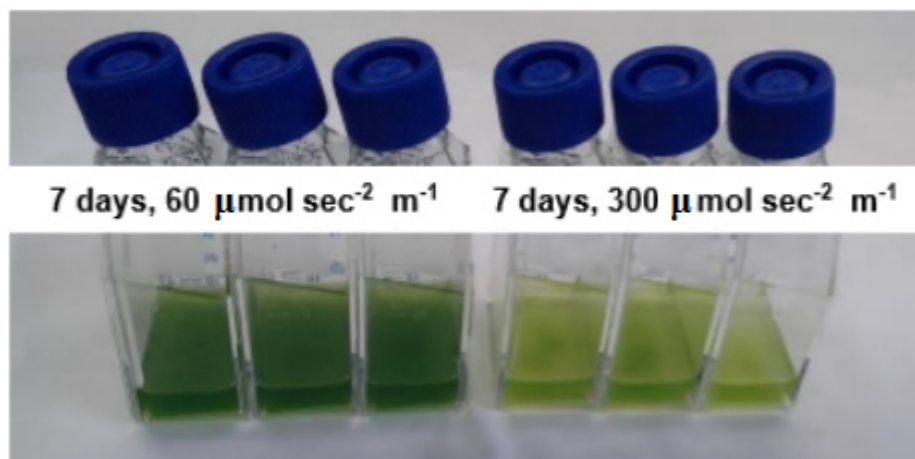


Figure 77. Difference in the culture coloration between WT12 *Chlamydomonas* cells grown in normal (on the left) and high (on the right) light conditions.

The literature reported the ascorbate peroxidase (APX1), one of the most important enzymes in the cell antioxidant system, is upregulated in both high light intensity and in presence of hydrogen peroxide (Caverzan et al., 2012). For this reason, exploiting the APX1 as positive control gene for both these stress conditions seemed legit.

As observed in the Figure 78, the positive control gene APX1 (green bars) increased its expression in both the treated samples as expected, providing the evidence that the two treatments induced an oxidative stress condition. Then it was noticed that the high light treatment did not lead to a decrease of the TRK1 gene expression (or it was not strong enough to decrease it), while the treatment with hydrogen peroxide led to a significant decrease by half in its expression levels (see the dark-grey bars in the graph).

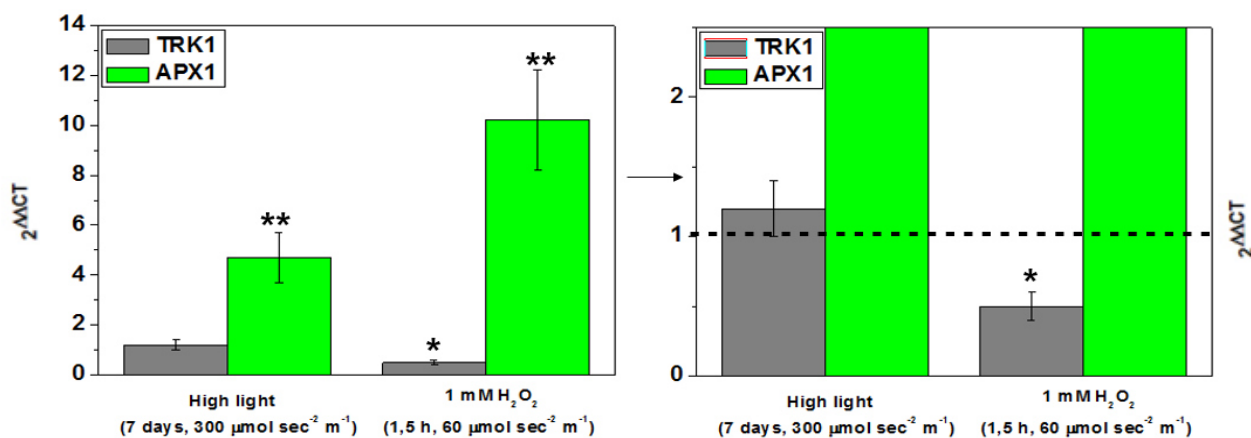


Figure 78. TRK1 (dark-grey columns) vs APX1 (green columns) expression levels. The $2^{\Delta\Delta CT}$ was measured following the qRT-PCR procedure described in Materials and Methods. Data represent the mean percentage \pm SD ($n = 6$). Significance of all the data was calculated using the Student's T-TEST. The significance of the results was expressed with *, corresponding to a p value ≤ 0.05 .

Discussion

Chapter 1

1. Comparison between the structure of the CrTK and the CrTK_{TPP/Mg}

The scientific literature suggests that almost all the TKs, with few exceptions, are homodimeric proteins (Lindqvist et al., 1992; Gerhardt et al., 2003). All the analysis performed on the CrTK (*i.e.* mass spectrometry, SEC, DLS and SDS-PAGE, corresponding respectively to the Figures 42, 43 and 44 in Paragraph 1 in Results and Figure 37 in Paragraph 7 in Materials and Methods) indicate that even in *Chlamydomonas reinhardtii* the transketolase has a dimeric nature.

The crystallographic investigation of the CrTK homodimer reveals its V-shaped quaternary structure (Figure 44) like the yeast and maize ones. Furthermore, the comparison of the structures between the CrTK_{apo} and the CrTK_{TPP/Mg} shows that the overall folding is highly conserved, with the exception for two portions (residues 239-247 and 433-437) which appear disordered and flexible in the CrTK_{apo} (Figure 47-A). The CrTK_{TPP/Mg} structure highlights that these protein regions are involved in the binding of cofactors (Figure 47-B) and they fold in an ordered manner composed by short helices and random coil segments only in presence of TPP and Mg²⁺. To note, these regions are located at the dimer interface and they form inter-chain interactions (Figure 47-C) in CrTK_{TPP/Mg}. The results of the thermal stability comparison between the CrTK and the CrTK_{TPP/Mg} are in concert with these structural observations: CrTK_{TPP/Mg} shows a T₅₀ significantly higher than CrTK, indicating that the presence of TPP and Mg²⁺ in the active site stabilizes the protein when exposed to high temperatures (Figure 48). This suggests that the TPP and Mg²⁺ binding provokes a concrete increase in the CrTK_{TPP/Mg} stability.

2. ICD signal analysis on the reduced and oxidized CrTK_{TPP/Mg}

Diverse papers suggest that the formation of the CrTK_{TPP/Mg} can be monitored by following the appearance of an ICD signal, represented by a negative band centered around at 325 nm in the CD spectrum (Wikner et al, 1994; Kovina et al. 2002). Accordingly, a TPP-induced CD signal at 325 nm was observed for the CrTK_{TPP/Mg} (Figure 62-A). This CD signal evolves by time, reaching its maximum value in about 3 hours. This data nicely agrees with the formation of a completely active CrTK_{TPP/Mg}, shown by Figure 51, confirming that the enzyme structure and function are prone for the catalytic action just after a three hours-incubation with both the cofactors.

The Mg²⁺ appears to be fundamental for this process since, when the chelating agent EDTA is added to the cuvette with the CrTK_{TPP/Mg}, it fully abolished the ICD band (Figure 62-B). Consequently, we can affirm that this cation is necessary for the binding/correct allocation of the TPP in the active site. In fact, the CrTK_{TPP/Mg} crystal structure shows that the metal ion is coordinated by two oxygen atoms of the TPP pyrophosphate moiety (Figures 45 and 46-B) as already reported for yeast and maize TKs (Schneider et al., 1998; Gerhardt et al., 2003).

The ICD signal was studied also for the oxidized CrTK_{TPP}: as shown in the Figures 63 and 64, the signal related to the oxidized protein rises much slower and do not saturate even after 24 hours, resulting in a band with a final (*i.e.* 24 hours) molar ICD intensity about three times lower than that of the reduced enzyme. This leads to two possible explanations: (I) as a result of the oxidation, the cofactor-apo protein interaction is impaired and consequently the ICD band intensity rises slowly; (II) the TPP enters the catalytic site of the CrTK, but its orientation, localization and, above all,

rearrangement of its chemical moieties could not be the same respect to that of the reduced protein.

3. The importance of Mg^{2+} for the CrTK activity

Different TKs activities were found to be tightly dependent on the presence of divalent cations (*e.g.* Mg^{2+} or Ca^{2+}) and TPP (Kochetov and Philippov 1970; Heinrich et al., 1972; Jung et al., 1988; Sprenger et al., 1995). The requirement of the cofactors TPP and Mg^{2+} was investigated in the CrTK to get insight into their role in the enzyme catalysis. We placed particular emphasis on the Mg^{2+} ion because, in photosynthetic organisms, one of the known effects induced by the dark-to-light transition is the increase of the Mg^{2+} concentration into the chloroplast stroma after its release from the thylakoids (Lin and Nobel, 1971; Ishijima et al., 2003).

The time required for reconstitution of the $CrTK_{TPP/Mg}$ in presence of saturating TPP is dependent on increasing Mg^{2+} concentrations in the incubation media (Figure 52). Interestingly, its activity is not influenced by the high content of divalent cations (*i.e.* 15 mM $MgCl_2$ and 5 mM $CaCl_2$) in the buffer assay (Figure 53, black squares), while the activity of the $CrTK_{TPP}$ is dependent just upon Mg^{2+} in the reaction mixture (Figure 53, white squares). These evidences suggested that the transition from the $CrTK_{TPP}$ (a partially active CrTK) to the $CrTK_{TPP/Mg}$ (a totally active CrTK) requires a long time (corresponding to about 3 hours) and it is not a quick process. This is in line with previous studies that analyzed the rate of transition from the apo- to the holo-form of yeast TK, demonstrating that the time needed to reach the maximal activity is strongly reduced upon pre-incubation with TPP and Mg^{2+} (Heinrich et al., 1972; Egan and Sable, 1981).

Therefore, we can reasonably sustain that Mg^{2+} -dependent activation of CrTK is consistent with slow protein conformational changes that allow a correct orientation/binding of the cofactor TPP in the catalytic center of the enzyme. In agreement with these results, it has been reported for yeast TK that the transition from the apo- to the holo enzyme is a multi-step process, influenced by slow rearrangements of the protein structure due to the cofactors' binding (Kochetov and Solovjeva, 2014).

4. The role of the Mg^{2+} in the TPP-induced absorption band

Different studies, mainly performed on the yeast TK, report that the formation of the catalytically active enzyme is parallel to the arise of a positive band in the absorption spectrum between 285 and 360 nm (Kochetov, 1982; Wikner et al., 1994).

The formation of this band was observed also for the $CrTK_{TPP/Mg}$ (Figure 56-A and Figure 56-B, black squares), but not for the $CrTK_{TPP}$ (Figure 56-B, white squares): this suggests that the Mg^{2+} can help in the stabilization of the activated TPP, supporting its right position in the catalytic center of the $CrTK_{TPP/Mg}$ and therefore the final V-shaped TPP conformation (Figure 46-A), required for the catalysis.

As shown in the Figure 56-B, the cation addition to the sole $CrTK_{TPP}$ led to a quick increase in the enzyme activity (red numbers in the Figure 56-B), which arrives to a plateau value after about 3 hours.

Unfortunately, we find no definitive explanation for the fact that the TPP-induced band associated with these activity measurements does not reach a saturating absorbance level: in fact, it continues to grow up even after different hours from the Mg^{2+} introduction in the cuvette with the $CrTK_{TPP}$. Actually, we can hypothesize that the behavior of this band is linked to a well-known phenomenon, called "band broadening": in brief, when the protein is exposed to certain temperatures (*e.g.* 25°C)

for many hours, the 280 nm-arising peak undergoes a time-dependent widening that is connected to the decline of the folding of the protein in question, an insuppressible and irreversible factor. Besides this explanation, all the articles talking about the TPP-induced absorption signal do not give a conclusive answer to this particular phenomenon (Kochetov, 1982; Wikner et al., 1994).

To sum up, these results suggest that the final conformation of the CrTK_{TPP/Mg} strongly depends on the presence of Mg²⁺ and not just on the TPP binding.

5. The redox sensitivity of the CrTK and the role of the Mg²⁺

The TRXs-dependent dithiol/disulfide interchanges represent the main mechanism involved in the control of the activity of CB enzymes during light-to-dark transitions (Michelet et al., 2013). The formation of regulatory disulfides is accompanied by structural changes that modulate the activity of CB enzymes allowing partial or complete inactivation. The regulation of CB enzymes also involves other factors, including, as already mentioned, light-dependent fluctuations of Mg²⁺ concentration (Lin and Nobel, 1971; El-Badry et al., 1974; Werdan et al., 1975; Ishijima et al., 2003).

In the last years, several proteomic studies identified the plant TKs as a putative target of TRXs-mediated regulation (Balmer et al., 2003; Balmer et al., 2004; Marchand et al., 2004; Marchand et al., 2006), suggesting the presence of regulatory cysteine residue(s). However, no biochemical study confirmed the TK sensitivity to redox transitions. Here, it was demonstrated that the CrTK_{TPP} is sensitive to oxidative deactivation, while the CrTK_{TPP/Mg} is protected by the inactivation induced by DTTox treatment (Figure 57), likely precluding the formation of one or more regulatory disulfide bond(s). This protection largely depends from the presence of the Mg²⁺; by contrast, both the CrTK and CrTK_{TPP}, which lack Mg²⁺ in their active sites, are strongly sensitive to reversible inhibition by oxidation (Figure 58 in Results and Figure 79 below).

The reversibility of both the CrTK and CrTK_{TPP} oxidations appears remarkable in the context of light-to-dark changes, reinforcing the hypothesis that CrTK can be regulated by disulfide bond(s) formation. The role of Mg²⁺ in modulating such oxidative regulation is also suited to the physiological context. In fact, it has been previously reported that the stromal Mg²⁺ content, ranging in millimolar concentration (Portis and Heldt, 1976), can vary according to several factor including light conditions (Shaul et al., 2002; Hermans et al., 2013). It is well known the stromal pH increases upon illumination, and the transfer of protons across the thylakoid membrane is believed to be electrically compensated by Mg²⁺ whose concentration increases in the stroma since the chloroplast envelope is relatively impermeable to this metal ion (Heldt et al., 1973; Hind et al., 1974; Tikhonov, 2013). For instance, in dark-kept intact chloroplasts from spinach, available Mg²⁺ concentration has been estimated to be 0.50 ± 0.53 mM, whereas its concentration raised to 1.95 ± 0.97 mM upon illumination (Ishijima et al., 2003). Although these values consist in raw estimations of Mg²⁺ content, its light-dependent fluctuation perfectly correlate with the strong dependency of CrTK activation upon increasing Mg²⁺ and oxidative inactivation observed under decreasing Mg²⁺ concentrations.

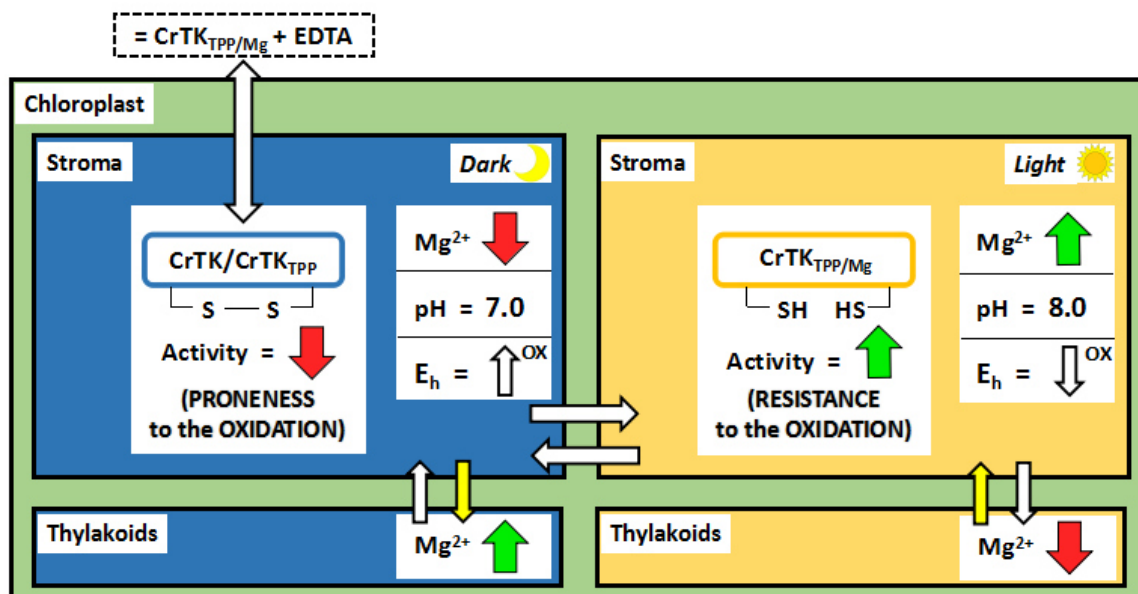


Figure 79. Scheme of the behaviour of the CrTK linking its redox status (oxidized/reduced) with the availability of the magnesium (presence/absence).

The Mg²⁺-dependent activation of CrTK and the role of the Mg²⁺ in the modulation of oxidative sensitivity are reminiscent with what previously observed for fructose-1,6-bisphosphatase (FBPase). In 1982, Minot et al. showed that the increase of Mg²⁺ concentration in the stroma participates to the light-dependent activation of the enzyme (Minot et al., 1982). This regulation was also found to act in concert with TRXs-dependent modulation of FBPase redox state, indicating that both factors are undoubtedly important to control the activity of this enzyme. In addition, it has been reported that Mg²⁺ protects FBPase from the oxidative deactivation, due to the stabilizing role of the complex with the substrate FBP and Mg²⁺ (Schurmann and Buchanan, 2008).

6. Effects of NEM and DTNB treatments on the CrTK_{TPP} activity

Our recombinant CrTK presents 12 cysteine residues mainly distributed in the middle domain (Cys58, 84, 173, 204, 210, 220 and 366) and in the Pyr domain (Cys386, 470, 484 and 582), while just the Cys638 is located in the C-terminal domain.

To verify the effects of the alkylation onto the CrTK_{TPP} activity, analysis with two different agents were carried out: (I) a treatment with N-ethylmaleimide (NEM) and (II) an incubation with di-thio-nitro-benzoic acid (DTNB). These molecules are known to be both alkylating substances, but (as already explained in Results, Paragraph 17) the NEM is able to conduct an irreversible alkylation, in contrast with the DTNB, whose action is reversible. Moreover, the DTNB displays not only an alkylating action, but even an oxidizing one, since it can form a mixed disulfide bridge with a free thiol residue.

As shown in the Figures 66 and 69, the alkylations induced by both NEM and DTNB played a clear effect on the CrTK_{TPP} enzymatic activity, leading to a decrease of this last respect to the control activity. This means that these agents alkylated some cysteine residues that are important for the catalytic activity of the enzyme. This hypothesis is beyond strengthened by the evident recovery of

the DTNB-oxidized CrTK_{TPP} activity after treatment with the strong reducing agent tri-carboxy-ethyl-phosphine (TCEP), as observed in Figure 69.

7. Gluthathionylation in the CrTK

To evaluate if the CrTK possesses potential cysteine residues target of glutathionylation, Western Blot analysis on BioGSSG-treated samples was performed (Figure 67 in Results), suggesting that one or more cysteines are subjected to this post-translational modification *in vitro*. This result is in nice agreement with the data of an *in vivo* proteomic study, which indicated that the Cys84 is a target of glutathionylation in CrTK (Zaffagnini et al., 2012a).

Thanks to the knowledge of the CrTK crystal structure, further analysis about the localization of the Cys84 in the CrTK have been carried out. After zooming the site where the residue in question is positioned, it is possible to notice that the Cys84 is located on a structural element that is quite exposed to the solvent. In fact, visualizing the water molecules near the Cys84, it is evident that H₂O molecules form a sort of “channel” connecting the Cys84 residue with the external solvent (Figure 80). For this reason, we can hypothesize that the oxidized glutathione (GSSG) could likely use this channel to reach and modify Cys84.

Moreover, another observation deriving from the study of the crystal structure of the CrTK shows that the Cys84 is very close to the TPP binding site: in fact there is a distance of about 7 Å between the sulfur atom of the cysteine and the oxygen atom of the TPP β (or distal) pyrophosphate group (as shown in Figure 81). This is to be considered in the light of a putative role of the glutathione in the displacement of the TPP molecule from its binding site or, at least, in a steric effect of the GSSG disturbing the TPP correct allocation/entrance in the enzymatic active cleft. To verify these hypothesis, other experiments are necessary, like for instance mass spectrometry analysis onto the glutathionylated CrTK or a CD analysis to check the presence of the TPP-induced signal in the GSSG-treated protein.

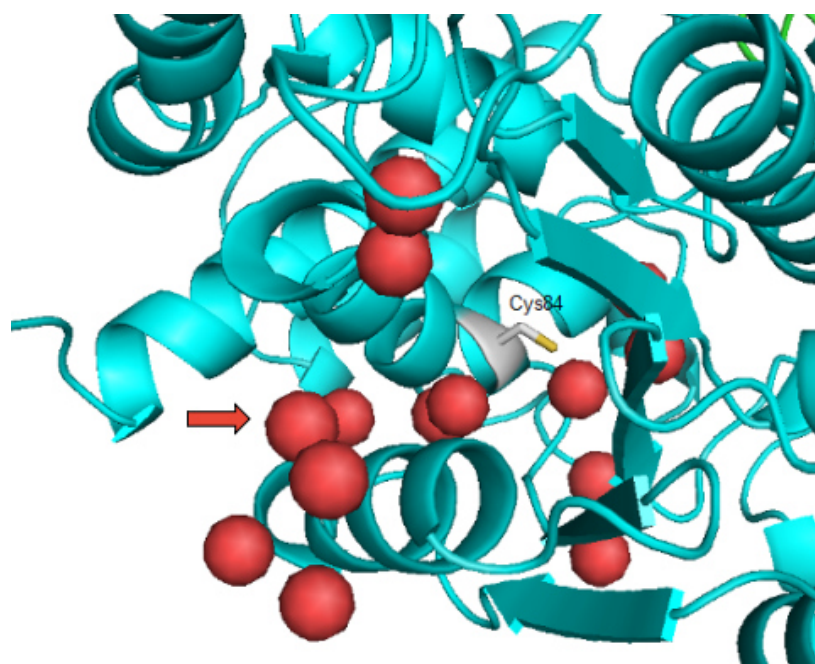


Figure 80. Enlargement of the Cys84 location, showing the solvent channel with the water molecules (red spheres): the solvent channel could be used by the GSSG to reach and modify the Cys84.

8. Titration of the free thiol residues and mass spectrometry analysis: identification of the Cys470-Cys484 disulfide bond

The DTNB thiol titration suggests that the number of free thiols in the control (not treated) CrTK corresponds to 14. Analyzing the sequence, it is evident that the recombinant CrTK possesses 12 cysteine residues: for this reason, the number that turned up from the titration is evaluated admissible if a minimal experimental error equal to ± 2 is considered.

Analyzing the calculations on the absorbance deriving from the Figure 70, it is clear that the glutathionylated CrTK sample shows a decreased number of DTNB-detected free thiol residues (14 free thiols in the untreated CrTK vs 8 free thiols in the glutathionylated CrTK). This means that the CrTK enzyme contains diverse cysteines with a proneness to be glutathionylated *in vitro*, likely depending from their localization in the protein structure and their accessibility to the GSSG molecule (see previous Paragraph on the Cys84).

The experiment in question also reveals that the number of unbound thiols upon DTTox-induced oxidation of the CrTK resulted lower than that of the untreated enzyme (14 free thiols in the not treated CrTK vs 10 free thiols in the oxidized CrTK, see Paragraph 18 in Results). To note, the value obtained for the oxidized CrTK is interestingly compatible with the formation of at least one disulfide bond - even if this number could suggest the appearance of two disulfides. In comparison with the number resulted from the GSSG-treated CrTK, it is assumable that the number of cysteine residues available for the oxidation is lower than that apt to be glutathionylated. This could be due to the fact that there is a few cysteines that are disposed so close in order to form a disulfide bridge between them. In fact, inspections of the CrTK_{TPP} structure showed that two cysteine residues, Cys470 and Cys484, are at suitable distance to bind themselves in a disulfide, without invoking huge conformational modifications of the protein structure.

In agreement with the biochemical data regarding the oxidation of the enzyme, the LC-ESI-MSMS analysis identified a disulfide bond between these two cysteines in the DTTox-treated CrTK. In fact, the mass spectrum of the oxidized CrTK (Figure 74) showed a oxidation-induced peptide (called PEP X = PEP 463-477 and PEP 478-495 linked by a cys470-cys484 disulfide) which is not present in the reduced protein spectrum (Figure 73) and whose molecular weight corresponds to the sum of the two peptides, arisen in the mass analysis of the reduced protein.

A detailed observation of the CrTK structure also unveiled a particular disposition of Cys470 and Cys484. In fact, these residues are located on two structural elements that are contiguous, forming a α -helix- β -sheet motif: the Cys470 is located on the α -helix, connected through a short loop to the β -sheet, on which the other cysteine residue is found (Figure 81). It is notable that the first residue of the whole structural motif is the Glu463: this amino acid plays a fundamental role in the enzymatic catalysis, since it can activate the TPP by giving one proton to the N1 in the aminopyrimidinic ring of the cofactor. This glutamate is present not only in all the reported transketolases, but it is conserved throughout evolution in all the TPP-dependent enzymes. Through its activation, the TPP will be able to attack the carbonyl group of the donor substrate in a nucleophilic manner with its C₂ carbanion (neighbor of the protonated N1).

Considering these observations, we can hypothesize that, when the Cys470 and the Cys484 are linked in a disulfide bond, the Glu463 could be slightly more distant from the TPP binding site and it could fail in the cofactor activation, resulting in a low CrTK activity; while when these cysteines are not involved in a disulfide bond, the Glu463 could get the optimal orientation/proximity to the TPP and contribute to the activation of the cofactor, leading to an increased enzyme activity (see scheme

on the right of the Figure 81). To confirm this hypothesis other experiments are needed, as for instance the site-directed mutagenesis of the residues Cys470 and Cys484.

If the proposed scheme will be confirmed, we will have a further demonstration of the importance of the cofactors in both the CrTK functioning and folding, to be connected with its redox status.

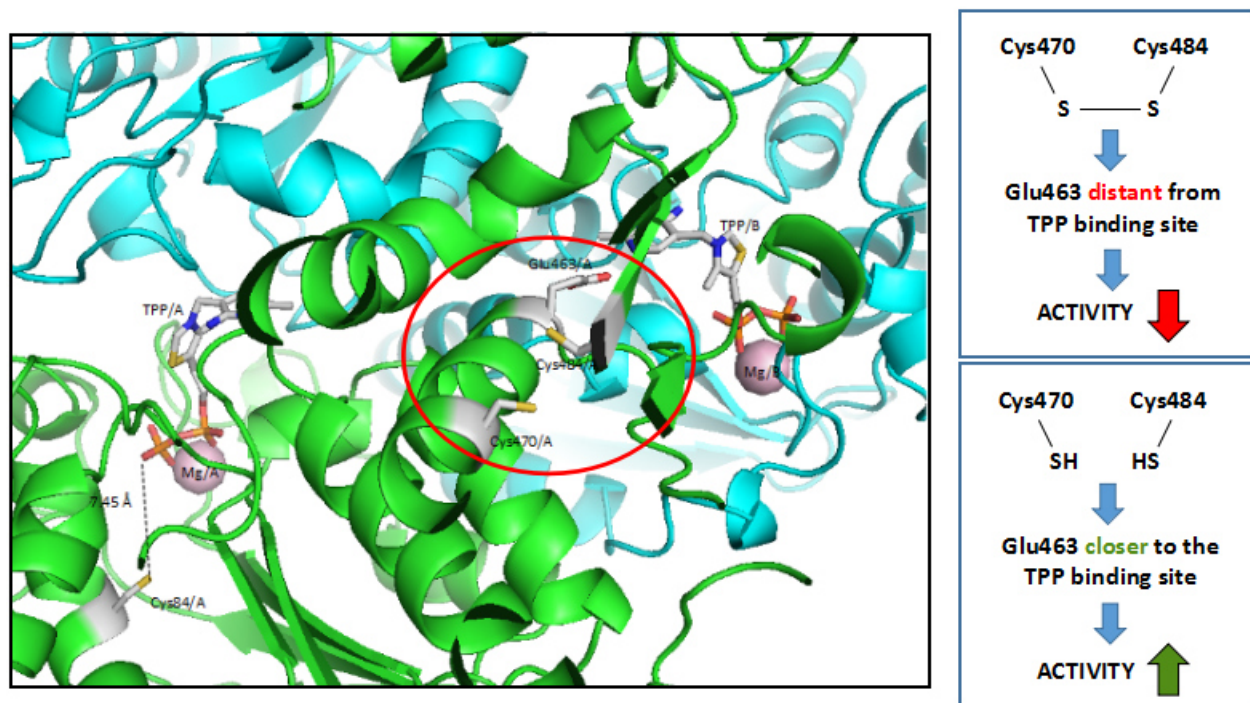


Figure 81. Left: Enlargement of the CrTK TPP binding sites, showing the disposition of the cysteine residues involved in the disulfide bridge respect to the position of the Glu463 (all in the red circle). Right: scheme of the effect of the formation of the disulfide bond on the localization of the Glu463 and on the CrTK activity.

In light of this hypothesis, the high similarity of the affinity constants for the fructose 6-phosphate (F6P) in the reduced and oxidized CrTK_{TPP} indicates that the substrate binding is not influenced by the oxidation of the enzyme. In fact, these values were found to be almost equal (K_m for the F6P in the reduced CrTK_{TPP} = 1.5 mM vs K_m for the F6P in the oxidized CrTK_{TPP} = 1.7 mM, Figure 65). Since the activity of the oxidized CrTK_{TPP} corresponds almost to one third of that of the reduced protein, the disulfide bridge would influence only the catalysis by changing the activation state of the TPP.

Chapter 2

1. Influence of intermediates of the TPP biosynthetic pathway on the TRK1 gene expression levels

Since the TPP was found to display a very important role in the CrTK, both from the structural and the functional point of view, the role of intermediates of the TPP biosynthetic pathway was investigated wondering if they could have some effects on the transketolase (TRK1) gene expression.

Growing concentrations of THI (thiamine), HET (hydroxyethylthiazole), HET/PYR (hydroxyethylthiazole + pyriothiamine) (0.1, 1 and 10 μM) and 10 μM 2HXMP (hydroxymethylpyrimidine) were used to treat the WT12 *Chlamydomonas* cultures. Experiments of qRT-PCR showed that the TRK1 expression was significantly decreased when the growth medium was supplemented with the highest concentration (10 μM) of THI, HET and HET/PYR (Figure 75 and gel in Figure 76, on the left), while it was basically unchanged when treated with 10 μM 2HXMP (Figure 76, on the right). The expression levels of the THI4 gene were measured simultaneously with the TRK1 gene expression, since its behavior in presence of compounds belonging to the TPP biosynthetic pathway is known. In fact, THI4 was found to contain a TPP riboswitch that can bind the thiamine and its intermediates, leading to a sequester of the ribosome binding site (RBS) on the mRNA and decreasing the expression of this gene when these molecules are present in the growth medium (Moulin et al., 2013).

To note, the TRK1 gene expression exactly follows the trend of the THI4 expression in all the analyzed cases, indicating that thiamine and the TPP intermediates act as repressors of the TRK1 gene expression. This result leads to the possibility to perform further studies aimed to find out the factor(s) able to display this control.

One of the possible checkpoints could be the riboswitch mechanism. However, at the moment, there is no evidence in literature about a possible RS regulation of the genes codifying for the Calvin Cycle enzymes. To confirm the presence of a riboswitch in the TRK1 gene, it would be necessary to perform *in silico* studies aimed to identify opportune structures on the messenger RNA that could be ascribable to the presence of a riboswitch. In particular, a region that could fold itself in a loop-like structure and that could bind chemical moieties of the TPP intermediates should be found to define the presence of a RS. Once pinpointed these structures, the creation of mutants lacking the putative riboswitch region or with mutations inserted in this region could be possible in order to evaluate the response of the TRK1 expression in presence of different intermediates of the TPP biosynthetic pathway.

2. Influence of stress agents on TRK1 gene expression

The literature suggested that the transketolase gene expression seemed to be influenced by oxidative stress conditions in a number of organisms, but with diverse results (*i.e.* upregulation in *Candida*, downregulation in yeast) (Ralser et al., 2009). The chosen stress agents were (I) hydrogen peroxide (H_2O_2), at a concentration of 1 mM, for 1.5 hours (after 7 days of algal cell growth) and (II) a high light intensity, corresponding to $300 \mu\text{mol sec}^{-2} \text{m}^{-1}$ (continuously for 7 days of growth).

The high light treatment did not lead to any changes in the TRK1 gene expression (or it was not strong enough to induce these modifications), while the treatment with hydrogen peroxide led to a significant decrease in its expression levels, equal to 50% of the control gene expression (Figure 78 in Results).

This behavior is reminiscent, as explained above, of what happens in *S. cerevisiae*: in fact, in this organism the transketolase gene (called TKL1) is strongly repressed after hydrogen peroxide treatment as a part of a general “metabolic shutdown” (Gasch et al., 2000) involving a high number of genes (*i.e.* codifying proteins important for the cell wall integrity and the cell cycle, the Heat Shock Proteins and Hsp70-related proteins).

Moreover, Ralser et al. explained that in the yeast, to survive oxidative perturbations, a major requirement is an immediate stabilization of the redox state to avoid the disruption of biochemical reactions, a potentially lethal situation (Ralser et al., 2009). In fact, following what Chechik et al. already suggested (Chechik et al., 2008) most genes encoding PPP enzymes are induced in the first minutes after the oxidative perturbations. They hypothesized that inactivation of GAPDH might occur quickly enough to explain the rapid increase of the PPP flux. Thus, reconfiguration of the carbohydrate flux precedes expression changes in the *S. cerevisiae* antioxidant response, allowing the cell to maintain its redox state within the first seconds after the contact with the stressor. These observations suggest the following timeline for the antioxidant response (Figure 82 from Ralser et al., 2009): first, a transcription-independent metabolic reconfiguration prevents a collapse of the cellular redox state; then later, gene expression-dependent systems act, allowing the cells to return to their normal metabolic activity.

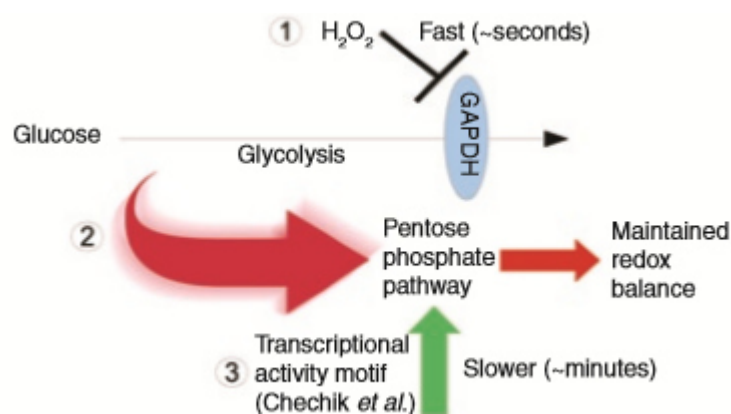


Figure 82. Proposed timeline for the antioxidant response in yeast.

Harking to the mechanisms described above, the results obtained for TRK1 seem to be contrasting. However, we cannot exclude that in the first minutes the hydrogen peroxide treatment of *Chlamydomonas* could have actually increased the level of the TRK1 gene expression. Unfortunately,

this hypothesis had not been analyzed, since the RNA extraction was performed only after 1.5 hours of H₂O₂ treatment.

Considering a longer oxidative stress, the TRK1 gene expression could be subjected to other changes (*i.e.* decrease/repression) due to the already mentioned “metabolic shutdown”, while instead other genes, like those codifying for the antioxidant enzymatic system, remain overexpressed even after different minutes after the impairing treatment (see the APX1 in Figure 78).

Surely, to better understand the overall situation after the exposure to this kind of stressor, it would be interesting: (I) to monitor the TRK1 gene expression in the time, setting up H₂O₂ treatments lasting from minutes to hours; (II) to evaluate even the CrTK protein activity after the described stressing treatments; (III) to check for putative responses (downregulation or upregulation) in the genes codifying for the other Calvin Cycle enzymes and (IV) to observe their catalytic activity upon these treatments.

Conclusions

The main results of this thesis about the structural and biochemical properties of the CrTK are that:

(I) The analyzed enzyme shows a high degree of similarity with the TKs of other organisms and it has a homodimeric quaternary structure (as observed through LC-ESI-MSMS, SDS-PAGE, DLS and SEC analysis).

(II) Its catalytic activity depends on a slow reconstitution process with both the cofactors, TPP and Mg^{2+} at saturating concentration (shown by CD spectroscopy and activity assays); this is connected to the fact that the Mg^{2+} is fundamental to ensure the correct orientation/allocation of the TPP molecule(s) in the CrTK active site(s).

(III) The cofactor binding leads the overall enzyme structure to assume a conformation that is more suitable for the catalytic mechanism, since two portions of the holo-enzyme, directly involved in the TPP and Mg^{2+} binding, were found to be more ordered in comparison with those observed in the apo-form (as pointed out from the crystallographic investigations); moreover, these evidences indicate that the presence of the Mg^{2+} is essential to allow gradual conformational arrangements apt to an optimal catalysis.

(IV) Oxidative treatments revealed that the Mg^{2+} participates in the redox control of CrTK by changing its propensity to be inactivated by oxidation; in fact, the activity of the holo-form (CrTK_{TPP/Mg}) is almost unaffected by the DTT_{ox}-induced oxidation, whereas CrTK_{apo} (apo-form) or CrTK_{TPP} (protein reconstituted with the sole TPP) show a strong sensitivity to the oxidative inactivation.

(V) A disulfide bond between the Cys470 and the Cys484, identified by mass spectrometry, is responsible for the decrease in the activities of CrTK_{apo} and CrTK_{TPP}.

For these reasons, it is possible to affirm that the formation of a disulfide bond and the role of the Mg^{2+} are synergistically involved in the control of the redox sensitivity of CrTK. These features can have a physiological role strictly related to the increase of the cation concentration in the stroma of chloroplasts during dark-to-light transition and to the thioredoxin-guided activation of the Calvin cycle enzymes, two of the three events (together with the stromal pH increase) allowing the “awakening” of the Calvin cycle enzymes.

The study of the redox modifications of CrTK should continue: (I) analyzing what type(s) of thioredoxins (TRXs) could act on the CrTK activation, trying to give a further physiological significance to the data exposed in this work; (II) performing a deeper mass spectrometry analysis, to understand if there could be other disulfide bridges in the oxidized enzyme; (III) carrying out experiments, always through mass spectrometry and activity assays, to find out if the CrTK can undergo additional post-translational modifications, like for instance the nitrosylation.

With regard to the experiments run in Cambridge, treatments with (I) the TPP-related molecules and (II) the stressor hydrogen peroxide lead to a slight but significant decrease in the transketolase (TRK1) gene expression in WT12 *Chlamydomonas* cultures. A putative continuation for these studies could be looking for a riboswitch in TRK1, starting from *in silico* analysis of the transcript structure.

Concerning the biotechnological applications of this research, the investigation on the transketolases is important, as already explained in the Introduction, also in light of their exploitation for industrial purposes, as the carbon-carbon bond synthesis: understanding, for example, how to enhance the enzyme catalysis should be very useful for the production of a number of molecules for pharmaceutical and food industries.

More in general, the analysis of the structure and functioning of the Calvin cycle enzymes will lead to a deeper comprehension of the photosynthetic pathways, even in light of the ambitious objective to recreate all these important mechanisms *in vitro*.

References

A

Agyei-Owusu K, Leeper FJ, Thiamin diphosphate in biological chemistry: analogues of thiamin diphosphate in studies of enzymes and riboswitches, *FEBS J.* 2009 (276) 2905-2916.

Ahn IP, Kim S, Lee YH, Vitamin B1 functions as an activator of plant disease resistance, *Plant Physiol.* 2005 (138) 1505-1515.

Allahverdiyeva Y, Suorsa M, Tikkanen M, Aro EM, Photoprotection of photosystems in fluctuating light intensities, *J Exp Bot.* 2015 (66) 2427-2436.

Allenmark S, Induced circular dichroism by chiral molecular interaction, *Chirality* 15 (2003) 409-422.

Arsova B, Hoja U, Wimmelbacher M, Greiner E, Ustün S, Melzer M, Petersen K, Lein W, Börnke F, Plastidial thioredoxin z interacts with two fructokinase-like proteins in a thiol-dependent manner: evidence for an essential role in chloroplast development in *Arabidopsis* and *Nicotiana benthamiana*, *Plant Cell.* 2010 (22) 1498-1515.

Astier J, Lindermayr C, Nitric oxide-dependent posttranslational modification in plants: an update, *Int J Mol Sci.* 2012 (13) 15193-15208.

B

Baldus IB, Gräter F, Mechanical force can fine-tune redox potentials of disulfide bonds, *Biophys J.* 2012 (102) 622-629.

Balmer Y, Koller A, del Val G, Manieri W, Schürmann P, Buchanan BB, Proteomics gives insight into the regulatory function of chloroplast thioredoxins, *Proc Natl Acad Sci USA.* 2003 (100) 370-375.

Balmer Y, Koller A, Val GD, Schürmann P, Buchanan BB, Proteomics uncovers proteins interacting electrostatically with thioredoxin in chloroplasts, *Photosynth Res.* 79 (2004) 275-280.

Barber J, Mills JB, Nicolson J, Studies with cation specific ionophores show that within the intact chloroplast Mg^{++} acts as the main exchange cation for H^+ pumping, *FEBS Letters* 1974 (49) 106-110.

Barber J, Ionic regulation in intact chloroplasts and its effect on primary photosynthetic processes. *The Intact Chloroplast.* Elsevier Biomedical Press, New York (1976) 80-134.

Bassham JA, Benson AA, Calvin M, The path of carbon in photosynthesis, *J Biol Chem.* 1950 (185) 781-787.

Benhar M, Forrester MT, Hess DT, Stamler JS, Regulated protein denitrosylation by cytosolic and mitochondrial thioredoxins, *Science.* 2008 (320) 1050-1054.

- Berkowitz GA, Wu W, Magnesium, potassium flux and photosynthesis. *Magnes Res.* 1993 (6) 257-265.
- Bienert GP, Møller AL, Kristiansen KA, Schulz A, Møller IM, Schjoerring JK, Jahn TP, Specific aquaporins facilitate the diffusion of hydrogen peroxide across membranes, *J Biol Chem.* 2007 (282) 1183-1192.
- Bishop DG, Lamellar structure and composition of chloroplasts in relation to photosynthetic electron transfer, *Photochem Photobiol.* 1974 (20) 281-299.
- Blaby-Haas CE, Merchant SS, The ins and outs of algal metal transport, *Biochim Biophys Acta.* 2012 (1823) 1531-1552.
- Blaby IK, Blaby-Haas CE, Tourasse N, Hom EF, Lopez D, Aksoy M, Grossman A, Umen J, Dutcher S, Porter M, King S, Witman GB, Stanke M, Harris EH, Goodstein D, Grimwood J, Schmutz J, Vallon O, Merchant SS, Prochnik S, The *Chlamydomonas* genome project: a decade on, *Trends Plant Sci* 2014 (19) 672-680.
- Bocobza S, Adato A, Mandel T, Shapira M, Nudler E, Aharoni A, Riboswitch-dependent gene regulation and its evolution in the plant kingdom, *Genes Dev.* 2007 (21) 2874-2879.
- Bocobza SE, Aharoni A, Small molecules that interact with RNA: riboswitch-based gene control and its involvement in metabolic regulation in plants and algae, *Plant J.* 2014 (79) 693-703.
- Bongs J, Hahn D, Schörken U, Sprenger GA, Kragl U, Wandrey C, Continuous production of erythrose using transketolase in a membrane reactor, *Biotechnology Letters* 1997 (19) 213-216.
- Bonomi M, Parrinello M, Enhanced sampling in the well-tempered ensemble, *Phys Rev Lett.* 2010 (104) 190601.
- Borkhsenius ON, Mason CB, Moroney JV, The intracellular localization of ribulose-1,5-bisphosphate Carboxylase/Oxygenase in *Chlamydomonas reinhardtii*, *Plant Physiol.* 1998 (116) 1585-1591.
- Brigelius-Flohé R, Flohé L, Basic principles and emerging concepts in the redox control of transcription factors, *Antioxid Redox Signal.* 2011 (15) 2335-2381.
- Brueggeman AJ, Gangadharaiyah DS, Cserhati MF, Casero D, Weeks DP, Ladunga I. Activation of the carbon concentrating mechanism by CO₂ deprivation coincides with massive transcriptional restructuring in *Chlamydomonas reinhardtii*, *Plant Cell.* 2012 (24) 1860-1875.
- Brünger AT, Adams PD, Clore GM, DeLano WL, Gros P, Grosse-Kunstleve RW, Jiang JS, Kuszewski J, Nilges M, Pannu NS, Read RJ, Rice LM, Simonson T, Warren GL, Crystallography & NMR system: A new software suite for macromolecular structure determination, *Acta Cryst. D* 54 (1998) 905-921.
- Butera D, Cook KM, Chiu J, Wong JW, Hogg PJ, Control of blood proteins by functional disulfide bonds, *Blood.* 2014 (123) 2000-2007.

Bykova IA, Solovjeva ON, Meshalkina LE, Kovina MV, Kochetov GA, One-substrate transketolase-catalyzed reaction, *Biochem Biophys Res Commun.* 2001 (280) 845-847.

C

Caverzan A, Passaia G, Rosa SB, Ribeiro CW, Lazzarotto F, Margis-Pinheiro M,

Plant responses to stresses: Role of ascorbate peroxidase in the antioxidant protection, *Genet Mol Biol.* 2012 (35) 1011-1019.

Cheah MT, Wachter A, Sudarsan N, Breaker RR, Control of alternative RNA splicing and gene expression by eukaryotic riboswitches, *Nature.* 2007 (447) 497-500.

Chechik G, Oh E, Rando O, Weissman J, Regev A, Koller D, Activity motifs reveal principles of timing in transcriptional control of the yeast metabolic network, *Nat Biotechnol.* 2008 (26) 1251-1259.

Choi H, Kim S, Mukhopadhyay P, Cho S, Woo J, Storz G, Ryu SE, Structural basis of the redox switch in the OxyR transcription factor, *Cell.* 2001 (105) 103-113.

Costelloe SJ, Ward JM, Dalby PA, Evolutionary analysis of the TPP-dependent enzyme family, *J Mol Evol.* 2008 (66) 36-49.

Couto N, Wood J, Barber J, The role of glutathione reductase and related enzymes on cellular redox homeostasis network, *Free Radic Biol Med.* 2016 (95) 27-42.

Couturier J, Chibani K, Jacquot JP, Rouhier N, Cysteine-based redox regulation and signaling in plants, *Front Plant Sci.* 2013 (4) 105.

Croft MT, Moulin M, Webb ME, Smith AG, Thiamine biosynthesis in algae is regulated by riboswitches, *Proc Natl Acad Sci USA.* 2007 (104) 20770-20775.

Cumming RC, Analysis of global and specific changes in the disulfide proteome using redox two-dimensional polyacrylamide gel electrophoresis, *Methods Mol Biol.* 2008 (476) 165-179.

D

Della Cioppa G, Garger SJ, Sverlow GG, Turpen TH, Grill LK, Melanin production in *Escherichia coli* from a cloned tyrosinase gene, *Biotechnology NY* 1990 (8) 634-638.

Demmig B, Gimmler H, Properties of the Isolated Intact Chloroplast at Cytoplasmic K Concentrations : I. Light-Induced Cation Uptake into Intact Chloroplasts is Driven by an Electrical Potential Difference, *Plant Physiol.* 1983 (73) 169-174.

Deponte M, Glutathione catalysis and the reaction mechanisms of glutathione-dependent enzymes. *Biochim Biophys Acta.* 2013 (1830) 3217-3266.

Dilley RA, Vernon LP, Ion and water transport processes related to the light-dependent shrinkage of spinach chloroplasts, *Arch Biochem Biophys.* 1965 (111) 365-375.

Duesterberg VK, Fischer-Hwang IT, Perez CF, Hogan DW, Block SM, Observation of long-range tertiary interactions during ligand binding by the TPP riboswitch aptamer, *Elife*. 2015 (4) e12362.

Dutcher SK, The awesome power of dikaryons for studying flagella and basal bodies in *Chlamydomonas reinhardtii*, *Cytoskeleton* 2014 (71)79-94.

E

Effenberger F, Null V, Ziegler T, Enzyme catalyzed reactions. 12. Preparation of optically pure L-2-hydroxyaldehydes with yeast transketolase, *Tetrahedron Lett*. 1992 (33) 5157-5160.

Egan RM, Sable HZ, Transketolase kinetics. The slow reconstitution of the holoenzyme is due to rate-limiting dimerization of the subunits, *J. Biol. Chem*. 1981 (256) 4877-4883.

El-Badry AM, Hexosediphosphatase from spinach chloroplasts purification, crystallization and some properties, *Biochim. Biophys. Acta* 333 (1974) 366-377.

Emsley P, Cowtan K, Coot: model-building tools for molecular graphics, *Acta Cryst. D* 60 (2004) 2126-2132.

Enser U, Heber U, Metabolic regulation by pH gradients. Inhibition of photosynthesis by indirect proton transfer across the chloroplast envelope, *Biochim Biophys Acta*. 1980 (592) 577-591.

Ensley BD, Ratzkin BJ, Osslund TD, Simon MJ, Wackett LP, Gibson DT, Expression of naphthalene oxidation genes in *Escherichia coli* results in the biosynthesis of indigo, *Science*. 1983 (222) 167-169.

Esakova OA, Meshalkina LE, Golbik R, Hubner G, Kochetov GA, Donor substrate regulation of Transketolase. *Eur. J. Biochem*. 2004 (271) 4189-4194.

Esnouf RM, An extensively modified version of MolScript that includes greatly enhanced coloring capabilities, *J Mol Graph Model*. 1997 (15) 132-134, 112-113.

Evans P, Scaling and assessment of data quality, *Acta Cryst. D* 62 (2006) 72-82.

F

Fang Z, Mi F, Berkowitz GA, Molecular and Physiological Analysis of a Thylakoid K⁺ Channel Protein, *Plant Physiol*. 1995 (108) 1725-1734.

Fang W, Si Y, Douglass S, Casero D, Merchant SS, Pellegrini M, Ladunga I, Liu P, Spalding MH, Transcriptome-wide changes in *Chlamydomonas reinhardtii* gene expression regulated by carbon dioxide and the CO₂-concentrating mechanism regulator CIA5/CCM1, *Plant Cell*. 2012 (24) 1876-1893.

Feechan A, Kwon E, Yun BW, Wang Y, Pallas JA, Loake GJ, A central role for S-nitrosothiols in plant disease resistance, *Proc Natl Acad Sci USA*. 2005 (102) 8054–8059.

Fernandes PA, Ramos MJ, Theoretical insights into the mechanism for thiol/disulfide exchange, *Chemistry*. 2004 (10) 257-266.

Finkel E, Disulfide bond switches, *Nat Biotechnol.* 2002 (20) 887.

Fomenko DE, Marino SM, Gladyshev VN, Functional diversity of cysteine residues in proteins and unique features of catalytic redox-active cysteines in thiol oxidoreductases, *Mol Cells.* 2008 (26) 228-235.

Friedemann R, Breitkopf C, Theoretical studies on thiamin-substrate adducts, *Bioorg. Chem.* 22 (1994) 119-127.

G

Ganem B, From glucose to aromatics: recent developments in natural products of the shikimic acid pathway, *Tetrahedron* 1978 (34) 3353-3383.

Gardemann A, Schimkat D, Heldt HW, Control of CO₂ fixation regulation of stromal fructose-1,6-bisphosphatase in spinach by pH and Mg²⁺ concentration, *Planta.* 1986 (168) 536-545.

Gasch AP, Spellman PT, Kao CM, Carmel-Harel O, Eisen MB, Storz G, Botstein D, Brown PO, Genomic expression programs in the response of yeast cells to environmental changes, *Mol Biol Cell.* 2000 (11) 4241-4257.

Gerhardt S, Echt S, Busch M, Freigang J, Auerbach G, Bader G, Martin WF, Bacher A, Huber R, Fischer M, Structure and properties of an engineered transketolase from maize, *Plant Physiol.* 132 (2003) 1941-1949.

Getz EB, Xiao M, Chakrabarty T, Cooke R, Selvin PR, A comparison between the sulfhydryl reductants tris(2-carboxyethyl)phosphine and dithiothreitol for use in protein biochemistry, *Anal Biochem.* 1999 (273) 73-80.

Govorunova EG, Sineshchekov OA, Chemotaxis in the green flagellate alga *Chlamydomonas*, *Biochemistry* 2005 (70) 717-725.

Goyer A, Thiamine in plants: aspects of its metabolism and functions, *Phytochemistry.* 2010 (71) 1615-1624.

Grossman AR, Catalanotti C, Yang W, Dubini A, Magneschi L, Subramanian V, Posewitz MC, Seibert M, Multiple facets of anoxic metabolism and hydrogen production in the unicellular green alga *Chlamydomonas reinhardtii*, *New Phytol.* 2011 (190) 279-288.

Grossman A, Acclimation of *Chlamydomonas reinhardtii* to its nutrient environment, *Protist.* 2000 (151) 201-224.

Guedich S, Puffer-Enders B, Baltzinger M, Hoffmann G, Da Veiga C, Jossinet F, Thore S, Bec G, Ennifar E, Burnouf D, Dumas P, Quantitative and predictive model of kinetic regulation by *E. coli* TPP riboswitches, *RNA Biol.* 2016 (13) 373-390.

Güttele DD, Roret T, Müller SJ, Couturier J, Lemaire SD, Hecker A, Dhalleine T, Buchanan BB, Reski R, Einsle O, Jacquot JP, Chloroplast FBPase and SBPase are thioredoxin-linked enzymes with similar architecture but different evolutionary histories, *Proc Natl Acad Sci U S A.* 2016 (113) 6779-6784.

H

Hägglund P, Bunkenborg J, Maeda K, Svensson B, Identification of thioredoxin disulfide targets using a quantitative proteomics approach based on isotope-coded affinity tags, *J Proteome Res.* 2008 (7) 5270-5276.

Hall A, Nelson K, Poole LB, Karplus PA, Structure-based insights into the catalytic power and conformational dexterity of peroxiredoxins. *Antioxid Redox Signal.* 2011 (15) 795-815.

Hammes HP, Du X, Edelstein D, Taguchi T, Matsumara T, Ju Q, Lin J, Bierhaus A, Nawroth P, Hannak D, Neumaier M, Bergfeld R, Giardino I, Brownlee M, Benfotiamine blocks three major pathways of hyperglycemic damage and prevents experimental diabetic retinopathy, *Nat. Med.* 2003 (9) 294-299.

Harris EH, Chlamydomonas as a model organism, *Annu Rev Plant Physiol Plant Mol Biol.* 2001 (52) 363-406.

Hashemy SI, Johansson C, Berndt C, Lillig CH, Holmgren A, Oxidation and S-nitrosylation of cysteines in human cytosolic and mitochondrial glutaredoxins: effects on structure and activity, *J Biol Chem.* 2007 (282) 14428-14436.

Hecquet L, Sancelme M, Bolte J, Demuynck C, Biosynthesis of 4-Hydroxy-2,5-dimethyl-3(2H)-furanone by *Zygosaccharomyces rouxii*, *J. Agric. Food Chem.* 1996 (44) 1357-1360.

Heinzel ML, Grossman AR, The GreenCut: re-evaluation of physiological role of previously studied proteins and potential novel protein functions, *Photosynth Res.* 2013 (11) 427-436.

Heinrich C, Steffen H, Janser P, Wiss O, Studies on the reconstitution of apotransketolase with thiamine pyrophosphate and analogs of the coenzyme, *Eur. J. Biochem.* 1972 (30) 533-541.

Heldt WH, Werdan K, Milovancev M, Geller G, Alkalization of the chloroplast stroma caused by light-dependent proton flux into the thylakoid space, *Biochim Biophys Acta* 314 (1973) 224-241.

Hermans C, Conn SJ, Chen J, Xiao Q, Verbruggen N, An update on magnesium homeostasis mechanisms in plants, *Metallomics* 5 (2013) 1170-1183.

Hind G, Nakatani HY, Izawa S, Light-dependent redistribution of ions in suspensions of chloroplast thylakoid membranes, *Proc Natl Acad Sci USA.* 1974 (71) 1484-1488.

Hisabori T, Hara S, Fujii T, Yamazaki D, Hosoya-Matsuda N, Motohashi K, Thioredoxin affinity chromatography: a useful method for further understanding the thioredoxin network, *Journal of Experimental Botany* 2005 (56) 1463-1468.

Hofbauer F, Frank I, Disulfide bond cleavage: a redox reaction without electron transfer, *Chemistry.* 2010 (16) 5097-5101.

Hogg PJ, Disulfide bonds as switches for protein function, *Trends Biochem Sci.* 2003 (28) 210-214.

Höhner R, Aboukila A, Kunz HH, Venema K, Proton Gradients and Proton-Dependent Transport Processes in the Chloroplast, *Front Plant Sci.* 2016 (7) 218.

Horecker BL, The pentose phosphate pathway, *J. Biol. Chem.* 2002 (277) 47965–47971.

Humphrey AJ, Parsons SF, Smith ME, Turner NJ, Synthesis of a novel N-hydroxypyrrolidine using enzyme catalysed asymmetric carbon–carbon bond synthesis, *Tetrahedron Lett.* 2000 (41) 4481-4485.

I

Ishijima S, Uchibori A, Takagi H, Maki R, Ohnishi M, Light-induced increase in free Mg^{2+} concentration in spinach chloroplasts: measurement of free Mg^{2+} by using a fluorescent probe and necessity of stromal alkalinization, *Arch Biochem Biophys.* 2003 (412) 126-132.

Issakidis-Bourguet E, Mouaheb N, Meyer Y, Miginiac-Maslow M, Heterologous complementation of yeast reveals a new putative function for chloroplast m-type thioredoxin, *Plant J.* 2001 (25) 127-135.

J

Jaffrey SR, Snyder SH, The biotin switch method for the detection of S-nitrosylated proteins, *Sci STKE.* 2001 2001 (86) 1.

Jancarik J, Kim SH, Sparse matrix sampling: a screening method for crystallization of proteins, *J. Appl. Cryst.* 24 (1991) 409-411.

Johnson X, Alric J, Central carbon metabolism and electron transport in *Chlamydomonas reinhardtii*: metabolic constraints for carbon partitioning between oil and starch, *Eukaryot Cell.* 2013 (12) 776-793.

Jordan A, Reichard P, Ribonucleotide reductases, *Annu Rev Biochem.* 1998 (67) 71-98.

Jung EH, Takeuchi T, Nishino K, Itokawa Y, Studies on the nature of thiamine pyrophosphate binding and dependency on divalent cations of transketolase from human erythrocytes, *Int J Biochem.* 1988 (20) 1255-1259.

Jurgenson CT, Ealick SE, Begley TP, Biosynthesis of Thiamin Pyrophosphate, *EcoSal Plus.* 2009 (3).

K

Kabsch W, XDS, *Acta Cryst. D* 66 (2010) 125-132.

Kern D, Kern G, Neef H, Tittmann K, Killenberg-Jabs M, Wikner C, Schneider G, Hübner G, How thiamine diphosphate is activated in enzymes, *Science* 275 (1997) 67-70.

Keten S, Chou CC, van Duin AC, Buehler MJ, Tunable nanomechanics of protein disulfide bonds in redox microenvironments, *J Mech Behav Biomed Mater.* 2012 (5) 32-40.

- Khailova LS, Severin SE, Hübner G, Neef H, Schellenberger A, Effect of pyruvate and its analogs on the thiamine pyrophosphate binding in the active center of muscle pyruvate dehydrogenase, *FEBS Lett.* 1982 (139) 49-52.
- Kianianmomeni A, Hallmann A, Algal photoreceptors: in vivo functions and potential applications, *Planta.* 2014 (239) 1-26.
- Kirk JT, Chloroplast structure and biogenesis, *Annu Rev Biochem.* 1971 (40) 161-196.
- Kobayashi NI, Tanoi K, Critical Issues in the Study of Magnesium Transport Systems and Magnesium Deficiency Symptoms in Plants, *Int J Mol Sci.* 2015 (16) 23076-23093.
- Kochetov GK, Philippov PP, The function of calcium - cofactor of transketolase from baker's yeast, *FEBS Lett.* 1970 (6) 49-51.
- Kochetov GA, Izotova AE, Reconstitution of holotransketolase from apotransketolase and thiamine diphosphate, *Biokhimiya* 1973 (38) 552–559.
- Kochetov GA, Philippov PP, Razjivin AP, Tikhomirova NK, Kinetics of reconstitution of holotransketolase, *FEBS Lett.* 1975 (53) 211-212.
- Kochetov GA, Meshalkina LE, Usmanov RA, The number of active sites in a molecule of transketolase, *Biochem Biophys Res Commun.* 1976 (69) 839-843.
- Kochetov GA, Transketolase from yeast, rat liver, and pig liver, *Methods Enzymol.* 1982 (90) 209–223.
- Kochetov GA, Solovjeva ON, Structure and functioning mechanism of transketolase, *Biochim Biophys Acta.* 2014 (1844) 1608-1618.
- Kovacs I, Lindermayr C, Nitric oxide-based protein modification: formation and site-specificity of protein S-nitrosylation, *Front Plant Sci.* 2013 (4) 229.
- Kovina MV, Selivanov VA, Kochevova NV, Kochetov GA, Kinetic mechanism of active site non-equivalence in transketolase, *FEBS Lett.* 1997 (418) 11-14.
- Kovina MV, Kochetov GA, Cooperativity and flexibility of active sites in homodimeric transketolase. *FEBS Lett.* 1998 (440) 81-84.
- Kovina MV, Bykova IA, Solovjeva ON, Meshalkina LE, Kochetov GA, The origin of the absorption band induced through the interaction between apotransketolase and thiamin diphosphate, *Biochem Biophys Res Commun.* 2002 (294) 155-160.
- Kovina MV, De Kok A, Sevostyanova IA, Khailova LS, Belkina NV, Kochetov GA, The molecular origin of the thiamine diphosphate-induced spectral bands of ThDP-dependent enzymes, *Proteins.* 2004 (56) 338-345.
- Kowalska E, Kozik A, The genes and enzymes involved in the biosynthesis of thiamin and thiamin diphosphate in yeasts, *Cell Mol Biol Lett.* 2008 (13) 271-282.

Kubodera T, Watanabe M, Yoshiuchi K, Yamashita N, Nishimura A, Nakai S, Gomi K, Hanamoto H, Thiamine-regulated gene expression of *Aspergillus oryzae* thiA requires splicing of the intron containing a riboswitch-like domain in the 5'-UTR; FEBS Lett. 2003 (555) 516-520.

L

Lacoste-Royal G, Gibbs SP, Immunocytochemical Localization of Ribulose-1,5 Bisphosphate Carboxylase in the Pyrenoid and Thylakoid Region of the Chloroplast of *Chlamydomonas reinhardtii*, Plant Physiol. 1987 (83) 602-606.

Lee U, Wie C, Fernandez BO, Feelisch M, Vierling E, Modulation of Nitrosative Stress by S-Nitrosoglutathione Reductase Is Critical for Thermotolerance and Plant Growth in Arabidopsis, Plant Cell. 2008 (20) 786–802.

Lee SB, Kim CK, Lee KH, Ahn JY, S-nitrosylation of B23/nucleophosmin by GAPDH protects cells from the SIAH1–GAPDH death cascade, J Cell Biol. 2012 (199) 65–76.

Leichert LI, Gehrke F, Gudiseva HV, Blackwell T, Ilbert M, Walker AK, Strahler JR, Andrews PC, Jakob U, Quantifying changes in the thiol redox proteome upon oxidative stress in vivo, Proc Natl Acad Sci USA. 2008 (105) 8197-8102.

León-Bañares R, González-Ballester D, Galván A, Fernández E, Transgenic microalgae as green cell-factories. Trends Biotechnol. 2004 (22) 45-52.

Leonard SE, Carroll KS, Chemical 'omics' approaches for understanding protein cysteine oxidation in biology, Curr. Opin. Chem. Biol. 2011 (15) 88-102.

Lillig CH, Berndt C, Glutaredoxins in thiol/disulfide exchange, Antioxid Redox Signal. 2013 (18) 1654-1665.

Lin DC, Nobel PS, Control of photosynthesis by Mg^{2+} , Arch. Biochem. Biophys. 145 (1971) 622-632.

Lindqvist Y, Schneider G, Ermler V, Sundstrom M, Three-dimensional structure of transketolase, a thiamine diphosphate dependent enzyme, at 2.5 Å resolution, EMBO J. 1992 (11) 2373–2379.

Liu JY, Timm DE, Hurley TD, Pyrithiamine as a substrate for thiamine pyrophosphokinase, J Biol Chem. 2006 (281) 6601-6607.

M

Machado CR, Praekelt UM, de Oliveira RC, Barbosa AC, Byrne KL, Meacock PA, Menck CF, Dual role for the yeast THI4 gene in thiamine biosynthesis and DNA damage tolerance, J Mol Biol. 1997 (273) 114-121.

Mandal M, Breaker RR, Adenine riboswitches and gene activation by disruption of a transcription terminator, Nat Struct Mol Biol. 2004 (11) 29-35.

Marchand C, Le Maréchal P, Meyer Y, Miginiac-Maslow M, Issakidis-Bourguet E, Decottignies P, New targets of Arabidopsis thioredoxins revealed by proteomic analysis, *Proteomics*. 2004 (4) 2696-2706.

Marchand C, Le Maréchal P, Meyer Y, Miginiac-Maslow M, Issakidis-Bourguet E, Decottignies P, New targets of Arabidopsis thioredoxins revealed by proteomic analysis, *Proteomics* 4 (2004) 2696-2706.

Marchand C, Le Maréchal P, Meyer Y, Decottignies P, Comparative proteomic approaches for the isolation of proteins interacting with thioredoxin, *Proteomics* 6 (2006) 6528-6537.

Mayfield SP, Manuell AL, Chen S, Wu J, Tran M, Siefker D, Muto M, Marin-Navarro J, Chlamydomonas reinhardtii chloroplasts as protein factories. *Curr Opin Biotechnol*. 2007 (18) 126-133.

Martin PR, Singleton CK, Hiller–Sturmhöfel S, The Role of Thiamine Deficiency in Alcoholic Brain Disease, *Alcohol Res Health*. 2003 (27) 134-142.

Matsuo T, Ishiura M, Chlamydomonas reinhardtii as a new model system for studying the molecular basis of the circadian clock, *FEBS Lett*. 2011 (585) 1495-1502.

Melis A, Seibert M, Ghirardi ML, Hydrogen fuel production by transgenic microalgae, *Adv Exp Med Biol*. 2007 (616) 110-121.

Merchant SS, Prochnik SE, Vallon O, Harris EH, Karpowicz SJ, Witman GB, Terry A, Salamov A, Fritz-Laylin LK, Maréchal-Drouard L, Marshall WF, Qu LH, Nelson DR, Sanderfoot AA, Spalding MH, Kapitonov VV, Ren Q, Ferris P, Lindquist E, Shapiro H, Lucas SM, Grimwood J, Schmutz J, Cardol P, Cerutti H, Chanfreau G, Chen CL, Cognat V, Croft MT, Dent R, Dutcher S, Fernández E, Fukuzawa H, González-Ballester D, González-Halphen D, Hallmann A, Hanikenne M, Hippler M, Inwood W, Jabbari K, Kalanon M, Kuras R, Lefebvre PA, Lemaire SD, Lobanov AV, Lohr M, Manuell A, Meier I, Mets L, Mittag M, Mittelmeier T, Moroney JV, Moseley J, Napoli C, Nedelcu AM, Niyogi K, Novoselov SV, Paulsen IT, Pazour G, Purton S, Ral JP, Riaño-Pachón DM, Riekhof W, Rymarquis L, Schroda M, Stern D, Umen J, Willows R, Wilson N, Zimmer SL, Allmer J, Balk J, Bisova K, Chen CJ, Elias M, Gendler K, Hauser C, Lamb MR, Ledford H, Long JC, Minagawa J, Page MD, Pan J, Pootakham W, Roje S, Rose A, Stahlberg E, Terauchi AM, Yang P, Ball S, Bowler C, Dieckmann CL, Gladyshev VN, Green P, Jorgensen R, Mayfield S, Mueller-Roeber B, Rajamani S, Sayre RT, Brokstein P, Dubchak I, Goodstein D, Hornick L, Huang YW, Jhaveri J, Luo Y, Martínez D, Ngau WC, Otilar B, Poliakov A, Porter A, Szajkowski L, Werner G, Zhou K, Grigoriev IV, Rokhsar DS, Grossman AR, The Chlamydomonas genome reveals the evolution of key animal and plant functions, *Science*. 2007 (318) 245-250.

Merchant SS, Kropat J, Liu B, Shaw J, Warakanont J, TAG, you're it! Chlamydomonas as a reference organism for understanding algal triacylglycerol accumulation, *Curr Opin Biotechnol*. 2012 (23) 352-363.

Meyer Y, Belin C, Delorme-Hinoux V, Reichheld JP, Riondet C, Thioredoxin and glutaredoxin systems in plants: molecular mechanisms, crosstalks, and functional significance, *Antioxid Redox Signal*. 2012 (17) 1124-1160.

- Meshalkina LE, Kochetov GA, The functional identity of the active centres of transketolase, *Biochim Biophys Acta*. 1979 (571) 218-223.
- Michelet L, Zaffagnini M, Morisse S, Sparla F, Pérez-Pérez ME, Francia F, Danon A, Marchand CH, Fermani S, Trost P, Lemaire SD, Redox regulation of the Calvin-Benson cycle: something old, something new, *Front Plant Sci*. 2013 (4) 470.
- Mieyal JJ, Gallogly MM, Qanungo S, Sabens EA, Shelton MD, Molecular mechanisms and clinical implications of reversible protein S-glutathionylation, *Antioxid Redox Signal*. 2008 (10) 1941-1988.
- Minagawa J, State transitions--the molecular remodeling of photosynthetic supercomplexes that controls energy flow in the chloroplast, *Biochim Biophys Acta*. 2011 (1807) 897-905.
- Minot R, Meunier JC, Buc J, Ricard J, The role of pH and magnesium concentration in the light activation of chloroplastic fructose biphosphatase, *FEBS Letters* 142 (1982) 118-120.
- Mitchell DA, Marletta MA, Thioredoxin catalyzes the S-nitrosation of the caspase-3 active site cysteine, *Nat Chem Biol*. 2005 (1) 154-158.
- Mitra RK, Woodley JM, Lilly MD, Escherichia coli transketolase-catalyzed carbon-carbon bond formation: biotransformation characterization for reactor evaluation and selection, *Enzyme and Microbial Technology* 1998 (22) 64-70.
- Mitschke L, Parthier C, Schröder-Tittmann K, Coy J, Lüdtkke S, Tittmann K, The crystal structure of human transketolase and new insights into its mode of action, *J Biol Chem*. 2010 (285) 31559-31570.
- Montrichard F, Alkhalifioui F, Yano H, Vensel WH, Hurkman WJ, Buchanan BB, Thioredoxin targets in plants: the first 30 years, *J Proteomics*. 2009 (72) 452-474.
- Morris KG, Transketolase from Escherichia coli: A practical procedure for using the biocatalyst for asymmetric carbon-carbon bond synthesis, *Tetrahedron Asymmetry* 1996 (7) 2185-2188.
- Moulin M, Nguyen GT, Scaife MA, Smith AG, Fitzpatrick TB, Analysis of Chlamydomonas thiamin metabolism in vivo reveals riboswitch plasticity, *Proc Natl Acad Sci USA*. 2013 (110) 14622-14627.
- Murshudov GN, Vagin AA, Dodson EJ, Refinement of macromolecular structures by the maximum-likelihood method, *Acta Cryst. D* 53 (1997) 240-255.
- Mustárdy L, Buttle K, Steinbach G, Garab G. The three-dimensional network of the thylakoid membranes in plants: quasi-helical model of the granum-stroma assembly, *Plant Cell*. 2008 (20) 2552-2557.

N

- Nagy P, Kinetics and mechanisms of thiol-disulfide exchange covering direct substitution and thiol oxidation-mediated pathways, *Antioxid Redox Signal*. 2013 (18) 1623-1641.
- Naula C, Alibu VP, Brock JM, Veitch NJ, Burchmore RJ, Barrett MP, A new erythrose 4-phosphate dehydrogenase coupled assay for transketolase, *J Biochem Biophys Methods*. 2008 (70) 1185-1187.
- Nauton L, Hélaine V, Théry V, Hecquet L, Insights into the Thiamine Diphosphate Enzyme Activation Mechanism: Computational Model for Transketolase Using a Quantum Mechanical/Molecular Mechanical Method, *Biochemistry* 55 (2016) 2144-2152.

Nemeria N, Chakraborty S, Baykal A, Korotchkina LG, Patel MS, Jordan F, The 1',4'-iminopyrimidine tautomer of thiamin diphosphate is poised for catalysis in asymmetric active centers on enzymes, *Proc Natl Acad Sci USA*. 2007 (104) 78-82.

Nielson KD, van Duin AC, Oxgaard J, Deng WQ, Goddard WA 3rd, Development of the ReaxFF reactive force field for describing transition metal catalyzed reactions, with application to the initial stages of the catalytic formation of carbon nanotubes, *J Phys Chem A*. 2005 (109) 493-499.

Nikkola M, Lindqvist Y, Schneider G, Refined structure of transketolase from *Saccharomyces cerevisiae* of 2.0 Å resolution, *J. Mol. Biol.* 1994 (238) 387-404.

Nilsson U, Meshalkina L, Lindqvist Y, Schneider G, Examination of substrate binding in thiamin diphosphate-dependent transketolase by protein crystallography and site-directed mutagenesis, *J Biol Chem*. 1997 (272) 1864-1869.

Nilsson U, Hecquet L, Gefflaut T, Guerard C, Schneider G, Asp477 is a determinant of the enantioselectivity in yeast transketolase, *FEBS Lett*. 1998 (424) 49-52.

Nishii W, Kukimoto-Niino M, Terada T, Shirouzu M, Muramatsu T, Kojima M, Kihara H, Yokoyama S, A redox switch shapes the Lon protease exit pore to facultatively regulate proteolysis, *Nat Chem Biol*. 2015 (11) 46-51.

Noctor G, Mhamdi A, Chaouch S, Han Y, Neukermans J, Marquez-Garcia B, Queval G, Foyer CH, Glutathione in plants: an integrated overview, *Plant Cell Environ*. 2012 (35) 454-484.

Nordlund P, Reichard P, Ribonucleotide reductases, *Annu Rev Biochem*. 2006 (75) 681-706.

P

Pan J, Misamore MJ, Wang Q, Snell WJ, Protein transport and signal transduction during fertilization in *Chlamydomonas*, *Traffic*. 2003 (4) 452-459.

Papenbrock J, Guretzki S, Henne M, Latest news about the sulfurtransferase protein family of higher plants, *Amino Acids*. (41) 43-57.

Philipps G, Krawietz D, Hemschemeier A, Happe T, A pyruvate formate lyase-deficient *Chlamydomonas reinhardtii* strain provides evidence for a link between fermentation and hydrogen production in green algae, *Plant J*. 2011 (66) 330-340.

Pletcher J, Sax M, Crystal and molecular structure of thiamine pyrophosphate hydrochloride, *J Am Chem Soc* 94 (1972) 3998-4005.

Portis AR Jr, Heldt HW, Light-dependent changes of the Mg²⁺ concentration in the stroma in relation to the Mg²⁺ dependency of CO₂ fixation in intact chloroplasts, *Biochim Biophys Acta*. 1976 (6) 434-436.

Pottosin II, Schönknecht G, Ion channel permeable for divalent and monovalent cations in native spinach thylakoid membranes, *J Membr Biol*. 1996 (152) 223-233.

Pribil M, Labs M, Leister DJ, Structure and dynamics of thylakoids in land plants. *Exp Bot*. 2014 (65) 1955-1972.

Pröschold T, Marin B, Schlösser UG, Melkonian M, Molecular phylogeny and taxonomic revision of *Chlamydomonas* (Chlorophyta). I. Emendation of *Chlamydomonas* Ehrenberg and *Chloromonas* Gobi, and description of *Oogamochlamys* gen. nov. and *Lobochlamys* gen. nov., *Protist* 2001 (152) 265-300.

Provencher SW, Glöckner J, Estimation of globular protein secondary structure from circular dichroism, *Biochemistry*. 1981 (20) 33-37.

Purczeld P, Chon CJ, Portis AR Jr, Heldt HW, Heber U. The mechanism of the control of carbon fixation by the pH in the chloroplast stroma. Studies with nitrite-mediated proton transfer across the envelope, *Biochim Biophys Acta*. 1978 (501) 488-498.

Pustynnikov MG, Neef H, Usmanov RA, Schellenberger A, Kochetov GA, The functional groups of thiamine pyrophosphate in holotransketolase. *Biokhimiya* 1986 (51) 1003-1016.

R

Ralser M, Wamelink MM, Latkolik S, Jansen EE, Lehrach H, Jakobs C, Metabolic reconfiguration precedes transcriptional regulation in the antioxidant response, *Nat Biotechnol*. 2009 (27) 604-605.

Rapala-Kozik M, Wolak N, Kujda M, Banas AK, The upregulation of thiamine (vitamin B1) biosynthesis in *Arabidopsis thaliana* seedlings under salt and osmotic stress conditions is mediated by abscisic acid at the early stages of this stress response, *BMC Plant Biol*. 2012 (12) 2.

Rasala BA, Mayfield SP, Photosynthetic biomanufacturing in green algae; production of recombinant proteins for industrial, nutritional, and medical uses, *Photosynth Res*. 2015 (123) 227-239.

Raschke M, Bürkle L, Müller N, Nunes-Nesi A, Fernie AR, Arigoni D, Amrhein N, Fitzpatrick TB, Vitamin B1 biosynthesis in plants requires the essential iron sulfur cluster protein, THIC, *Proc Natl Acad Sci USA*. 2007 (104) 19637-19642.

Reddie KG, Seo YH, Muse WB, Leonard SE, Carroll KS, A chemical approach for detecting sulfenic acid-modified proteins in living cells, *Mol Biosyst*. 2008 (4) 521-531.

Rehder DS, Borges CR, Cysteine sulfenic acid as an intermediate in disulfide bond formation and non-enzymatic protein folding, *Biochemistry*. 2010 (49) 7748-7755.

Rocha AG, Mehlmer N, Stael S, Mair A, Parvin N, Chigri F, Teige M, Vothknecht UC, Phosphorylation of *Arabidopsis* transketolase at Ser428 provides a potential paradigm for the metabolic control of chloroplast carbon metabolism, *Biochem. J*. 458 (2014) 313-322.

Rochaix JD, *Chlamydomonas reinhardtii* as the photosynthetic yeast, *Annu Rev Genet*. 1995 (29) 209-230.

Rochaix JD, Lemeille S, Shapiguzov A, Samol I, Fucile G, Willig A, Goldschmidt-Clermont M, Protein kinases and phosphatases involved in the acclimation of the photosynthetic apparatus to a changing light environment, *Philos Trans R Soc Lond B Biol Sci*. 2012 (367) 3466-3474.

Roos G, Geerlings P, Messens J, Enzymatic catalysis: the emerging role of conceptual density functional theory, *J Phys Chem B*. 2009 (113) 13465-13475.

Roos G, Messens J, Protein sulfenic acid formation: from cellular damage to redox regulation, *Free Radic Biol Med*. 2011 (51) 314-326.

Rosales-Mendoza S, Paz-Maldonado LM, Soria-Guerra RE, *Chlamydomonas reinhardtii* as a viable platform for the production of recombinant proteins: current status and perspectives, *Plant Cell Rep*. 2012 (31) 479-494.

Rosales-Mendoza S, Future directions for the development of *Chlamydomonas*-based vaccines, *Expert Rev Vaccines*. 2013 (12) 1011-1019.

S

Sager R, Granick S, Nutritional studies with *Chlamydomonas reinhardtii*, *Ann N Y Acad Sci*. 1953 (56) 831-838.

Sahrawy M, Hecht V, Lopez-Jaramillo J, Chueca A, Chartier Y, Meyer Y, Intron position as an evolutionary marker of thioredoxins and thioredoxin domains, *J Mol Evol*. 1996 (42) 422-431.

Salmeen A, Andersen JN, Myers MP, Meng TC, Hinks JA, Tonks NK, Barford D, Redox regulation of protein tyrosine phosphatase 1B involves a sulphenyl-amide intermediate, *Nature*. 2003 (423) 769-773.

Salinas T, Larosa V, Cardol P, Maréchal-Drouard L, Remacle C, Respiratory-deficient mutants of the unicellular green alga *Chlamydomonas*: a review, *Biochimie*. 2014 (100) 207-218.

Sarkar N, Lemaire S, Wu-Scharf D, Issakidis-Bourguet E, Cerutti H, Functional specialization of *Chlamydomonas reinhardtii* cytosolic thioredoxin h1 in the response to alkylation-induced DNA damage, *Eukaryot Cell*. 2005 (4) 262-273.

Schellenberger A, Sixty years of thiamin diphosphate biochemistry, *Biochim Biophys Acta*. 1998 (1385) 177-186.

Schenk G, Duggleby RG, Nixon PF, Properties and functions of the thiamine diphosphate dependent enzyme transketolase, *Int. J. Biochem. Cell Biol*. 1998 (30) 1297-1318.

Schmidt B, Ho L, Hogg PJ, Allosteric disulfide bonds, *Biochemistry* 2006 (45) 7429-7433.

Schneider G, Lindqvist Y, Crystallography and mutagenesis of transketolase: mechanistic implications for enzymatic thiamin catalysis, *Biochim Biophys Acta*. 1998 (1385) 387-398.

Schürmann P, Buchanan BB, The ferredoxin/thioredoxin system of oxygenic photosynthesis, *Antioxid Redox Signal*. 2008 (10) 1235-1274.

Schütte LD, Baumeister S, Weis B, Hudemann C, Hanschmann EM, Lillig CH, Identification of potential protein dithiol-disulfide substrates of mammalian Grx2, *Biochim Biophys Acta*. 2013 (1830) 4999-5005.

Selivanov VA, Kovina MV, Kochevova NV, Meshalkina LE, Kochetov GA, Studies of thiamine diphosphate binding to the yeast apotransketolase, *J. Mol. Catal. B: Enzymatic* 2003 (26) 33-40.

Shaul O, Magnesium transport and function in plants: the tip of the iceberg, *Biometals*. 2002 (15) 309-323.

Smith GM, The nature of sexuality in *Chlamydomonas*, *Am J Bot.* 1946 (33) 625-630.

Skjånes K, Rebours C, Lindblad P, Potential for green microalgae to produce hydrogen, pharmaceuticals and other high value products in a combined process, *Crit Rev Biotechnol.* 2013 (33) 172-215.

Solovjeva ON, Bykova IA, Meshalkina LE, Kovina MV, Kochetov GA, Cleaving of ketosubstrates by transketolase and the nature of the products formed, *Biochemistry* 2001 (66) 932-936.

Sparla F, Zaffagnini M, Wedel N, Scheibe R, Pupillo P, Trost P, Regulation of photosynthetic GAPDH dissected by mutants, *Plant Physiol.* 138 (2005) 2210-2219.

Sprenger GA, Schörken U, Sprenger G, Sahm H, Transketolase A of *Escherichia coli* K12. Purification and properties of the enzyme from recombinant strains, *Eur J Biochem.* 1995 (230) 525-532.

Sundstrom M, Lindqvist Y, Schneider G, Three-dimensional structure of apotransketolase, *FEBS Lett.* 1992 (3) 229-231.

T

Tedesco D, Bertucci C, Induced circular dichroism as a tool to investigate the binding of drugs to carrier proteins: classic approaches and new trends, *J Pharm Biomed Anal.* 113 (2015) 34-42.

Teige M, Melzer M, Süß KH, Purification, properties and in situ localization of the amphibolic enzymes D-ribulose 5-phosphate 3-epimerase and transketolase from spinach chloroplasts, *Eur J Biochem.* 1998 (252) 237-244.

Tester M, Blatt MR, Direct measurement of k channels in thylakoid membranes by incorporation of vesicles into planar lipid bilayers, *Plant Physiol.* 1989 (91) 249-252.

Thaler M, Simonis W, Schönknecht G, Light-Dependent Changes of the Cytoplasmic H and Cl Activity in the Green Alga *Eremosphaera viridis*, *Plant Physiol.* 1992 (99) 103-110.

Thore S, Leibundgut M, Ban N, Structure of the eukaryotic thiamine pyrophosphate riboswitch with its regulatory ligand, *Science.* 2006 (312) 1208-1211.

Thore S, Frick C, Ban N, Structural basis of thiamine pyrophosphate analogues binding to the eukaryotic riboswitch, *J Am Chem Soc.* 2008 (130) 8116-8117.

Tikhonov AN, pH-dependent regulation of electron transport and ATP synthesis in chloroplasts, *Photosynth Res.* 116 (2013) 511-534.

Touisni N, Charmantray F, Helaine V, Forano C, Hecquet L, Mousty C, Optimized immobilization of transketolase from *E. coli* in MgAl-layered double hydroxides, *Colloids Surf B Biointerfaces*. 2013 (112) 452-459.

Touisni N, Charmantray F, H elaine V, Hecquet L, Mousty C, An efficient amperometric transketolase assay: towards inhibitor screening, *Biosens Bioelectron*. 2014 (62) 90-96.

Tunc-Ozdemir M, Miller G, Song L, Kim J, Sodek A, Koussevitzky S, Misra AN, Mittler R, Shintani D, Thiamin confers enhanced tolerance to oxidative stress in *Arabidopsis*. *Plant Physiol*. 2009 (151) 421-432.

U

Umen JG, Evolution of sex and mating loci: an expanded view from Volvocine algae, *Curr Opin Microbiol*. 2011 (14) 634-641.

Usmanov RA, Kochetov GA, Interaction of baker's yeast transketolase with substrates, *Biochem International* 1982 (5) 727-734.

V

Vagin A, Teplyakov A, Molecular replacement with MOLREP, *Acta Cryst. D* 66 (2010) 22-25.

Van Laer K, Oliveira M, Wahni K, Messens J, The concerted action of a positive charge and hydrogen bonds dynamically regulates the pKa of the nucleophilic cysteine in the NrdH-redoxin family, *Protein Sci*. 2014 (23) 238-242.

Vinick FJ, Jung S, A superior synthesis of aspartame, *Tetrahedron Letters* 1982 (23) 1315-1318.

W

Wachter A, Tunc-Ozdemir M, Grove BC, Green PJ, Shintani DK, Breaker RR, Riboswitch control of gene expression in plants by splicing and alternative 3' end processing of mRNAs, *Plant Cell*. 2007 Nov;19(11):3437-50.

Wang H, Xian M, Chemical methods to detect S-nitrosation, *Curr Opin Chem Biol*. 2011 (15) 32-37.

Wang Y, Duanmu D, Spalding MH, Carbon dioxide concentrating mechanism in *Chlamydomonas reinhardtii*: inorganic carbon transport and CO₂ recapture, *Photosynth Res*. 2011 (109) 115-122.

Wang ZY, Portis AR, Dissociation of ribulose-1,5-bisphosphate bound to ribulose-1,5-bisphosphate carboxylase/oxygenase and its enhancement by ribulose-1,5-bisphosphate carboxylase/oxygenase activase-mediated hydrolysis of ATP, *Plant Physiol*. 1992 (99) 1348-1353.

Warner KD, Homan P, Weeks KM, Smith AG, Abell C, Ferré-D'Amaré AR, Validating fragment-based drug discovery for biological RNAs: lead fragments bind and remodel the TPP riboswitch specifically, *Chem Biol.* 2014 (21) 591-595.

Weerapana E, Wang C, Simon GM, Richter F, Khare S, Dillon MB, Bachovchin DA, Mowen K, Baker D, Cravatt BF, Quantitative reactivity profiling predicts functional cysteines in proteomes, *Nature.* 2010 (4685) 790-795.

Werdan K, Heldt HW, Milovancev M, The role of pH in the regulation of carbon fixation in the chloroplast stroma. Studies on CO₂ fixation in the light and dark, *Biochim Biophys Acta.* 1975 (396) 276-292.

Wikner C, Meshalkina L, Nilsson U, Nikkola M, Lindqvist Y, Sundström M, Schneider G, Analysis of an invariant cofactor-protein interaction in thiamin diphosphate-dependent enzymes by site-directed mutagenesis. Glutamic acid 418 in transketolase is essential for catalysis. *J Biol Chem.* 1994 (269) 32144-32150.

Wilson NF, Iyer JK, Buchheim JA, Meek W, Regulation of flagellar length in *Chlamydomonas*, *Semin Cell Dev Biol.* 2008 (19) 494-501.

Winkler W, Nahvi A, Breaker RR, Thiamine derivatives bind messenger RNAs directly to regulate bacterial gene expression, *Nature.* 2002 (419) 952-956.

Wiita AP, Perez-Jimenez R, Walther KA, Gräter F, Berne BJ, Holmgren A, Sanchez-Ruiz JM, Fernandez JM, Probing the chemistry of thioredoxin catalysis with force, *Nature.* 2007 (450) 124-127.

Wittorf JH, Gubler CJ, Coenzyme binding in yeast pyruvate decarboxylase. A fluorescent enzyme-inhibitor complex, *Eur J Biochem.* 1970 (14) 53-60.

Wolak N, Tomasi M, Kozik A, Rapala-Kozik M, Characterization of thiamine uptake and utilization in *Candida* spp. subjected to oxidative stress, *Acta Biochim Pol.* 2015 (62) 445-455.

Wolosiuk RA, Ballicora MA, Hagelin K, The reductive pentose phosphate cycle for photosynthetic CO₂ assimilation: enzyme modulation, *FASEB J.* 1993 (7) 622-637.

Wood MJ, Storz G, Tjandra N, Structural basis for redox regulation of Yap1 transcription factor localization, *Nature.* 2004 (430) 917-921.

Y

Yi D, Devamani T, Abdoul-Zabar J, Charmantray F, Helaine V, Hecquet L, Fessner WD, A pH-based high-throughput assay for transketolase: fingerprinting of substrate tolerance and quantitative kinetics, *Chembiochem.* 2012 (13) 2290-2300.

Z

Zaffagnini M, Michelet L, Massot V, Trost P, Lemaire SD, Biochemical characterization of glutaredoxins from *Chlamydomonas reinhardtii* reveals the unique properties of a chloroplastic CGFS-type glutaredoxin, *J Biol Chem.* 2008 (283) 8868-8876.

(a) Zaffagnini M, Bedhomme M, Groni H, Marchand CH, Puppo C, Gontero B, Cassier-Chauvat C, Decottignies P, Lemaire SD, Glutathionylation in the Photosynthetic Model Organism *Chlamydomonas reinhardtii*: A Proteomic Survey, *Mol Cell Proteomics*. 2012 (11) M111.014142.

(b) Zaffagnini M, Bedhomme M, Lemaire SD, Trost P, The emerging roles of protein glutathionylation in chloroplasts, *Plant Sci*. 2012 (185) 86-96.

Zhou B, Baldus IB, Li W, Edwards SA, Gräter F, Identification of allosteric disulfides from prestress analysis, *Biophys J*. 2014 (107) 672-681.

Acknowledgements

In tre anni di dottorato si cresce, ed io sono contenta della mia crescita, lavorativa e non. Sono assolutamente sicura del fatto che da sola non ce l'avrei mai fatta.

Innanzitutto, vorrei ringraziare le due figure professionali che mi sono state più vicine in tale percorso: il Prof. Francia e Mirko. Due persone che con costanza e pazienza mi hanno guidata verso il mio obiettivo, che mi hanno accolta pur essendo, all'inizio, una totale sconosciuta della biochimica e della fisiologia vegetali, e che, parlando linguaggi a volte diversi tra loro, mi hanno insegnato che è possibile analizzare un problema da tanti punti di vista. Spero che questi anni insieme siano stati piacevoli per voi così come lo sono stati per me.

Ringrazio anche tutti i collaboratori, preziosi per completare al meglio i nostri studi e per la scrittura e (speriamo!) la pubblicazione del mio primo articolo a primo nome: Simona, Daniele, Marina, Chiara e il Prof. Bertucci; la Prof. Vothknecht dall'Università di Bonn; il Prof. Lemaire dal CNRS di Parigi e Antonino, che mi ha aiutato negli esperimenti nel suo internato per conseguire la laurea magistrale e mi ha "insegnato ad insegnare". Sono inoltre grata per la possibilità di aver potuto usufruire dei Fondi FARB nell'ambito del progetto «Studi funzionali e strutturali di enzimi coinvolti nell'organizzazione del carbonio nella microalga *Chlamydomonas reinhardtii*: effetto di modificazioni redox a carico di tioli proteici.»

Vorrei poi ringraziare gli amici, di laboratorio e non, che hanno sempre contribuito ad alleggerire lo stress che inevitabilmente subiamo facendo il mestiere del ricercatore: gli amici dell'orto botanico, gli ex-compagni di corso, le ragazze della palestra, i "mitici" di Sax, gli amici del paese natale e soprattutto le persone fantastiche conosciute nel breve periodo trascorso a Cambridge.

Mi sono sempre chiesta se fossi stata in grado di lavorare (e di sopravvivere!) all'estero. Ne ho avuto, con tanto sollievo, la conferma lo scorso anno, proprio in Inghilterra, a Cambridge. Non posso descrivere quanto quell'esperienza sia stata importante per me: non solo mi sono messa alla prova con tecniche che non conoscevo, ma sono entrata in un mondo in cui ho vissuto a pieno ogni momento, sia dal punto di vista professionale che umano. Assolutamente doveroso è ringraziare Alison, che mi ha permesso di frequentare il suo laboratorio per quattro mesi. Alison è stata un modello di donna e di ricercatrice per me: sempre (e dico sempre) disponibile per tutti, preparatissima e molto sensibile a tutti i problemi del gruppo di ricerca. Spero un giorno di diventare un'unghia di quello che lei è adesso.

Ringrazio il programma MarcoPolo per aver finanziato questa piccola fantastica permanenza a Cambridge.

Dulcis in fundo, non posso non dire grazie alla mia famiglia e a Jacob, che mi hanno sempre sostenuta (e sopportata nei periodi più tesi!). Non tutti hanno la fortuna di essere circondati da persone pronte a tutto per loro. Davvero grazie per essermi vicini! Mi auguro che un giorno siate fieri di me e di quello che costruirò.